UNIVERSITY OF UDINE

DOCTORATE COURSE IN
BIOMEDICAL AND BIOTECHNOLOGICAL SCIENCES
CICLE XXVII

RESEARCH DOCTORATE THESIS

THE MEF2-HDAC AXIS CONTROLS PROLIFERATION OF MAMMARY EPITHELIAL CELLS AND ACINI FORMATION IN VITRO.

Tutor:

Professor Claudio Brancolini

Candidate:

Giulia Viviani

Supervisor:

Andrea Clocchiatti

ACADEMIC YEAR 2014-2015

INDEX

ABSTRACT

It is currently unclear how mammary epithelial cells organize in acinar structures and which genetic signals are involved in this process, even though distinct patterns of gene expression are considered the base to orchestrate fine tuned cellular decisions. MEF2 transcription factors are important players driving and controlling morphogenetic and differentiation processes in several districts of the body and their activity is highly and tightly regulated by class IIa HDACs. Despite described their central role during development, MEF2 factors and class IIa HDACs involvement in epithelial morphogenesis is still not characterized. Here, using 3D culture of human mammary MCF-10A acini as a model of study, we investigated the effect of the MEF2-HDAC pathway to elucidate its contribution in the epithelial side and its alteration by HER2, a known oncogene in breast cancer. We showed that MEF2-dependent transcription is up-regulated during acini formation and is coupled to a down-regulation of HDAC7, the most expressed class IIa HDAC in our model, which occurs independently from changes in mRNA levels, proteasome or autophagy mediated degradation. Pertubation of MEF2 activity, using shRNA lentiviral vectors or overexpressing a MEF2 or HDAC7 inducible form, affects cell proliferation controlling the expression of the cyclin-dependent kinase inhibitor 1A (CDKN1A). Only in proliferating cells HDAC7 can bind the first intron of the CDKN1A gene, a region characterized by epigenetic markers of active promoters/enhancers. In cells overexpressing the HER2 oncogene 3D epithelial morphogenesis is altered, HDAC7 is continuously expressed and MEF2-dependent transcription is repressed. Importantly reactivation of MEF2 transcription in these cells, blocking HER2 activity or enhancing MEF2 function, reverted the proliferative defect and re-established normal acini morphogenesis.

INTRODUCTION

The Myocyte Enhancer Factor 2 (MEF2) family of transcription factors.

Structure of the MEF2 family members.

MEF2s, Myocyte Enhancer Factor 2, belong to the MADS (MCM1, agamous, deficiens, SRF) family of transcription factors (TFs). *Saccharomyces cerevisiae, Drosophila*, and *C. elegans* possess a single MEF2 gene, while in vertebrates the family of MEF2s includes four transcriptional activators: MEF2A, -B, -C, and –D, which are located on different chromosomes. Members of this family share a highly conserved 57 amino acid (AA) region, known as MADS-box domain, with the other MADS-box proteins, located at the extreme amino-terminal region and an adjacent 29 amino acid (AA) motif, termed MEF2 domain, exclusive to the MEF2 factors. Together these two domains mediate the homo- and heterodimerization of MEF2 proteins, the binding to a conserved A-T rich DNA consensus sequence, YTA(A/T)4TAR, and the interactions with transcriptional co-factors and co-regulators (Black and Olson, 1998)(Timothy A. McKinsey et al., 2002). The carboxyl-terminal region of MEF2 proteins is more divergent and variable between individual MEF2 family members. It contains a potent transcriptional activation domain (TAD) and a nuclear localization signal (NLS) and it is subject to complex patterns of alternative splicing (Figure 1)(J. F. Martin et al., 1994)(Potthoff and Olson, 2007). Members of the MEF2 family are relatively weak transcriptional activators and they cooperate and associate with other transcription factors to control and drive the expression of specific set of downstream target genes involved in different cellular programs.

Tissue and cell type distribution of MEF2 proteins.

In vertebrates MEF2 factors show distinct, but overlapping, expression patterns during the process of embryogenesis and in adult tissues (Potthoff and Olson, 2007). MEF2A, -B, and -D proteins are ubiquitously expressed, whereas MEF2C shows mainly expression in skeletal muscle, heart and brain. MEF2 factors have a very important role and function in the differentiation processes of several cell types, including muscle (cardiac, smooth and skeletal), neurons, chondrocytes and lymphocytes. In these tissues their expression is concomitant with the activation of differentiation programs, which are highly controlled by different regulatory mechanisms. Members of MEF2 family interact and associate with a variety of transcriptional co-factors that modulate MEF2 activity in a positive or negative manner during the tissue development (Arnold et al., 2007)(Lu et al., 2000)(Verzi et al., 2007).

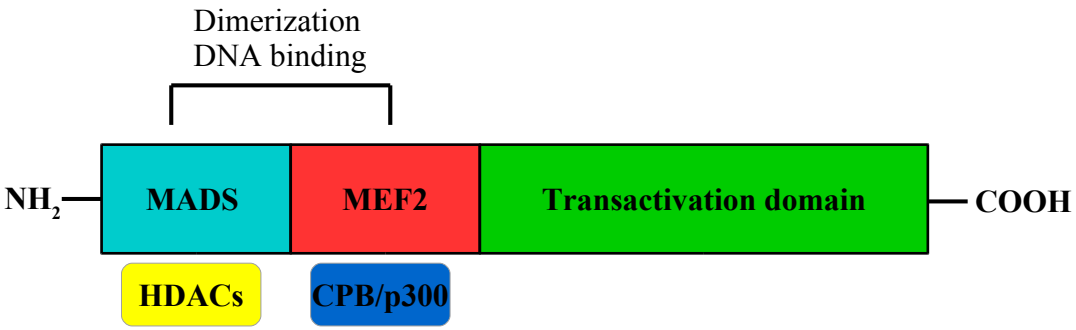

Figure 1: Schematic diagram of MEF2 structure and protein interaction domains.

A schematic representation of the MEF2 structure, including binding sites for key repressors (HDACs) and transcription activators (CBP/p300). MEF2 proteins are comprised of three domains: the N-terminal MADS-box and MEF2 domains, and the C-terminal transactivation domain. The N-terminal domains are responsible for DNA binding, dimerization and co-factors interactions, whereas the C-terminal domain contains the transactivation domain (adapted from Timothy A. McKinsey et al., 2002).

Function and regulation of MEF2 activity.

The transcription factors of MEF2 family act as transcriptional activators or repressors through the direct binding to the promoters or enhancers of a variety of specific genes, thus mediating and controlling multiple and different cellular functions. In this way MEF2 proteins cooperate through protein-protein interactions with other transcriptional factors to control specific sets of target genes. MEF2 expression and activity is under a tight and complex regulation that occurs through different and complex transcriptional, translational and post-translational mechanisms. This complexity provides the possibility to regulate and govern the function of the family members at multiple time points during cell differentiation and growth.

Regulation of MEF2 activity by post-translational modifications.

Many post-translational modifications (PTMs) including phosphorylation, sumoylation, methylation, and acetylation, can influence and govern positively or negatively activity of MEF2 factors, enhancing or suppressing their activities during different cellular programs.

Phosphorylation plays an important role in the regulation and activation of MEF2 family members. MEF2 proteins contain a single conserved phosphorylation serine residue in the

MADS-box domain (Molkentin et al., 1996) and multiple phosphorylation sites in the transactivation domain (Cox et al., 2003). The phosphorylation in the MADS-domain induces conformational changes, which lead to the activation of MEF2 factors. Kinases involved include members of the mitogen-activated protein (MAP) kinase family. The MAPKs, such as p38, JNK and ERK5 can enhance the transcriptional activity of MEF2s in a variety of cell types, by phosphorylating MEF2s in the transactivation domain without affecting DNA binding (H G Kasler et al., 2000)(Miska et al., 2001). Conversely the cyclin-dependent kinase 5 (Cdk5) phosphorylates MEF2s in the transactivation domain (Ser444 in MEF2D) and inhibits MEF2 activity (Gong et al., 2003)(Gregoire et al., 2006). During muscle differentiation, phosphorylation of MEF2D by protein kinase A (PKA) determines the interaction of the transcriptional factor with class II HDACs, mediating MEF2 transcriptional repression (Sebastian et al., 2013).

MEF2 family members undergo also to tissue-specific alternative splicing in the transactivation domain, changing the regulation of MEF2 factors and producing a greater diversity of MEF2 functions.

Many calcium-regulated protein kinases also modulate MEF2s activities through the association with intermediary factors. Calmodulin and CaMK can activate MEF2 by repressing its repressors, respectively cabin and HDACs. Calmodulin, when activated by calcium, binds cabin on the MEF2 binding domain, thus impeding interaction with the transcription factors. When activated, the cabin inhibits MEF2 by recruiting class I HDACs inhibiting calcineurin and preventing the interaction between MEF2 and ERK5 (Youn et al., 1999)(H G Kasler et al., 2000).

MEF2 activity is also regulated through many protein phophatases. Among them, calcineurin can directly stimulate and active MEF2-dependent transcription, dephosphorylating NFAT and recruiting p300 (Wu et al., 2000)(Grégoire et al., 2006).

MEF2 proteins are also modified by sumoylation on conserved lysine residues (Grégoire et al., 2006)(Kang et al., 2006)(Riquelme et al., 2006)(Zhao et al., 2005). This post-translational modification, which occurs on lysine 391 in MEF2C and on lysine 439 in MEF2D inhibits transcriptional activity and it is mediated by class IIa HDACs (Grégoire et al., 2006).

Recent studies have identified a novel post-translational modification. MEF2D activity is regulated by lysine 267 methylation in the transactivation domain, as operated by the co-repressor G9a. G9a controls and represses MEF2 activity during skeletal muscle differentiation through its interaction with cabin and HDACs (J. Choi et al., 2014).

The acetylation of MEF2 is also required for efficient DNA binding (K. Ma et al., 2005). The histone acetyltransferases (HATs) p300, PCAF, and CBP acetylate MEF2 proteins on lysine conserved residues in the MADS-domain (K. Ma et al., 2005), promoting MEF2 activity. The MADS-domain is also critical for the interaction of MEF2 with class IIa HDACs, repressors of MEF2 activity. In this manner the cells can operate by providing a model of dual mutually exclusive signaling for MEF2, important for the regulation of different biological outputs such as differentiation and growth (Timothy A. McKinsey et al., 2002).

Modulation of MEF2 activity by class IIa HDACs.

Class IIa HDACs are widely recognized as the most important transcriptional repressors of genes regulated by MEF2 (Timothy A. McKinsey et al., 2002). Class IIa HDACs act by binding to the MEF2/MADS-domain, without affecting the DNA binding, thus promoting the formation of multiproteins repressive complexes on the regulatory regions of MEF2-dependent genes. Class IIa HDACs lead to suppression of transcription through multiple mechanisms: the exclusion of transcriptional co-activators such as p300/CBP in a sort of competitive binding, or by recruiting class I histone deacetylases, which can deacetylate and switch off MEF2s, as in the case of HDAC3 that binds the complex N-CoR/SMRT (Lu et al., 2000)(Grégoire et al., 2006)(A. Han et al., 2005). Phosphorylation cascades affect MEF2 activity by modifying interactions with their co-repressors. In response to developmental and pathological signaling phosphorylation of class IIa HDACs on conserved serine residues creates docking sites for the intracellular chaperone proteins 14-3-3, promoting the export of histone deacetylases out of the nucleus into the cytoplasm. This re-localization results in the subsequent activation of MEF2 transcription (Wang et al., 2000)(S. J. Choi et al., 2001)(Clocchiatti et al., 2011)(Di Giorgio et al., 2014)(Figure 2). The interaction of MEF2s with HDACs works as a switch in several contexts during both adaptive and differentiative responses as, for example, in the regulation of skeletal muscle differentiation (T A McKinsey et al., 2000).

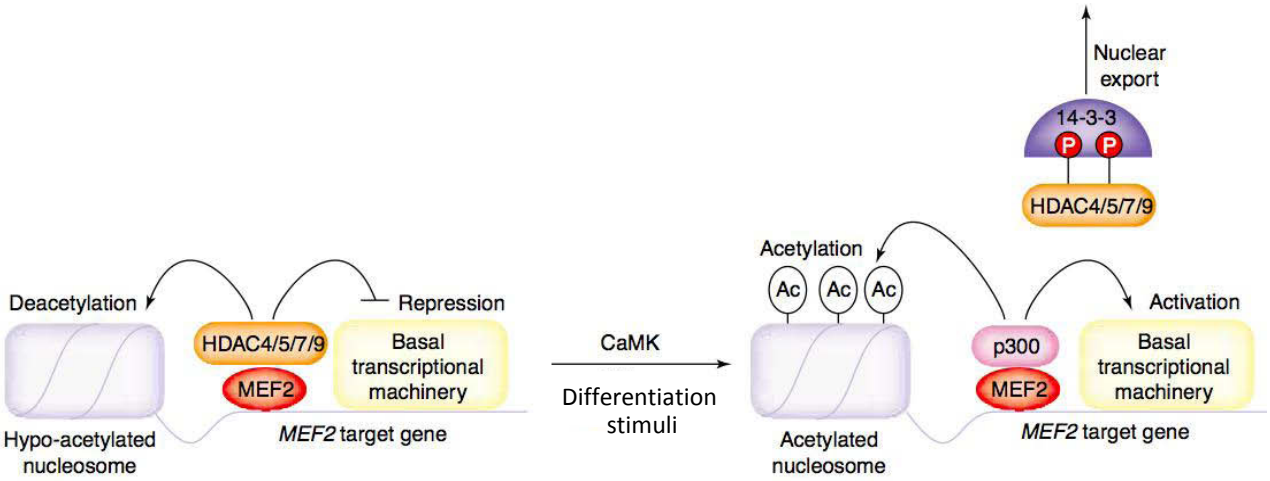

Figure 2: Repression of the transcriptional activation of MEF2 by class IIa HDACs.
Image adapted from (Timothy A. McKinsey et al., 2002).

The histone deacetylase (HDAC) family.

The human genome encodes for eighteen different histone deacetylases (HDACs), which are grouped in four different classes on the basis of sequence homology to yeast counterparts, different catalytic activity, subcellular localization and interacting partners (Xiang-Jiao Yang and Seto, 2008).

- Class I HDACs includes HDAC1, -2, -3, and -8 that present a high homology with yeast enzyme Rpd3, are expressed ubiquitously across cell types, have mainly a nuclear localization and exert a high catalytic activity versus histone and non-histone substrates.
- Class II HDACs are subdivided into class IIa (HDAC4, -5, -7, and -9) and class IIb (HDAC6, and -10). These deacetylases are structurally related to yeast HDA1, they can shuttle between the nucleus and the cytoplasm in a phosphorylation state-dependent manner and they have a tissue-specific pattern of expression.
- Class III HDACs includes the Sirtuins (SIRT1-7), which are homologous to yeast Sir2 and are localized in different cellular compartments.
- Class IV HDACs is composed only by HDAC11 that shares homology and displays common characteristics with both class I and class II (Figure 3).

HDACs are enzymes known to play an important role in the regulation of gene expression both in physiological processes, such as cell proliferation and differentiation, and pathological conditions (Barneda-Zahonero and Parra, 2012). In addition to histones, an increasing list of

other non-histone proteins can also be deacetylated by HDACs, including transcription factors, chaperones, as well as different regulators involved in several different cellular processes (Peng and Seto, 2011)(X-J Yang and Seto, 2007). Since HDACs do not directly bind to DNA sequences, histone deacetylases are recruited to chromatin, after interactions with specific transcription factors to assert their repressive effect.

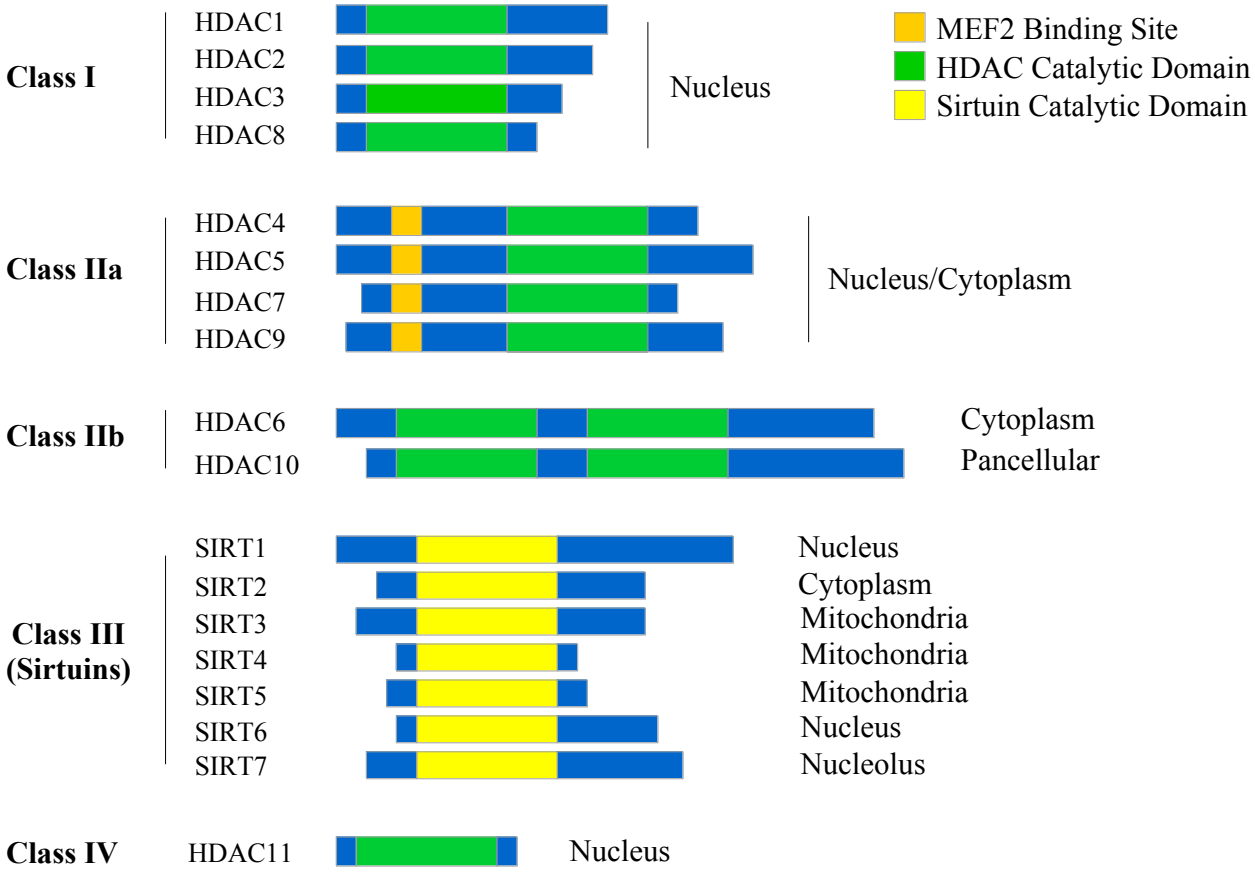

Figure 3: The histone deacetylase family.

The histone deacetylase family is subdivided into four different subclasses according to sequence homology to yeast prototypes, subcellular localization, different catalytic activity and interacting partners (adapted from Barneda-Zahonero and Parra, 2012).

Class IIa histone deacetylases: function and structure.

Class IIa HDACs, which comprises HDAC4, -5, -7, and -9, are expressed in many different tissues such as brain, skin, skeletal, cardiac and smooth muscle, bone, cardiovascular and hematopoietic system, and are involved in different developmental and differentiation processes (Clocchiatti et al., 2011).

Unlike other HDACs, class IIa histone deacetylases present a peculiar structural organization. This is appreciated by a bipartite organization consisting of two distinct regions: an extended N-terminal regulatory domain and a C-terminal catalytic domain (Haberland et al., 2009). The N-terminal region (~450–600 amino acids) is involved in different regulatory functions. It mediates protein–protein interactions with a variety of DNA-binding transcription factors, transcriptional co-repressors and chaperone proteins (M. Martin et al., 2007)(Verdin et al., 2003), among them MEF2 TFs are the best characterized. The N-terminal adaptor domain contains also a nuclear localization signal (NLS) and several serine residues, which are subject to phosphorylation, a post-translational modification that regulates the subcellular localization of these enzymes (T A McKinsey et al., 2001). The conserved C-terminal domain (~400–450 amino acids) of class IIa HDACs contains the catalytic deacetylase domain (HDAC domain) and a nuclear export signal (NES)(M. Martin et al., 2007)(Figure 4).

Unlike other members of HDAC family, class IIa members have a weak intrinsic HDAC activity because of a substitution of a tyrosine residue in the catalytic site, highly conserved among class I enzymes, with a histidine (Lahm et al., 2007). HDAC activity of class IIa members is dependent on the formation of a multiprotein repressor complex at the C-terminal domain, which comprises HDAC3, the co-repressors SMRT (silencing mediator for retinoid and thyroid hormone receptor) and N-CoR (nuclear receptor co-repressor 1)(Fischle et al., 2002).

MEF2 as a regulator of differentiation programs and growth.

MEF2 factors are highly expressed in skeletal, cardiac and smooth muscle cells, as well as in neurons (Edmondson et al., 1994)(Lyons et al., 1995), and at lower levels in several other cell types. The MEF2 family of transcription factors plays important functions in tissue development and homeostasis both in embryonic tissues and in fully differentiated tissues. In developing tissues, such as bone tissue, muscle and nervous system, the expression of MEF2s marks and influences the beginning of the differentiation process and is inversely correlated with the repressive activity of class IIa HDACs (Arnold et al., 2007)(Lu et al., 2000)(Verzi et al., 2007).

The important and critical role of MEF2 factors in developmental processes of various tissues has been illustrated by loss-of-function mutations of each single MEF2 gene. Genetic studies in mice have proved the important contribution of MEF2A to the regulation of heart development (Naya et al., 2002). Likewise, defects in MEF2C impact on cardiovascular system, causing mice to die at stage E9.5 (Q. Lin, 1997)(Qing Lin et al., 1998). By contrast, homozygous mutations in MEF2D are viable, probably because of overlapping expression patterns with other MEF2 members (Arnold et al., 2007). Conditional, cell lineage specific deletions of MEF2s have proved additional roles of these TFs during B-cells development (I. Debnath et al., 2013) and bone homeostasis (Collette et al., 2012)(Kramer et al., 2012). In adult tissues MEF2s regulate stress responses, such as cardiac hypertrophy (C. L. Zhang et al., 2002)(Potthoff et al., 2007), remodeling programs, cell survival and proliferation, for example, by stimulating apoptosis of thymocytes via Nur77 (Dequiedt et al., 2005) or of neurons (Bolger and Yao, 2005), and cell division, via activation of the transcription of c-jun by MEF2D (T. H. Han and Prywes, 1995). The ability of MEF2 proteins to control such diverse and opposing cellular decisions like differentiation, proliferation and apoptosis depends on their regulatory mechanisms, such as specific post-translational modifications and interactions with transcriptional co-factors and co-regulators.

The MEF2-class IIa HDACs axis regulates differentiation programs and cell growth.

MEF2 proteins and class IIa HDACs are co-expressed in several, almost all cell types, including neurons, chondrocytes, muscle cells and lymphocytes. The interaction and the balance between the repressive function of class IIa HDACs and the transcription-activating functions of MEF2 factors play an important and essential role in regulating developmental and differentiation processes in different tissues. As mentioned above class IIa HDACs have a weak deacetylase activity and for this reason they principally act as a bridge between the enzymatically active transcriptional repressor complex (SMRT/N-CoR/HDAC3) and MEF2s to modulate and regulate the transcription of target genes implicated in tissues development and cell differentiation.
Studies in mice, using both gain and loss-of-function approaches, have suggested that several tissue specific cellular programs are regulated by the MEF2-class IIa HDACs axis, such as myogenesis, cardiovascular development, bone formation, endothelial function and the development of the immune system.
The first association between class IIa HDACs and MEFs was described in myocytes. During skeletal muscle differentiation the interaction of HDAC4, HDAC5 and HDAC9 with MEF2s

results in the repression of MEF2 activity and suppression of myogenesis (Lu et al., 2000)(Haberland et al., 2007)(Potthoff and Olson, 2007). MEF2-class IIa HDACs axis has a functional role also in cardiomyocyte differentiation and cardiac hypertrophy (C. L. Zhang et al., 2002). MEF2C controls and regulates the heart development through the expression of numerous cardiac structural and contractile proteins. HDAC5 and HDAC9 are active regulators of cardiac development by repressing MEF2s, Campta2 (calmodulin binding transcription activator 2) and Srf (serum response factor) transcriptional activities (Song et al., 2006). During chondrocyte differentiation, the maturation of immature chondrocytes to hypertrophic chondrocytes is controlled by parathyroid hormone-related peptide (PTHrP), which induces the dephosphorylation of HDAC4 and its translocation into the nucleus, resulting in the repression of MEF2 transcriptional activity (Arnold et al., 2007)(Potthoff and Olson, 2007). MEF2 factors control and regulate the development, differentiation and activation of thymocytes (T-cells) by association with transcriptional co-repressors, like HDAC7 and cabin, which inhibit Nur77 expression in resting thymocytes (Parra et al., 2007)(Herbert G Kasler and Verdin, 2007). It has been shown an important contribution of the MEF2-HDACs axis in vascular integrity and remodeling. During embryogenesis MEF2 proteins regulate and promote endothelial cell survival, directly stimulating the expression of matrix metalloproteinase 10 (Mmp10), that degrades the extracellular matrix. HDAC7, which is highly expressed in endothelial cells during development, represses this activation, thus maintaining vascular integrity (Chang et al., 2006).

MEF2-class IIa HDACs axis in cancer.

Histone deacetylases (HDACs), together with histone acetyltransferases (HATs), are enzymes responsible for chromatin remodeling and thereby play an important role in gene transcription. Simply via MEF2 interaction, they are able to regulate cell proliferation, differentiation, apoptosis and many other cellular processes. Dysregulated MEF2-trascriptional activities due to alteration of class IIa HDACs and MEF2 factors interaction are observed in certain cancers (Di Giorgio et al., 2014)(Clocchiatti et al., 2011).

In the last few years, numerous studies have demonstrated that alterations of the MEF2-class IIa HDACs axis appear to play a crucial role in cancer initiation and progression. For this reason there is an increasing interest in identifying and developing small molecules targeting the axis, in order to understand the functional relationships between the two players and to acquire knowledge to design, test and develop specific drugs for the treatment of cancer.

In acute myelogenous leukemia, high expression levels of MEF2C are correlated with the aggressive nature of this tumor (Schwieger et al., 2009). Activation of MEF2C has an oncogenic role also in human acute lymphoblastic leukemia (ALL)(Homminga et al., 2011). In hepatocellular carcinoma MEF2D is overexpressed and high expression levels of this transcription factor are associated with a poor prognosis (L. Ma et al., 2014). Recent results have discovered alterations in MEF2 levels and transcription in breast tumors (Schuetz et al., 2006) and the repressive activity of class IIa HDACs on MEF2 transcriptional activity has been related to poor prognosis of a subset of these tumors. In particular in ER+ tumors, repression of putative MEF2-target genes correlates with aggressiveness and high class IIa HDACs expression is associated with reduced patients survival (Clocchiatti et al., 2013). By contrast, in recurrent ER- mammary cancers, expression of MEF2s correlates with NOTCH1 (Pallavi et al., 2012). Although some reports point to a contribution of MEF2-dependent transcription in the mammary gland neoplastic pathogenesis, data on the role of the MEF2-HDAC axis during normal gland development/homeostasis are lacking and only few information are available on the role accomplished by the axis in epithelial cells (Ishikawa et al., 2010).

Morphogenesis and oncogenesis in the mammary gland.

The mammary gland is an organ that presents a remarkable feature: its development begins during embryonic life but reaches the complete functional form only during adulthood. The study of morphogenetic processes not only contributes to answer key questions in developmental biology, but also contributes to our understanding of several cancer related features. In fact, several oncogenes significantly modify epithelial structures providing compensations and reverting morphogenetic signaling. For this reason the comprehension of how mammary epithelial units are formed, which signals are required and which targets they use to transmit these information are of valuable interest. To better understand the molecular and cellular mechanisms involved in developmental (formation and function) and pathological processes, it is necessary to take advantage from appropriate experimental research models aimed to reproduce the complexity of the mammary gland environment but that also permit simple manipulations and observations.

The mammary gland structure in development and cancer.

The mammary epithelium is a bilayered polarized structure composed of an inner layer of luminal epithelial cells, facing the lumen, immediately surrounded by an outer layer of myoepithelial cells (Mina J. Bissell et al., 2002). Given this organization the epithelial luminal cells do not directly contact the basement membrane and the stroma (Figure 4).

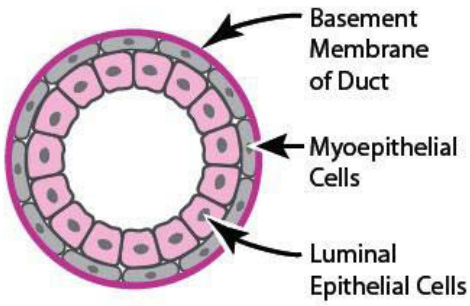

Figure 4: Schematic representation of the structure of mammary epithelium.

The mammary epithelial tree is embedded in a complex stroma, where several different cell types participate like adipose and immune cells, fibroblasts and endothelial cells (Hansen and Bissell, 2000)(Weigelt and Bissell, 2008). Two cellular compartments contribute to the development of the mammary gland: the epithelial and the stromal, both arising from different origin during embryonic life, the ectoderm and the mesoderm respectively. In the mouse ectodermal placodes form around embryonic day 10 and organize linearly, giving rise to the so called milk line (Robinson, 2007). The placodes evolve in buds, which continue to grow with the stimulation of the underlying mesenchyme. At birth, cell proliferation and branching activities govern the generation of a small ductal tree. This rudimental structure remains silent up to puberty when, under the influence of sexual hormones, epithelial cells manifest a significant ductal growth and branching in the stroma (Smalley and Ashworth, 2003). The adult mammary gland is now composed of an extensive network of ducts that branches out in smaller ductules and terminates in lobules. In the human gland the lobules end forming the terminal ductal lobular unit (TDLU)(Visvader, 2009). It is only with pregnancy that, under the influence of additional hormonal stimulation, the mammary tree undergoes an extensive proliferation burst followed by a terminal differentiation that results in milk secretion (L Hennighausen and Robinson, 2001)(Figure 5).

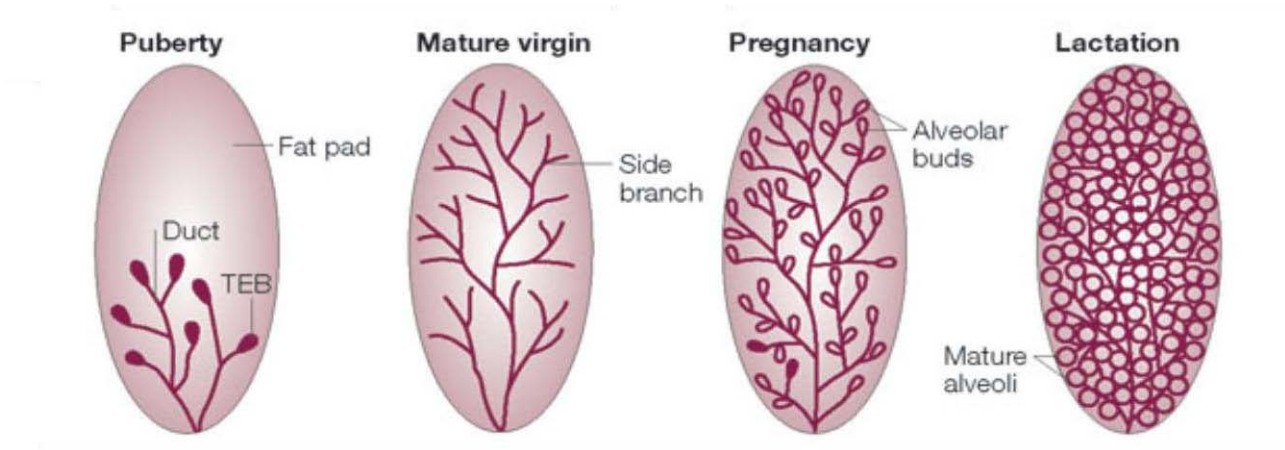

Figure 5: Evolution of the mammary gland.

Schematic representation of different stages of the mammary gland development from puberty to pregnancy and lactation (adapted from Lothar Hennighausen and Robinson, 2005).

The analysis of the structure of the mammary gland is of relevance also for pathological processes. In fact, to establish a correct diagnosis and eventual prognosis of breast carcinoma, pathologists rely on two different parameters: the degree of architectural disorder and the variability in size and shape of cells and nuclei. This classification, that differs from the canonical TNM (tumor dimension and presence of lymph node and distant metastasis), has proven useful in predicting the mammary and prostate cancer aggressiveness and is generally called grading (American Joint Committee on Cancer. *AJCC Cancer Staging Manual*. 7th ed. New York, NY: Springer; 2010). In particular this system is based on the identification of:

- Architectural maintenance, which describes how much the neoplasm preserves the original ductal/lobular structure. The loss of basement membrane integrity and presence of cancer cells in the stroma identifies invasive carcinoma. Conversely, premalignant lesions, confined within an integral basement membrane, are classified as Ductal Carcinoma In Situ (DCIS). However these structures may manifest different degree of luminal filling and the presence of a necrotic centre.
- Nuclear appearance, which evaluates the degree of alterations of the nuclear shape and size in histological sections.
- Proliferation index and counts the number of actively dividing cells, which generally is dependent on the Ki67 staining.

Defining the appropriate research model.

Over the years, biological research has contributed significantly to the understanding and answering important questions through the use of in vitro cell culture in a monolayer and with animal models. These experimental approaches have been particularly useful for mammary gland development and breast cancer. Both systems have some limitations and in vivo studies can pose ethical constrains.

Conventional cell culture has been useful for the identification of dysregulated pathways, given the wide number of cancer cell lines established, their simple manipulation and propagation. Additional advantages are the relative low costs and a quite high level of reproducibility. Moreover, cancer cell lines frequently display alterations commonly found in human tissue neoplastic specimens and recapitulate the great heterogeneity found in primary neoplasms (Neve et al., 2006). However common cell lines are generally established from metastasis and may not reflect the properties of primary tumors, as evidenced for ER+ breast tumors. Moreover, conventional in vitro culture models create an environment for the cells that markedly differs from the microenvironment that is present in tissues in vivo (Gogola et al., 2007), loosing many characteristics and cues that could have important influences in tissue morphogenesis and function (Mina J. Bissell et al., 2002). In vivo cells are organized in three-dimensional structures, where they are dependent on the ECM and the neighboring cells. Plastic has long been recognized as a stiffer substratum compared to the physiological matrix found in mammary gland.

The use of mouse models to study mammary gland development and cancer has given invaluable results. Generation of genetically modified animals permitted the identification of several transcription factors required for embryonic development like Lef1 and Tbx3, during puberty like the ER or for mammary terminal differentiation as STAT5a (Reichenstein et al., 2011). Moreover, they also significantly contributed to understanding the effect of commonly found alteration as TP53, HER2 or MYC (Jackson and Lozano, 2013)(Hutchinson and Muller, 2000), providing models that frequently recapitulate human histology in the context of preserved physiological architecture and cell-cell communication. Unfortunately, they are also associated with long time required for experimental observations, relatively reduced possibilities of samples manipulation and sometimes they do not permit basic molecular and biological observations, as for example, lumen translocation or precise metabolic measurements of oncogene expressing cells.

The three-dimensional cultures bridge the gap between a very simple and tractable model and a very sophisticated and elegant one. 3D cultures closely mimic the biological microenvironment and physiological cell-cell and cell-extracellular matrix interactions, reproducing and maintaining critical aspects of tissue architecture (growth, organization and differentiation), making these models attractive for studies on tissue morphogenesis and cancer. Three-dimensional cultures have contributed significantly to the understanding of the complexity of cues that play a pivotal role in the organ morphogenesis. This achievement has been possible through the use of three-dimensional substrates for studying cell-cell and cell-extracellular matrix interactions. A common method utilized for this type of research is the cultivation of the cells in a reconstituted basement membrane matrix (rBM) derived from a special type of mouse tumor, the Engelbreth Holm-Swann (EHS) murine sarcoma, commonly referred to as Matrigel (J. Debnath et al., 2003). This proteinous gel is mainly rich in laminin and contains also other extracellular matrix components such as collagen, fibronectin, nidogen and proteoglycans (Kleinman et al., 1986), thus partially recreating a similar environment found for example in human mammary gland.

Besides to these "monotypic" 3D culture models, other systems better mimicking *in vivo* conditions have been described and established over the years. For example epithelial cells can be co-cultured with other mammary gland cell types, enabling the investigation of cells-extracellular matrix interaction effects *in vitro*, or transplanted into an *ex vivo* system, cleared fat pad (stroma tissue), or can be grown as whole organ culture *in vitro* (Schmeichel and Bissell, 2003).

3D morphogenic model of mammary gland.

Mammary morphogenesis is characterized by the presence of several different instructive signals, which provide the correct stimulation to generate the proper glandular architecture. These structures transit from a disorganized state to an ordered epithelial organization modulating polarity, proliferation, and luminal cells clearance (J. Debnath and Brugge, 2005), which resemble events found *in vivo*. Specifically, the immortalized non transformed human mammary epithelial cell line, MCF-10A, is an example of a cell line capable of forming acinar-like spheroids/structures, which are similar to those found in the mammary gland, when it is cultured on a reconstituted extracellular matrix, (J. Debnath et al., 2002).

Initially, each single cell proliferates to generate a filled spheroid. During the first period epithelial cells are characterized by a rotational motion, with a complete revolution every four

hours. The movement is independent from cell proliferation, as it is still noticeable after treatment with mitomicin C and stops at day eight. Interestingly this motion is dependent on microtubules, as testified by nocodazole treatment, and by polarity proteins, like Scribble and PAR3, whose knock-down completely blocks this feature. Moreover the rotational movement seems to favor Golgi reorganization and apical side definition, events required for a proper cell polarization. At this point the structures present an outer layer of cells contacting the ECM, that manifest a correct apical-basal polarity, and an inner core of cells, lacking basement membrane contacts, that are subjected to a series of stress events and compensations. These eventually enter an apoptotic and a non-apoptotic cell death processes, or both (J. Debnath et al., 2002)(Mills et al., 2004). Curiously forced expression of anti-apoptotic proteins in MCF-10A cells (such as Bcl-2 or Bcl-xL) does not prevent lumen formation, but only delays it appearance (J. Debnath et al., 2002). These observations suggest that additional events take place to ensure the correct acinar morphogenesis. Moreover cells not in direct contact with the matrix perceive an increase metabolic stress, related to a depletion in glucose uptake. These matrix orphan cells manifest increase in ROS production and stimulate autophagy which, interestingly, is stimulated by the up-regulation of TRAIL (Mills et al., 2004). ROS inhibition with scavengers like Trolox or N-acety-L-lcysteine (NAC) confers a protection from cell death in Bcl-2 overexpressing cells, indicating that metabolic impairment may plays a role in luminal cell survival (Schafer et al., 2009). Autophagy seems to be a primary response to cell detachment and provides an initial strategy for survival of these matrix deprived cells. Accordingly inhibition of the autophagic machinery or depletion of central ATG genes fosters luminal cell death in the acinar lumen (Fung et al., 2008).

An interesting link between lumen formation and matrix detachment involves integrin signaling. Integrins play a key role at different steps of this morphogenetic process (Reginato et al., 2003)(Lee and Streuli, 2014). The absence of integrin-mediated pro-survival signals (anoikis) negatively affects the expression of the pro-survival RTK epidermal growth factor receptor (EGFR), which is internalized and degraded (Reginato et al., 2003). This creates an imbalance between apoptotic and non-apoptotic members as the expression and activity of pro-apoptotic factors like Bim and Bmf increase (Reginato et al., 2005)(Schmelzle et al., 2007), which results in cell death. Interestingly recent evidences support a role for integrin dependent lumen formation, which is independent from apoptosis but rather involves the formation of a correct polarization process (Lee and Streuli, 2014). In particular beta-1 integrin collaborates with microtubules to ensure a spatial reorganization of the Golgi apparatus and to define the basolateral surface, by removing tight junctions. This discovery made on primary cells

corroborates a previous finding where beta-1 integrin blockage using specific antibodies suppressed acinar polarization (Nedvetsky et al., 2012). The control in junctional proteins seems to be achieved through the control of endocytic trafficking, which is generally influenced by the microtubule network. It is curious to note that not only altered integrin signaling but also a modification of environmental stiffness, which differentially engages integrins, modulates lumen formation. In fact, in MCF-10A cells cultured onto a collagen matrix, which is stiffer compared to laminin, the apoptotic and non-apoptotic death responses were completely abrogated. This altered response generated acinar structures that remain without cavity (Butcher et al., 2009). In addition the abrogation of the function of other players, needed to establish epithelial polarity, significantly impacts on lumen formation. The deregulation of Scribble, a component of the protein machinery needed to define the basolateral surface, perturbs not only Golgi disposition but also the luminal clearance (Godde et al., 2014). Its loss is even capable of blocking myc induced apoptosis in MCF-10A cells cultured in 3D. Similarly loss of LKB1, a master kinase regulating PAR3 and apical side determination, blocks cell polarization and confers resistance to luminal cell death (Klefstrom et al., 2007). Although signals provided by the extracellular microenvironment are necessary to determine the complete morphogenesis, also the medium in which cells grow exerts an important contribution. Generally MCF-10A cells are routinely cultured with cholera toxin, an agent that stimulates cAMP production. Removal of this component from the medium results in filled structures (Nedvetsky et al., 2012). This effect is dependent on a decreased Bim expression and to a decreased pERK signaling. ERK phosphorylation was previously identified as an important signal that modulate the response to anoikis (Reginato et al., 2003) and its down-regulation favors cell survival. Interestingly cAMP stimulation has an effect on α6-integrin, promoting its recruitment towards the ECM, an event linked to cell polarization.

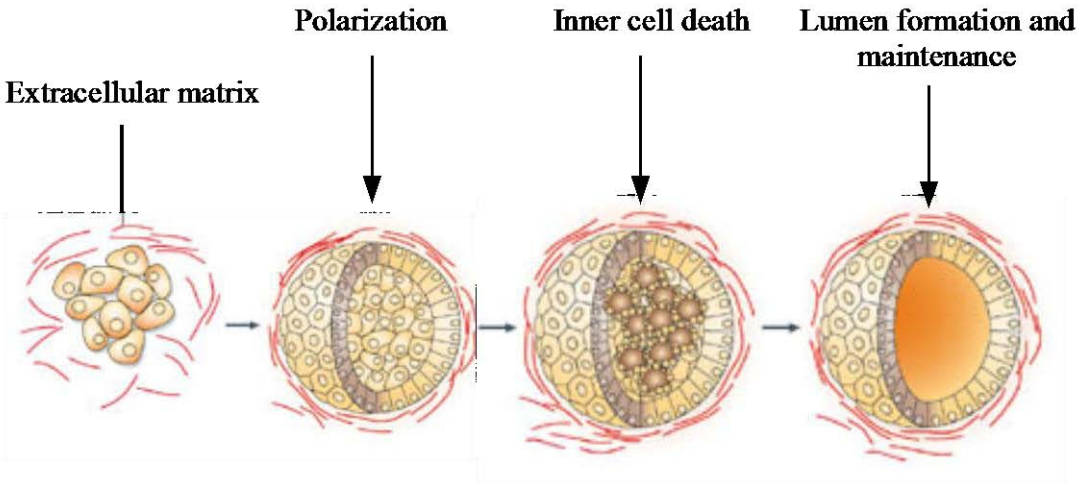

Figure 6: Formation of the MCF-10A mammary epithelial acinus in 3D culture.

Schematic representation of the processes that take place after seeding MCF-10A cells within ECM: at the beginning cells undergo a few cycles of proliferation, forming small spheroids. Next the outer layer of cells in direct contact with ECM develops an axis of apicobasal polarity, while the centrally localized cells lacking the necessary signals from the matrix die through both apoptotic and non-apoptotic processes, leading to lumen formation (adapted from J. Debnath and Brugge, 2005).

Modeling breast tumorigenesis in 3D culture.

The epithelial tissues are structures of polarized and specialized cells, strictly organized by cell-cell contacts. The disruption of normal tissue architecture is frequently associated to a dysregulated control of proliferation and altered cell survival (J. Debnath et al., 2003)(M J Bissell, 2007). The 3D cultures have been used extensively as experimental model systems to investigate and study the roles and effects of cancer genes and pathways associated with breast cancer progression (J. Debnath and Brugge, 2005).

Initially observations were focused on the understanding of the role of characterized mutations and activated pathways in breast tumors. One of the features of neoplastic cells is the unrestrained proliferation. In this light initial work was carried out to address the specific consequences of boosting cell cycle in mammary epithelial cells in 3D cultures. The rational of this approach finds justification by the fact that cyclin D is also frequently amplified in breast cancer (Gillett et al., 1994)(Bartkova et al., 1994). Overexpression of the pro-proliferative factor cyclin D1 (CCND1) increases proliferation in MCF-10A 3D structures, which results in larger acini, but does not lead to luminal filling due to a compensatory increase in luminal apoptosis (J. Debnath et al., 2002)(Shaw et al., 2004). Inhibition of apoptosis or an increase in cell proliferation alone are not sufficient to alter and prevent luminal clearance; instead the

combination of the two alterations does not lead to the formation of a hollow lumen (J. Debnath et al., 2002).

Similarly inactivation of critical cell cycle checkpoint proteins, such as the retinoblastoma protein Rb by the E7 viral product of human papilloma virus, leads to a similar phenotype with increased growth but hollow lumen and with MYC overexpression (J. Debnath et al., 2002). A frequent oncogenic event in breast cancer is represented by the loss or the mutation of the master regulator TP53. TP53 knock-down is associated with a reduced luminal cell clearance and related to an altered establishment of polarity. Similarly, overexpression of mutant versions of p53 promotes luminal cell filling related to a decrease in apoptotic proteins like Bax and Puma (Y. Zhang et al., 2011). Depletion of mutant p53 in breast cancer cell lines cultured onto laminin rich gels restores the correct round shape morphology with a hollow cavity (Freed-Pastor et al., 2012). Interestingly, the mutant p53 effect is related to its ability to associate with SREBP transcription factors and foster the mevalonate pathway, which is highly activated in human breast cancer samples harboring p53 mutations. Pharmacological inhibition of this pathway mimics, at least partially, the effect of mutant p53 knock-down and restores a normal architecture.

An additional frequent lesion, associated with poor prognosis is the amplification of the HER2 oncogene, a tyrosine kinase receptor member of the EGF pathway (Sørlie et al., 2001). HER2 overexpression in normal mammary epithelial cells cultivated in 3D significantly compromises the acinar morphogenetic program (Muthuswamy et al., 2001). In MCF-10A cells that express an inducible version of ErbB2/HER2, its activation even in growth-arrested, polarized acini resulted in a re-initiation of proliferation and formation of multi-acinar structures with luminal filling (Muthuswamy et al., 2001). Interestingly HER2 is capable of fostering cell growth even when just a single cell is overexpressing in the context of a well formed, resting acinar structure. Differentially, sporadic up-regulation of MYC, CCND1, E7 or AKT are incapable of producing growth, indicating that the environmental and structural architecture are posing a barrier to luminal outgrowth at early stage (Leung and Brugge, 2012). To achieve this effect HER2 not only boosts cell proliferation but also favors luminal cell translocation dependent on the stimulation of the MAPK activity. Furthermore to reach a filled lumen, HER2 disrupts cell polarity through the direct binding of Par6. Disruption of HER2-Par6 interaction does not impair cell proliferation but restrains its effect on cell survival indicating the need of coupling apoptotic resistance to cell proliferation to generate filled acinar structures (Aranda et al., 2006). Of note, MCF-10A cells overexpressing HER2 resemble ductal carcinoma in situ (DCIS) lesions but are not associated with invasion. In human samples HER2 and 14-3-3z are often co-expressed in

invasive breast cancer. 14-3-3z in combination with HER2 influences epithelial features by favoring epithelial mesenchymal transition (EMT) and therefore migration. This effect is dependent at least in part by the activation of the transforming growth factor beta (TGFβ) signaling pathway, caused by an increased expression of TGFβ1 receptor. It should be noted that 14-3-3z overexpression does not stimulate cell proliferation but affects luminal cell clearance by affecting the levels of p53. In particular its down-regulation seems to be dependent on the increased expression of MDM2, stimulated by the enhanced activity of pAKT.

In epithelial cancer increased activity of the phosphoinositide (PI) 3-kinase pathway is a frequent event and in breast cancer samples PI3K is frequently mutated. Moreover overexpression of receptor tyrosine kinases (RTK) like HER2 impinges on the signaling, by enhancing its activity. Overexpression of a mutant form of PI3K H1047R in MCF-10A cells leads to the formation of bigger multi-acinar structures (Chakrabarty et al., 2010). Curiously activation of PI3K does not suppress the autophagic program in cells cultured in 3D. The knock-down of basic autophagy-related genes (ATG), like Atg7 and Atg12, in this context is followed by a concomitant increase in cell death, further indicating that autophagy in this model is primarily a pro-survival response. However, the concomitant increase in cell death is paralleled by a massive burst in proliferation as a result of an increase in ERK-MAPK activation. AKT activity in 3D cultures, using an inducible model, demonstrated this downstream arm is able to increase acinar size and can delay apoptotic clearance but does not confer luminal filling phenotype.

Abrogation of PI3K signaling in cancer cells is generally associated with a homeostatic/resistance response, which involves the up-regulation of RTKs expression to balance the inhibition of the pathway (Chandarlapaty et al., 2011). Pharmacological inhibition of PI3K in cancer cell lines cultured in 3D leads to a dichotomous response where matrix deprived cells undergo cell death while matrix attached survive (Muranen et al., 2012). Abrogation of this signaling pathway is associated with feedback loop responses that up-regulate EGFR and Bcl2. Particularly interesting is Bcl2 because its synthesis appears in a condition in which normal CAP dependent translation is inhibited (PI3K inhibition). Restraining from this block is possible because of the presence of an IRES motif in the 5' UTR of the Bcl2 transcript. Concomitant inhibition of PI3K and Bcl2 elicits massive cell death and disintegration of acinar structures made by cancer cell lines but not in the case of untransformed cells like MCF-10A. These findings not only point to this drug combination as efficient anti-cancer treatment to eradicate neoplastic cells but also underline how the use of 3D cultures can be extremely useful to better understand compound sensitivity and to discover mechanisms of resistance to targeted therapeutics, not achievable with conventional standard cultures.

MATERIALS AND METHODS

Cell cultures and reagents.

Human normal immortalized epithelial breast cells (MCF-10A) and MCF-10A cells expressing HER2 were maintained in Ham's F12/DMEM 1:1 medium (Sigma-Aldrich) supplemented with 5% horse serum (Gibco), penicillin (100U/ml), streptomycin (100µg/ml), L-glutamine (2mM) (Lonza), insulin (0,01mg/ml), hydrocortisone (500ng/ml), cholera toxin (100ng/ml)(Sigma-Aldrich), and epithelial growth factor (20ng/ml)(Peprotech). HEK-293T cells were grown in Dulbecco's modified Eagle's medium (DMEM) supplemented with 10% fetal bovine serum (FBS), L-glutamine (2mM), penicillin (100U/ml), and streptomycin (100µg/ml)(Lonza). Cells expressing inducibile forms of MEF2 and HDAC7 were grown in complete F12/DMEM medium without phenol red (Sigma-Aldrich) and with 5% charcoal stripped horse serum. The proteasome inhibitor bortezomib (LC Laboratories) was used at 250nM for 8h. The lysosomal/autophagy inhibitor cloroquine (Sigma-Aldrich) was used at 10µM for 8h. The CRM1 inhibitor, leptomycin-B (LC Laboratories), was used at 5ng/ml. 4-hydroxytamoxifen (4-OHT)(Sigma-Aldrich) was used at 1µM. The inhibitor of HER2 lapatinib (LC Laboratories) was used at 1µM for 2h.

Three-dimensional morphogenetic assay.

3D morphogenetic assays were conducted as previously described (J. Debnath et al., 2003). Briefly, to obtain mammospheres, cells ($3x10^4$) were plated in a thick layer of ~1-2mm of laminin-rich extra-cellular matrix (Cultrex-Trevigen). Cultrex was overlaid with cells grown in medium containing 5ng/ml EGF along with 2%v/v cultrex. Cells were maintained at 37ºC and 5%CO2 and the culture medium was changed every 4 days. Images of mammospheres were collected by using a Leica AF 6000LX microscope. Acinar area measurements were determined using Volocity 3D image analysis software.

Plasmid construction, transfection, retroviral and lentiviral infection, and silencing.

pWZL-Hygro-MEF2C-VP16-ER was previously described (Di Giorgio et al., 2013). The ligand binding domain of ER was PCR amplified from pCDNA MEF2-VP16-ER (Flavell et al., 2006) and cloned in pWZL-Hygro. To generate pWZL-Hygro-HDAC7/SA-ER, an EcoRI fragment of HDAC7/SA point mutant (Di Giorgio et al., 2013) was cloned into pWZL-Hygro-ER. MCF-10A cells expressing MEF2-VP16-ER or HDAC7/SA-ER transgenes were generated by retroviral

infection as described previously (Cernotta et al., 2011). 293T packaging cells were transfected 24h after plating by calcium-phosphate precipitation. After 48-72h the virus-containing medium was filtered and added to target cells. Recombinant lentiviruses (Sigma-Aldrich) were produced by tranfection of 293T cells. Briefly, subconfluent 293T packaging cells were co-transfected with 20μg of lentiviral vector plasmids, 15μg of pCMV-ΔR8.91, and 5μg of VSVG envelope plasmid by calcium-phosphate precipitation. After 24h medium was changed, and recombinant lentiviruses vectors were harvested 24-36h later.

Immunofluorescence, antibody production and immunoblotting.

For immunofluorescence, cells were fixed in 3% paraformaldehyde and permeabilized with 1% Triton-X100 in PBS for 15min. Next, coverslips were incubated with primary antibodies anti-HDAC4 (Paroni et al., 2004), anti-HDAC7 (Santa Cruz Biotechnology), anti-MEF2D (BD Transduction Laboratories), and anti-GM130 (BD Transduction Laboratories). Then, they were incubated with 488-Alexa or 546-Alexa Fluor conjugated secondary antibodies (Life Technologies). Finally, coverslips were incubated for 15min with 5μM TOPRO-3 (Life Technologies) to label nuclei. Cells were imaged with a Leica confocal scanner SP equipped with a 488 λ Ar laser and a 543 to 633λ HeNe laser. Representative confocal images were shown as equatorial cross sections through the middle of acini.

For antibody production, rabbits were immunized with recombinant histidine-tagged HDAC5 fragment 1132-2040 purified from Escherichia coli. For anti-HDAC5 antibody purification from antiserum, HDAC5 was fused to glutathione S-transferase (GST) and cross-linked to glutathione-Sepharose as described previously (Paroni et al., 2001).

Cell lysates after SDS-PAGE and immunoblotting were incubated with the following primary antibodies anti: HDAC4 (Paroni et al., 2004), HDAC7, MEF2A (Santa Cruz Biotechnology), MEF2D (BD Transduction Laboratories), AKT (Cell Signaling Technology), p53 (Santa Cruz Biotechnology), p62 (BD Transduction Laboratories), LC3 (Demarchi et al., 2006), VP16 (Santa Cruz Biotechnology), p120 (BD Transduction Laboratories), ERK, P-ERK (Cell Signaling Technology). Secondary antibodies were obtained from Sigma-Aldrich, and blots were developed with Super West Dura (Pierce). For antibody stripping, blots were incubated for 30min at 60ºC in stripping solution containing 100mM β-mercaptoethanol. DNA staining was performed as described previously (Cernotta et al., 2011). For S-phase analysis, cells were grown for 3h with 100uM bromodeoxyuridine (BrdU). After fixation, coverslips were treated with 1N HCl (10min, in ice), followed by 20min with 2N HCl at room temperature. Mouse anti-BrdU

(Sigma-Aldrich) was used as primary antibody. Nuclei were stained with Hoechst 33258 (Sigma-Aldrich).

RNA extraction and quantitative qRT-PCR.

Cells were lysed using RiboEx (GeneAll Biotechnology Co., LTD). 1 μg of total RNA was retro-transcribed by using 100 units of M-MLV reverse transcriptase (Life Technologies). qRT-PCRs were performed using the Bio-Rad CFX96 apparatus and SYBR Green technology (Resnova). Data were analyzed with the ΔΔCt method, using GAPDH (glyceraldehydes 3-phosphate dehydrogenase) and HPRT (hypoxanthine phosphor-ribosyltransferase) as normalizer genes. All reactions were done in triplicate. To evaluate the mRNA copies/μg of retro-transcribed RNA for each class IIa HDACs, standard curves of qRT-PCR amplification were obtained using defined concentrations of the relative cDNAs.

Chromatin immunoprecipitation.

For immunoprecipitations, DNA-protein complexes were cross-linked with 1% formaldehyde (Sigma-Aldrich) in phosphate-buffered saline (PBS) for 15min at room temperature. After quenching and two washes in PBS, cells were collected and then lysed for 10min with lysis buffer (5mM PIPES, 85mM KCl, 0.5% NP-40) containing protease inhibitor cocktail (Sigma-Aldrich). The pellets were resuspended in RIPA-100 and sonicated using Bioruptor UCD-200 (Diagenode) with pulses of 30s for 15min, resulting in an average size of ~500 bp for genomic DNA fragments. Samples were pre-cleared and immunoprecipitated overnight with 1μg of anti-HDAC7, followed by incubation with protein A beads (GE Healthcare Bio-Sciences) blocked with BSA and salmon sperm DNA (1μg/μl) at 4ºC for 2h. Beads and inputs were treated with proteinase K overnight at 68ºC to degrade proteins and reverse cross-linking. Genomic DNA finally purified with Qiagen QIAquick PCR purification kit and eluted in 100 μl of water.
Graphic representation of the CDKN1A locus and its chromatin organization in human mammary epithelial cells was obtained from ENCODE (http://genome.ucsc.edu/ENCODE/). Analysis of putative binding site for MEF2D was carried out with JASPAR (jaspar.genereg.net/).

Cell cycle analysis.

Before measuring, cells were detached by trypsin and fixed in 70% ethanol. After some washing cells were resuspended in PBS supplemented with 1% Triton-X100 and RNAse-A 100 ug/ml and incubated 30min at 37°C. DNA staining was performed incubating cells with propidium iodide at 50ug/ml for 45min at RT. Cells were then passed through a flow cytometer equipped with the Cell Quest software by using a 488-nm argon ion laser (FACScan, BD Biosciences). A minimum of 10.000 events per sample was analyzed. Data analysis was performed by FCS Express 4 Plus Research Edition software.

Gene set enrichment analysis (GSEA).

Analyses were performed using the GSEA software (http://www.broadinstitute.org/gsea/index.jsp). The list of MEF2-target genes was obtained from the Molecular Signature Database (http://www.broadinstitute.org/gsea/msigdb/index.jsp). Dataset for MCF-10A cells was obtained from GEO (http://www.ncbi.nlm.nih.gov/geo/) GSE26148 (Simpson et al., 2011). Human normal and breast tumor samples were taken from Curtis and colleagues (Curtis et al., 2012) with accession number EGAS00000000083 deposited at the European Genome-Phenome Archive (EGA, http://www.ebi.ac.uk/ega/).

Statistics.

Results were expressed as means ± standard deviations of at least three independent experiments, except for CHIP experiments where standard error was used. Statistical analysis was performed using a Student's t test with the level of significance set at $P < 0.05$. Data from 3D acinar area measurement were determined using Volocity 3D image analysis software and analyzed using Non-parametric Mann-Whitney test (Prism GraphPad Software). Data were from at least three independent experiments. *P<0.05; **P<0.01; ***P<0.005.

RESULTS

Regulation of the MEF2-HDAC axis during acini morphogenesis.

As a first step to investigate and study the role of the MEF2-HDAC axis in mammary epithelial morphogenesis, we compared expressed sequence tag (EST) profiles between skeletal muscle and breast tissue, for class IIa HDACs and MEF2A, C, and D (Fig. 1A). As expected, in skeletal muscle MEF2C, HDAC4, and HDAC5 are the most expressed members of each family. By contrast in breast tissue MEF2A, MEF2D, and HDAC7 are the uppermost expressed isoforms. Furthermore, Gene Set Enrichment Analysis (GSEA), using a signature of putative MEF2-target genes, suggests that MEF2-dependent transcription is positively modulated during MCF-10A acinar morphogenesis (Fig. 1B). Hence, we selected MCF-10A cells as model to investigate the role of the MEF2-HDAC axis during mammary epithelial morphogenesis. When plated on a laminin-rich extracellular matrix (3D culture), MCF-10A cells transit from an initial proliferative, disorganized state (Fig. 1C, day 4), evidenced by the presence of several mitotic figures per acinus (Fig. 1D) and by the random orientation of the Golgi, to a quiescent polarized condition, marked by Golgi re-orientation, formation of a hollow lumen, and the absence of mitotic figures (Fig. 1C, day 16, and 1D).

qRT-PCR experiments showed that, although with different magnitudes, the mRNA levels of certain MEF2-target genes, KLF2, KLF4, NR4A1, END1, and RHOB, were augmented when the acinar morphogenesis was completed, at day 16 (Fig. 2A). Together with MEF2-target genes, MEF2D mRNA levels rise, as similarly described during muscle differentiation (Nebbioso et al., 2009)(Sebastian et al., 2013)(Fig. 2B). The expression of HDAC5 and HDAC9 also increase during acinar developmental process, while HDAC4 and HDAC7 remain constant (Fig. 2B). The up-regulation of CDKN1A was selected as marker of growth arrest (Besson et al., 2008), whereas BMF and BIM sign the appearance of apoptosis (Mailleux et al., 2008).

To clarify the apparent paradox of the MEF2-dependent transcriptional stimulation coupled to the up-regulation of HDAC5 and HDAC9 mRNAs, we carried out an absolute quantification of class IIa HDACs expression (Fig. 2C). This analysis suggests that in MCF-10A cells HDAC7 and HDAC4 mRNA levels are largely dominant over the other class IIa deacetylases and therefore even a six fold increase in HDAC5 mRNA could be irrelevant in the context of the MEF2-dependent transcription. We also performed immunoblot analysis (Fig. 2D), which confirmed the up-regulation of MEF2D and HDAC5 during acinar morphogenesis and evidenced a dramatic down-regulation of HDAC7 levels. This drastic reduction of HDAC7 could explain the up-regulation of MEF2-dependent transcription. Since HDAC7 down-regulation was uncoupled to a decrease in mRNA levels, to gain insight on the mechanism entangled in such

task, MCF-10A cells grown for 4 or 16 days, under 3D conditions, were treated with bortezomib, to block proteasome-mediated degradation, and with chloroquine, to block lysosomal/autophagy degradation, or with a combination of both drugs. Although class IIa proteins can be target of the proteasome (Potthoff et al., 2007)(Cernotta et al., 2011), HDAC7 down-regulation was unaffected by both drugs (Fig. 2E), thus indicating that other proteolytic events or different mechanisms control HDAC7 protein levels during acini formation.

Class IIa HDACs nucleo-cytoplasmic shuttling is under the influence of multiple signaling pathways (Xiang-Jiao Yang and Seto, 2008)(Clocchiatti et al., 2011), mainly described during tissue differentiation, such as skeletal myogenesis (T A McKinsey et al., 2000). We therefore investigated the subcellular localization of MEF2D, HDAC4 (Fig. 2F), and HDAC7 (Fig. 2G) in cells grown for 4 or 16 days under 3D conditions. MEF2D localizes in the nucleus and both deacetylases show either a nuclear and cytoplasmic distribution. Treatment of MCF-10A cells with leptomycin B promoted the nuclear accumulation of HDAC7, thus indicating that the deacetylase undergoes nucleo-cytoplasmic shuttling. Similar results were observed at 16 days and for HDAC4 (data not shown).

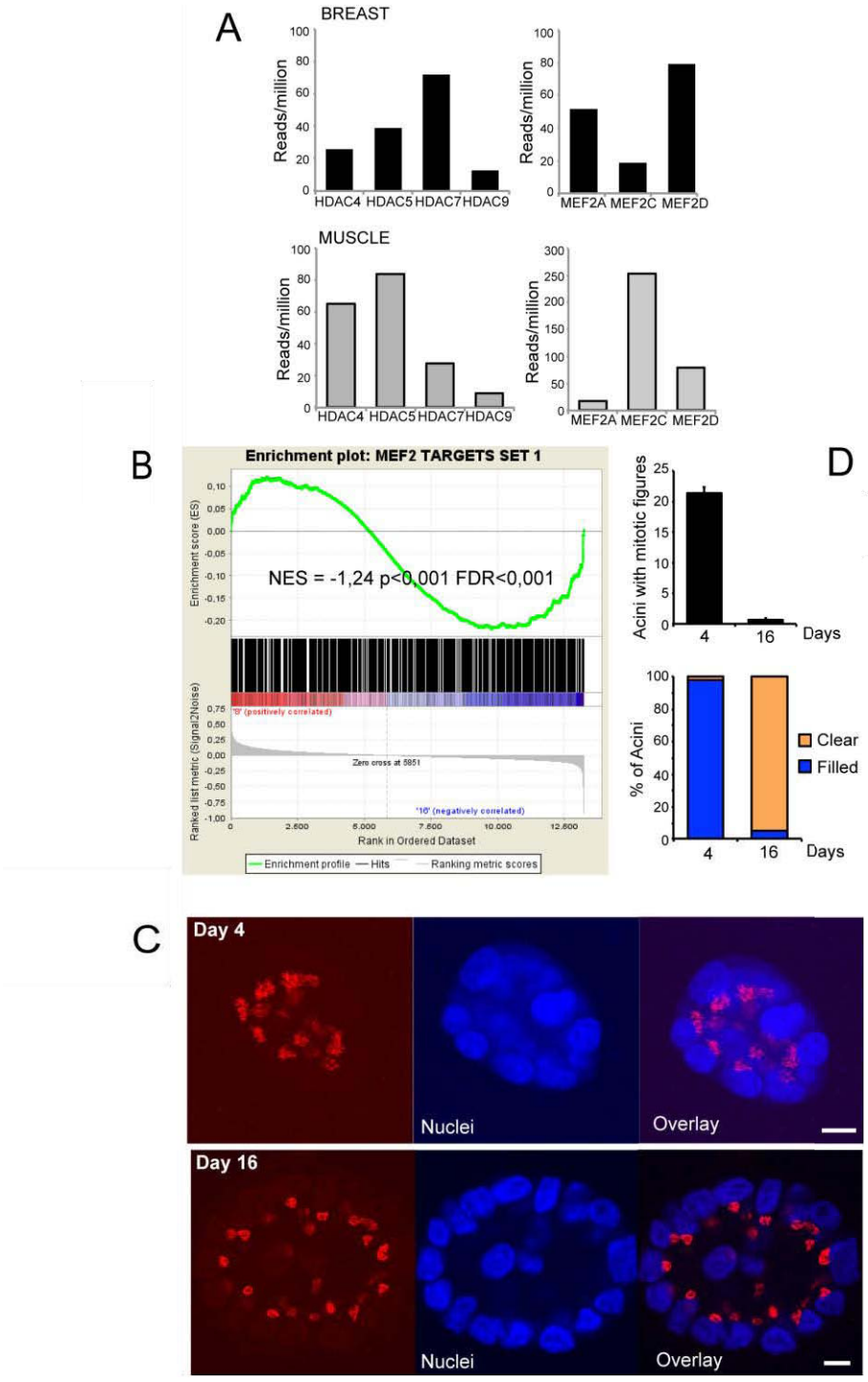

Figure 1: The MEF2-HDAC axis in mammary gland.

A: Plots illustrating the frequency of EST tags for class IIa HDACs and MEF2s family members in skeletal muscle and breast tissue.

B: GSEA analysis of a list of 900 putative MEF2-target genes in expression data from MCF-10A cells cultured in 3D comparing day 8 with 16.

C: Confocal images comparing the distribution of the Golgi apparatus, using GM130 marker (red), and nuclei (blue), using TOPRO-3 staining, between MCF-10A cells grown in 3D culture for 4 and 16 days. Images are shown in pseudocolors. Scale bars, 50 µm.

D: Quantification of mitotic figures and luminal filling in acini generated by MCF-10A cells grown in 3D for 4 or 16 days.

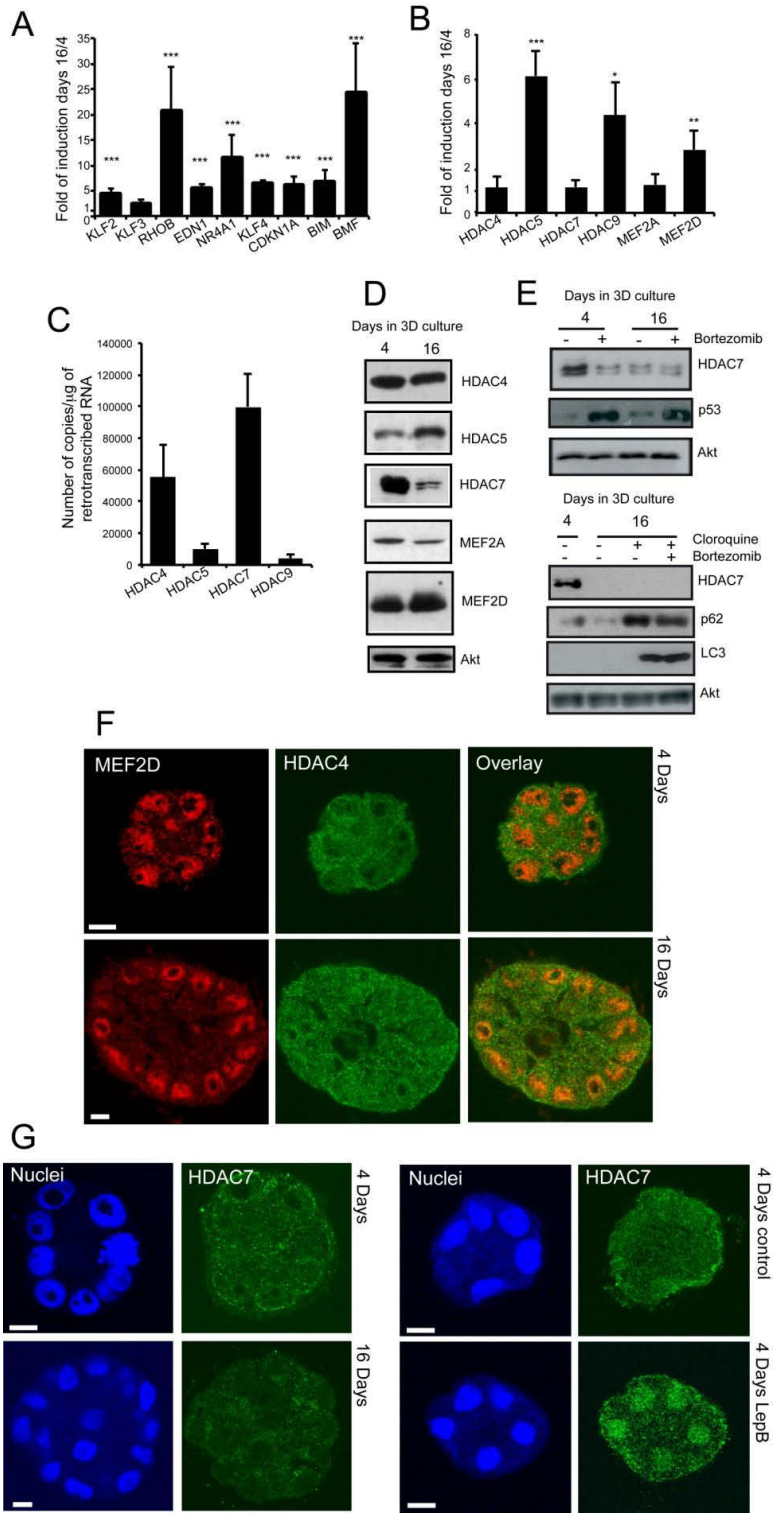

Figure 2: Analysis of MEF2-dependent transcription and class IIa HDACs expression in MCF-10A breast epithelial cells during acinar morphogenesis.

A: qRT-PCR analysis was performed to quantify mRNA levels of MEF2-target genes, of the cell-cycle inhibitor CDKN1A and of the pro-apoptotic genes BIM and BMF in MCF-10A cells grown in 3D culture for 4 and 16 days. Fold induction was calculated as the ratio relative to 4 days of culture.

B: qRT-PCR was performed to quantify mRNA levels of class IIa members (HDAC4, HDAC5, HDAC7, and HDAC9) and MEF2 members (MEF2A, MEF2C, and MEF2D) in MCF-10A cells grown in 3D for 4 and 16 days. Fold induction was calculated as the ratio relative to 4 days of culture.

C: qRT-PCR analysis was performed to quantify mRNA levels of all class IIa members (HDAC4, HDAC5, HDAC7, and HDAC9) in MCF-10A cells. The expression was calculated as number of copies relative to µg of retrotranscribed RNA.
D: Immunoblot analysis of MEF2 family members and class IIa HDACs in MCF-10A cells grown in 3D for 4 and 16 days. Akt was used as loading control.
E: Immunoblot analysis of HDAC7 levels in 3D culture of MCF-10A cells at 4 and 16 days treated or not with bortezomib or bortezomib in association with chloroquine for 8h. p53 was used as positive control for proteasome-mediated degradation inhibition. p62 and LC3 were used as positive controls of blocking lysosomal/autophagy degradation. Akt was used as loading control.
F: Confocal images illustrating the subcellular localization of MEF2D (red) and HDAC4 (green) in MCF-10A cells grown in 3D culture for 4 and 16 days. Images are shown in pseudocolors. Scale bars, 50 µm.
G: Confocal pictures exemplifying the subcellular localization of HDAC7 in MCF-10A cells cultured in 3D for 4 and 16 days and for 4 days treated or not with leptomycin-B for 1h. Nuclei (blue) were stained with TOPRO-3. Images are shown in pseudocolors. Scale bars, 50µm.

MEF2D down-regulation does not affect acinar morphogenesis but elicits different compensatory mechanisms.

To comprehend the role of MEF2 in mammary epithelial cells, we silenced MEF2D expression by shRNA lentiviral infection. We selected MEF2D because MEF2D is the highest expressed isoform in breast tissue (Fig. 1A) and its expression is up-regulated during morphogenesis (Fig. 2B and D). Despite an evident down-regulation of MEF2D at protein (Fig. 3A) and mRNA levels (Fig. 3B) in MCF-10A cells expressing two different shRNAs, we did not evidenced any negative alteration in the expression of the MEF2-target genes (Fig. 3B). Instead unexpectedly, END1 mRNA levels were augmented (Fig. 3B). In cells with down-regulated MEF2D acinar morphogenesis appeared normal, as proved by scoring luminal filling per strucure and Golgi orientation, with the GM130 marker (Fig. 3C). We also evaluated whether the absence of MEF2D could influence the initial proliferation phase by measuring the acinar size. Here again MEF2D seems to be dispensable (Fig. 3D). The absence of evident phenotypes in cells silenced for MEF2D could be the consequence of redundancy and/or of compensatory mechanisms as observed in other contexts (N. Liu et al., 2014). In fact, MCF-10A cells with down-regulated MEF2D revealed an increase in MEF2A protein levels in association with a down-regulation of HDAC4 and HDAC5 (Fig. 3A).

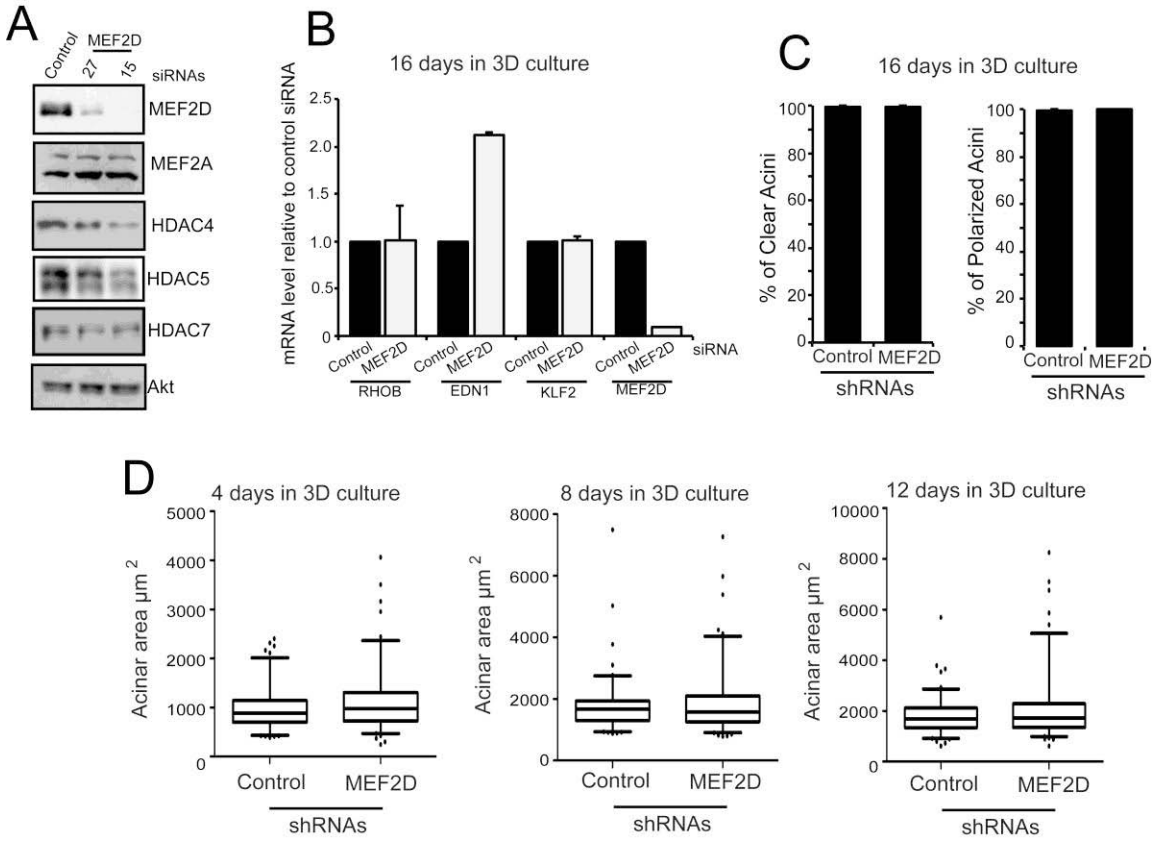

Figure 3: Effects of MEF2D down-regulation on acinar morphogenesis.

A: Immunoblot analysis of MEF2 family members and class IIa HDACs levels in MCF-10A cells expressing two different shRNAs against MEF2D or a control shRNA. Akt was used as loading control.

B: qRT-PCR was performed to evaluate mRNA levels of MEF2-target genes and of MEF2D in MCF-10A cells expressing the shRNA15 or the control shRNA and cultured in 3D for 16 days.

C: Quantification of luminal filling per structure and acini polarization, scoring Golgi orientation, in MCF-10A cells expressing the shRNA15 or the control shRNA and grown in 3D for 16 days.

D: Acinar area (μm^2) of individual acini, generated in 3D culture by MCF-10A cells expressing the shRNA15 or the control shRNA at 4, 8 and 12 days, plotted as a boxplot.

Unscheduled expression of MEF2 compromises cell proliferation and reduces acini size.

To understand the contribution of the MEF2-HDAC axis in the context of mammary epithelial cells, we decided to use an alternative strategy. We introduced in MCF-10A cells a conditionally active form of MEF2 fused to VP16 virus activation domain and to the ligand binding domain of the estrogen receptor (Flavell et al., 2006), as a control a DNA-binding defective mutant (ΔDBD) was used (Fig. 4A). In 2D culture, activation of MEF2-VP16 by 4-hydroxytamoxifen (4-OHT), but not the control construct, efficiently promoted MEF2-target genes transcription (Fig. 4B). Importantly, the magnitude of induction perfectly mirrors changes observed during acini morphogenesis in 3D culture (compare fig. 4B and 2A). Induction of MEF2 transcription

by 4-OHT in 2D cultured MCF-10A cells has a profound effect on proliferation (Fig. 4C). This anti-proliferative effect was observed also when cells were grown in 3D culture. Time course analysis indicated that stimulation of MEF2 activity within the first four days constrains acinar size (Fig. 4D). At day 4, in the presence of an unscheduled MEF2 transcriptional activity, acinar structures are smaller and populated by a reduced number of cells (Fig. 4E and F). To understand if MEF2 elicits a growth repressive effect during different phases of acini formation, we selectively stimulated its activity for four days starting from day 4, 8, or 12. Boosting MEF2 transcription from day 4 to 8 still interferes with the proliferation of MCF-10A cells, as evidenced by the reduced acini size (Fig. 4G), number of cells (Fig. 4H), and the dramatic decrease of mitotic activity (Fig. 4I). Noteworthy, activation of MEF2 during the next time intervals (8 or 12 days in culture) does not exert any effect on acinar diameter (Fig. 4J and K), cells number, or luminal cell death (data not shown), thus indicating that MEF2 perturbations are principally linked to the initial proliferative phase of the morphogenetic process. Overall these data suggest that, in order to proceed with a normal morphogenetic process in mammary epithelial cells, MEF2 transcriptional activity must be limited during the initial proliferative state.

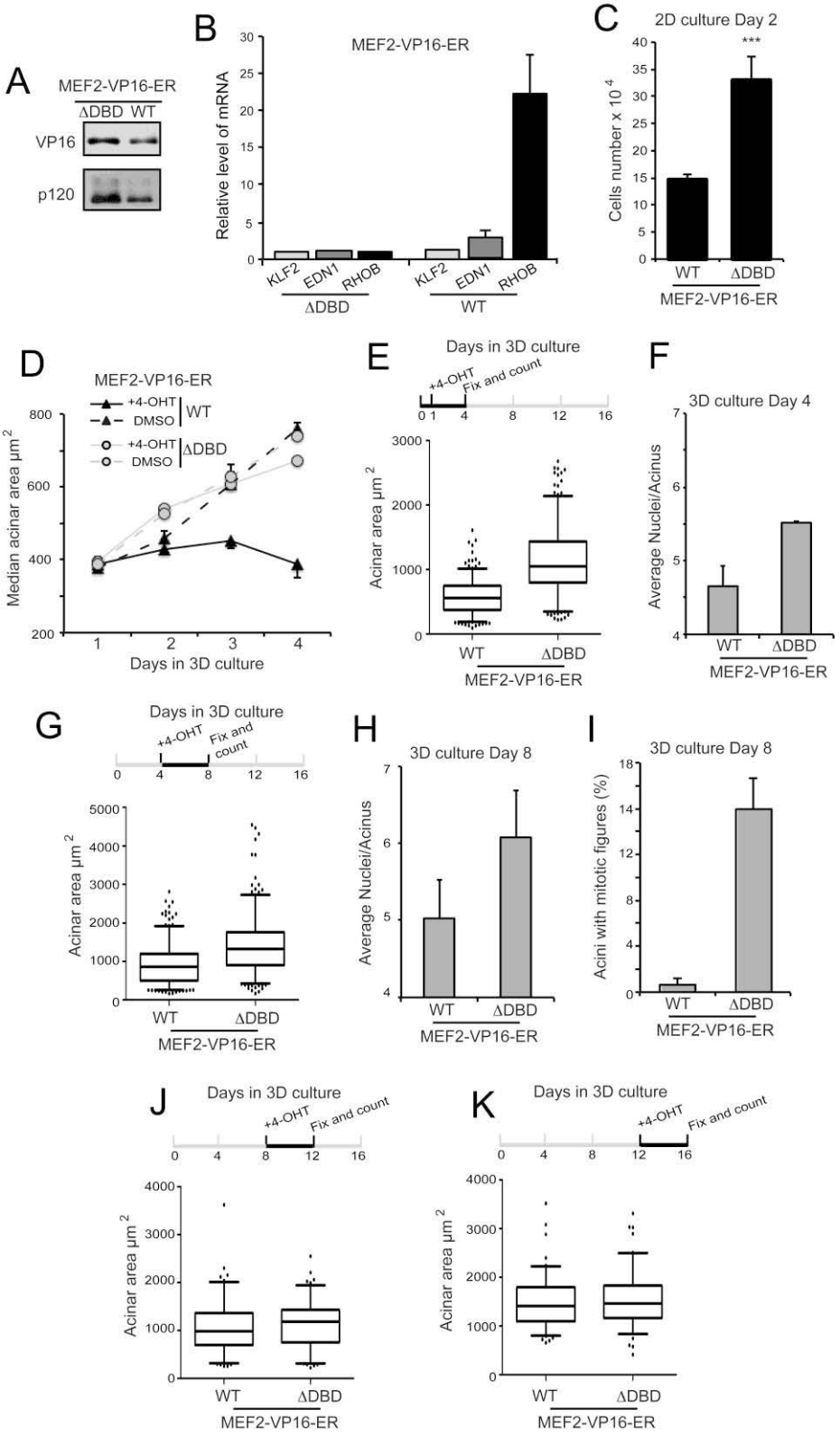

Figure 4: MEF2 transcriptional activity can compromise cell proliferation and acini size during the normal morphogenetic process in mammary epithelial cells.

A: Immunoblot analysis of MEF2-VP16-ER levels in MCF-10A cells expressing MEF2-VP16-ER chimera or its mutant defective in DNA binding MEF2-ΔDBD-VP16-ER. MEF2-VP16-ER-dependent transcription was induced by treating cells with 4-OHT for 24h. p120 was used as loading control.

B: mRNA levels of selected MEF2-target genes were measured by using qRT-PCR in MCF-10A cells expressing MEF2-VP16-ER or the mutant MEF2-ΔDBD-VP16-ER following 4-OHT treatment in 2D culture.
C: Quantitative analysis of cell proliferation of MCF-10A cells expressing the two MEF2 inducible forms. The day after seeding, 4-OHT was added to culture medium and cells number scored 24h later.
D: Time course analysis of acinar area (μm^2) for the indicated times, as generated by MCF-10A cells expressing the two MEF2 inducible forms. The day after seeding, 4-OHT was added to the culture medium.
E: Acinar size (μm^2) of MCF-10A cells, expressing the two MEF2 chimeras, in 3D culture for 4 days were analyzed. The day after seeding, 4-OHT was added to culture medium.
F: Number of nuclei per acinus as generated by the different transgenic MCF-10A cells after 4 days in 3D culture.
G: Acinar size (μm^2) of MCF-10A cells, expressing the two MEF2 chimeras, in 3D culture for 8 days were analyzed. The fourth day in culture, 4-OHT was added to culture medium.
H: Number of nuclei per acinus as generated by the different transgenic MCF-10A cells after 8 days in 3D culture.
I: Number of acini with mitotic figures, as generated by the different transgenic MCF-10A cells after 8 days in 3D culture.
J: Acinar size (μm^2) of MCF-10A cells, expressing the two MEF2 inducible forms, in 3D culture for 12 days were analyzed. 4-OHT was added to culture medium as indicated.
K: Acinar size (μm^2) of MCF-10A cells, expressing the two MEF2 inducible forms, in 3D culture for 16 days were analyzed. 4-OHT was added to culture medium as indicated.

Sustained HDAC7 activity promotes cell proliferation and affects acinar morphogenesis.

The demonstration of a role of MEF2-dependent transcription in limiting proliferation of mammary epithelial cells suggests that the down-regulation of HDAC7, observed during the morphogenetic process could be instrumental to drive the exit from the cell cycle. To verify this hypothesis we generated MCF-10A cells expressing a conditionally active form of HDAC7, fused to the ligand-binding domain of the estrogen receptor (Fig. 5A). This mutant, named HDAC7/SA-ER, presents the substitution of four serine residues with alanines, in the amino-terminal region. These serines once phosphorylated by various kinases become binding sites for 14-3-3 proteins and are required for the efficient nuclear export of the deacetylase (M. Martin et al., 2007)(Xiang-Jiao Yang and Seto, 2008). Hence, upon 4-OHT treatment, this chimera should promptly accumulate in the nucleus and repress MEF2-dependent transcription. Figure 5A shows that the fused protein is expressed at the expected size and, after 4-OHT addition to MCF-10A cells in 2D culture, it efficiently accumulates in the nucleus (Fig. 5B). Moreover, HDAC7/SA-ER effectively represses MEF2-dependent transcription, as evidenced by the decrease in RHOB mRNA levels after eight days in 3D culture (Fig. 5C). To determine the effect of an unscheduled HDAC7 repressive activity during morphogenesis, we observed acinar size at 4, 8, and 12 days in 3D culture after induction with 4-OHT. Acini generated by MCF-10A cells expressing HDAC7/SA-ER are bigger at all time points analyzed (Fig. 5D). This raise in size depends on an increase in the number of nuclei per acinus (Fig. 5E). The increased number of epithelial structures presenting the lumen partially filled (Fig. 5F and quantitative analysis in fig. 5G)

confirmed the pro-growth effect of HDAC7. However HDAC7/SA-ER acini were also characterized by higher picnotic and fragmented nuclei (Fig. 5F arrows and quantitative analysis in fig. 5H), pointing to an increase in the apoptotic activity, as a counterbalance to restrain excessive proliferation. These data indicate that although HDAC7 can stimulate epithelial cell growth, compensatory mechanisms are engaged that limit this potential harmful effect.

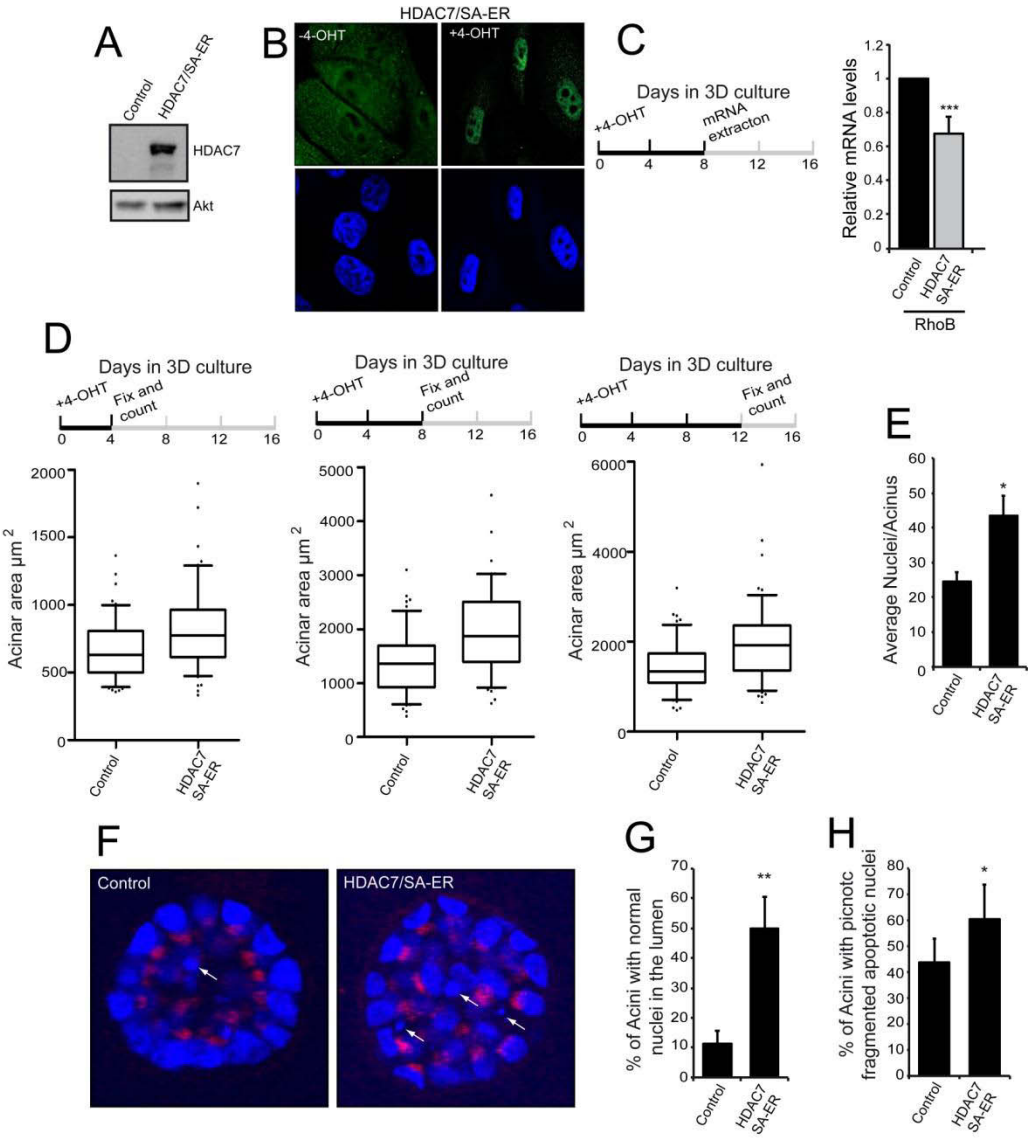

Figure 5: Sustained HDAC7 activity promotes cell proliferation and affects acinar morphogenesis.
A: Immunoblot analysis of transgene HDAC7 levels in MCF-10A cells expressing a mutant form of HDAC7 defective in the four serine residues, binding sites for 14-3-3 proteins (HDAC7/SA-ER). HDAC7/SA-ER activity was induced by treating cells with 4-OHT for 24 h. AKT was used ad loading control.
B: Confocal pictures of MCF-10A cells showing HDAC7/SA-ER nuclear accumulation (green) after the induction with 4-OHT. Nuclei were stained with Hoechst 33258. Images are shown in pseudocolors.

C: mRNA expression levels of the MEF2-target gene RHOB were measured by using qRT-PCR in MCF-10A cells expressing HDAC7/SA-ER or control grown in 3D culture for 8 days. 4-OHT was added to culture medium the day of seeding and the fourth day of culture.
D: Acinar size (μm^2) of MCF-10A cells, expressing HDAC7/SA-ER, in 3D culture for 4, 8, and 12 days. When cells were seeded, 4-OHT was added to culture medium as well as every fourth day in culture.
E: Number of nuclei per acinus, as generated by MCF-10A cells expressing HDAC7/SA-ER or the control, after 12 days in 3D culture.
F: Confocal images comparing the presence of picnotic fragmented apoptotic nuclei in the lumen of acini generated by MCF-10A cells, expressing HDAC7/SA-ER or the control, grown in 3D culture for 12 days. Nuclei were stained with Hoechst 33258. Images are shown in pseudocolors.
G: Quantification of number of acini with normal nuclei in the lumen, as generated by MCF-10A expressing the different transgenes after 12 days in 3D culture.
H: Quantification of the number of apoptotic cells per acini, as generated by MCF-10A expressing the different transgenes after 12 days in 3D culture.

MEF2-dependent transcription and HDAC7 levels are regulated during growth arrest in mammary epithelial cells.

The discovery that MEF2 activity influences cell cycle progression encouraged us to address whether this response can be observed also independently from the epithelial morphogenetic process. As alternative conditions for G0 induction, exit from the cell cycle was promoted by density dependent inhibition and by growth factors starvation. Under contact inhibition MEF2A and MEF2D protein levels increase in the absence of appreciable rises of the relative mRNAs (Fig. 6A and B). As above described for 3D culture, HDAC7 protein levels decrease and HDAC5 increase (Fig. 6A). Expression of KLF2, RHOB, and HDAC5 augments, whereas HDAC7 mRNA levels are unchanged (Fig. 6B). Similar results were obtained when G0 entering was elicited by serum and growth factors deprivation (Fig. 6C and D). Serum starvation promoted the down-regulation of HDAC4 as previously observed (Cernotta et al., 2011). Induction of HDAC7 repressive activity using the HDAC7/SA-ER chimera in MCF-10A cells subjected to growth factors deprivation limited the up-regulation of RHOB mRNA expression levels (Fig. 7A), sustained cell proliferation (Fig. 7B), and DNA synthesis (Fig. 7C). An increase in cell proliferation (Fig. 7B) and in S phase (data not shown) can also be achieved using a conditionally active mutant form of HDAC4. Compared to the results obtained in presence of epidermal growth factor (EGF) in the medium, the HDAC7/SA-ER chimera is less capable to repress RHOB and sustain DNA synthesis. This partial effect depends on the dramatic decrease in its expression observed when cells are deprived of serum and growth factors (Fig. 7D and E). The most prominent effect of cell cycle exit on the MEF2-HDAC axis, in both 3D and 2D culture models, is the down-regulation of HDAC7. To verify whether the up-regulation of MEF2-target genes depends on the release of a repressive influence operated by the deacetylase

on the promoter of such genes, we performed CHIP analysis. The RHOB promoter was selected as a prototype for MEF2-target gene. Figure 6E illustrates that HDAC7 binds the RHOB proximal promoter during the proliferative phase, whereas the binding is clearly reduced upon growth arrest as induced by either density dependent inhibition or serum starvation.

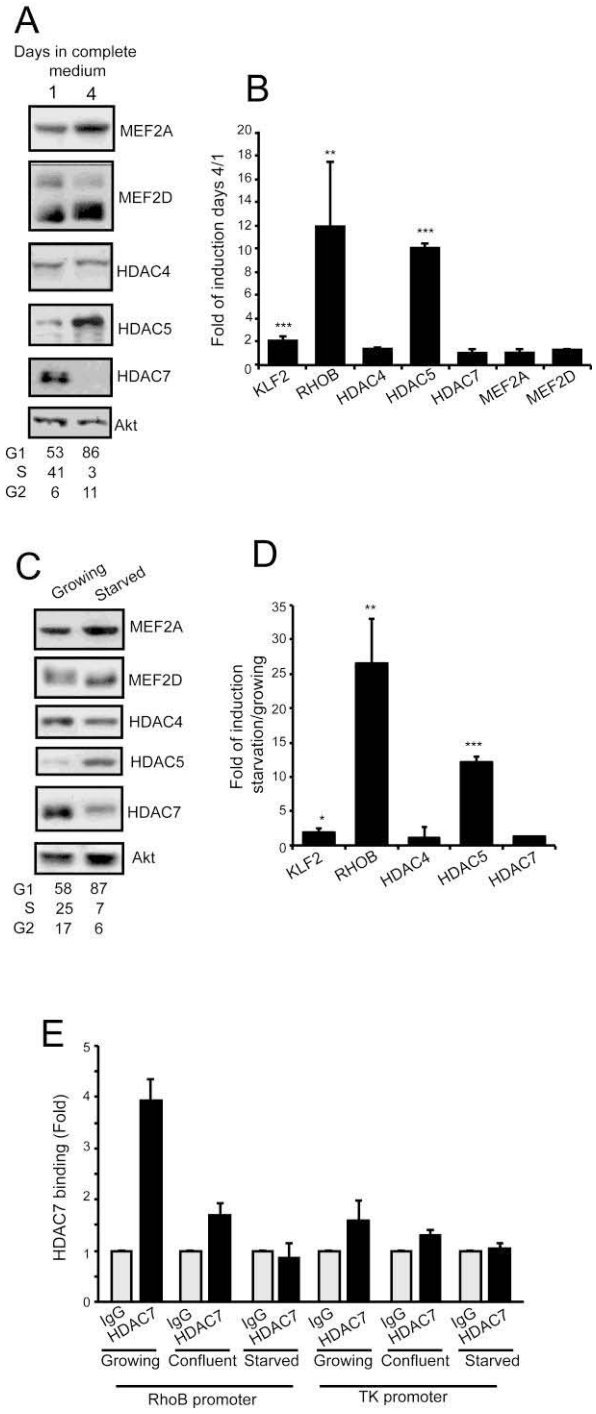

Figure 6: MEF2-dependent transcription and HDAC7 levels are regulated during growth arrest in mammary epithelial cells.

A: Immunoblot analysis of MEF2 family members and class IIa HDACs levels in MCF-10A cells, seeded in complete medium, at the indicated time points. Akt was used as loading control. Cell cycle analysis is provided.

B: qRT-PCR was performed to quantify mRNA levels of class IIa members (HDAC4, HDAC5, and HDAC7) as well as of MEF2s members (MEF2A, and MEF2D) and MEF2-taget genes (KLF2, and RHOB) in MCF-10A cells. Fold induction was calculated as the ratio relative to 1 day of culture in complete medium.
C: Immunoblot analysis of MEF2 family members and class IIa HDACs levels, in MCF-10A cells cultured at different growing conditions. Akt was used as loading control. Cell cycle analysis is provided.
D: qRT-PCR was performed to quantify mRNA levels of class IIa members (HDAC4, HDAC5, and HDAC7) as well as of MEF2s members (MEF2A, and MEF2D) and MEF2-taget genes (KLF2, and RHOB) in MCF-10A cells. Fold induction was calculated as the ratio relative to growing condition.
E: qRT-PCR analysis on chromatin immunoprecipitated with the indicated antibodies in different conditions as showed.

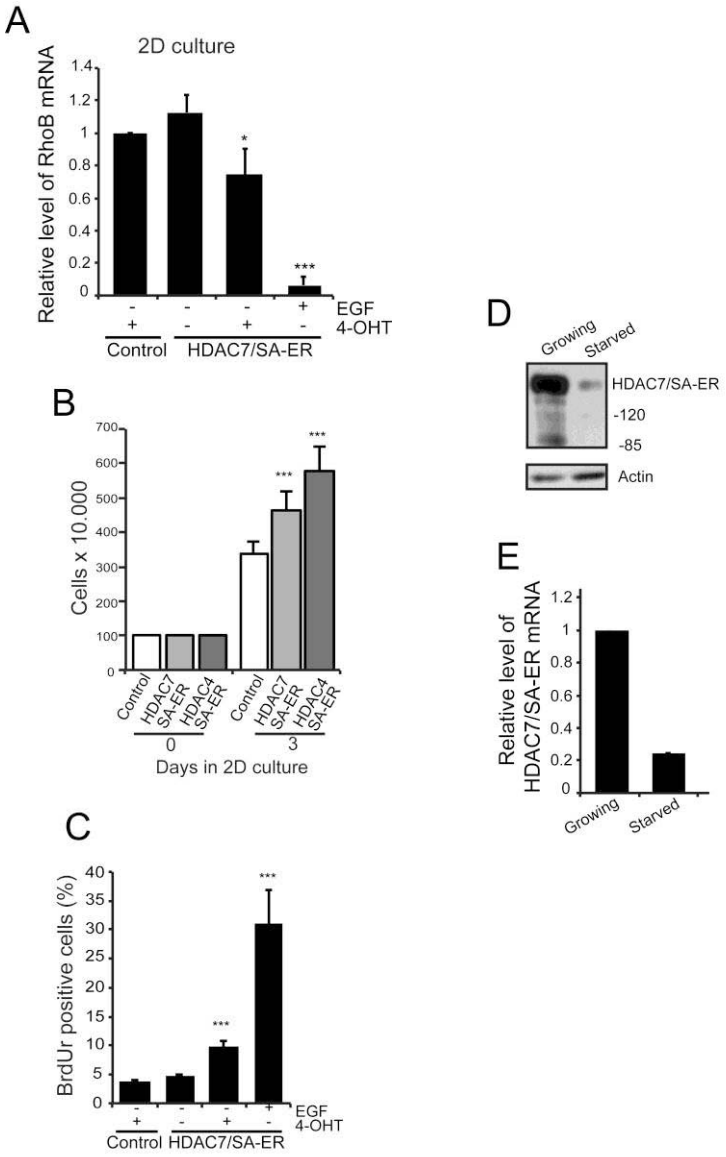

Figure 7: HDAC7 influences MEF2-dependent transcription and cell proliferation in mammary epithelial cells.

A: qRT-PCR was performed to evaluate RHOB mRNA levels in MCF-10A cells expressing ER or HDAC7/SA-ER chimera.

B: MCF-10A cells expressing the indicated transgenes were grown in normal medium deprivated of EGF.

C: MCF-10A cells expressing ER or HDAC7/SA-ER chimera were seeded and after 24h BrdU was added for 2h, and then cells were processed for immunofluorescence.

D: Immunoblot analysis of HDAC7/SA-ER in MCF-10A cells expressing HDAC7/SA-ER chimera subjected or not to serum and growth factors deprivation. Actin was used as loading control.
E: qRT-PCR was performed to evaluate HDAC7/SA-ER mRNA levels in MCF-10A cells expressing HDAC7/SA-ER chimera subjected or not to serum and growth factors deprivation.

HDAC7 binds the p21 promoter.

Cyclin-dependent kinases (CDKs) are master regulators of cell cycle progression and cell proliferation. The CDK inhibitor 1A (CDKN1A), also named p21, is a well-known negative regulator of proliferation, under the control of multiple signals, including growth factors and differentiation (Besson et al., 2008). Some reports have suggested that class IIa HDACs could be involved in the regulation of CDKN1A transcription (Wilson et al., 2008)(Mottet et al., 2009)(R. Liu et al., 2009). To explore whether MEF2 factors and class IIa HDACs control p21 expression during acinar morphogenesis, we initially interrogated the ENCODE database to map the epigenetic status of CDKN1A promoter in human mammary epithelial cells (HMEC)(Ernst et al., 2011)(Rosenbloom et al., 2013). We have considered the genomic region comprised between two insulators (CTCF). Histone 3 lysine 4 trimethylation (H3K4me3) and histone 3 lysine 27 acetylation (H3K27Ac), well-known markers of open chromatin status and characteristics of active promoter and enhancer regions, define the first intron as the important element involved in CDKN1A transcription (Fig. 8A). A similar pattern can be observed also in human lymphoblastoid GM12878 cells (Fig. 8B) and in leukemia K562 cells (data not shown). Interestingly available ENCODE data for GM12878 and K562 cell lines highlighted a conserved binding of MEF2 factors in the promoter/enhancer elements (Fig. 8C), although with a slight variation in the position.

Next we screened for potential MEF2 binding sites a 20 Kb genomic region of CDKN1A, comprising the first intron, containing the active chromatin markers above described. The enlargement in figure 8A illustrates the presence of several potential MEF2 binding sites in the analyzed genomic region and particularly in the first intron, where epigenetic signatures mark active enhancers.

To evaluate the involvement of HDAC7 in the regulation of the CDKN1A transcription, we decided to investigate its ability to bind the regions highlighted in figure 8A. CHIP experiments proved that HDAC7 binds preferentially the region containing the MEF2 binding site at +1.5 Kb from the transcription start site. Importantly, this binding is abolished or dramatically reduced when growth arrest was induced by growth factor starvation or high confluence (Fig. 9A).

The involvement of the MEF2-HDAC axis in the regulation of CDKN1A transcription was confirmed after induction of the MEF2-VP16-ER chimera in 2D conditions (Fig. 9B and C) and by the repression operated by the HDAC7/SA-ER chimera in 3D conditions (Fig. 9D).

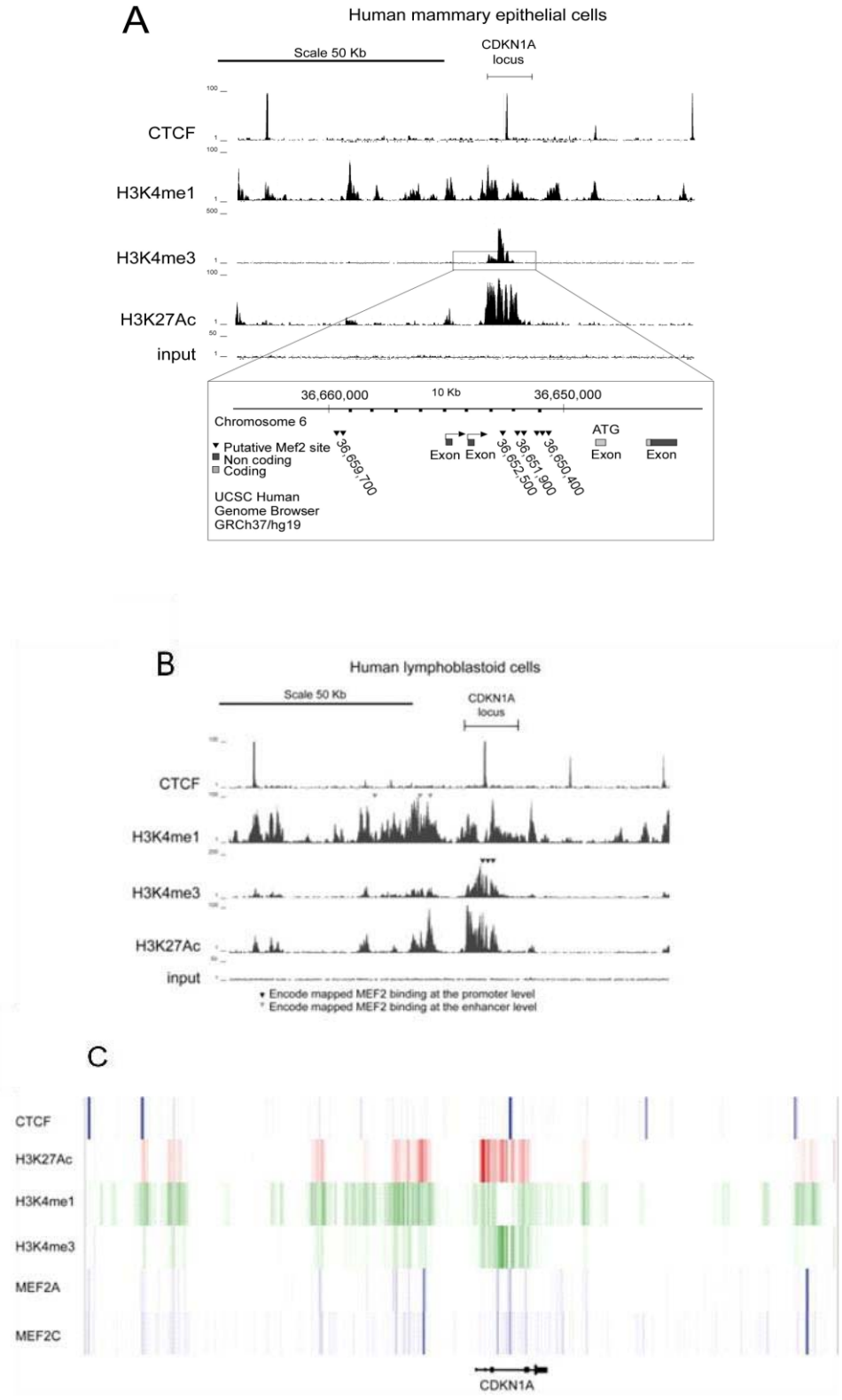

Figura 8: Epigenetic status of p21 promoter.

A: Schematic representation of the epigenetic status of the CDKN1A locus in human mammary epithelial cells, as mapped with the ENCODE project. The analyzed region was comprised within two insulator CTCF peaks and the promoter has been identified through H3K4me3 and H3K27Ac signals. A region of 20 Kb, highlighted in the black box, including the promoter, has been selected and scanned for putativeMEF2 binding sites.
B: Schematic representation of the epigenetic status of the CDKN1A locus in human lymphoblastoid GM12878 cells, as mapped with the ENCODE project. The analyzed region was comprised within two insulator CTCF peaks and the promoter has been identified through H3K4me3 and H3K27Ac signals. Arrows mark MEF2 binding sites identified by ECODE consortium.
C: Schematic representation of the MEF2A and MEF2C peaks in the CDKN1A locus in human lymphoblastoid GM12878 cells, as mapped with the ENCODE project. MEF2 factors associate with regions marking both promoter (H3K4me3) and enhancer (H3K4me1) elements.

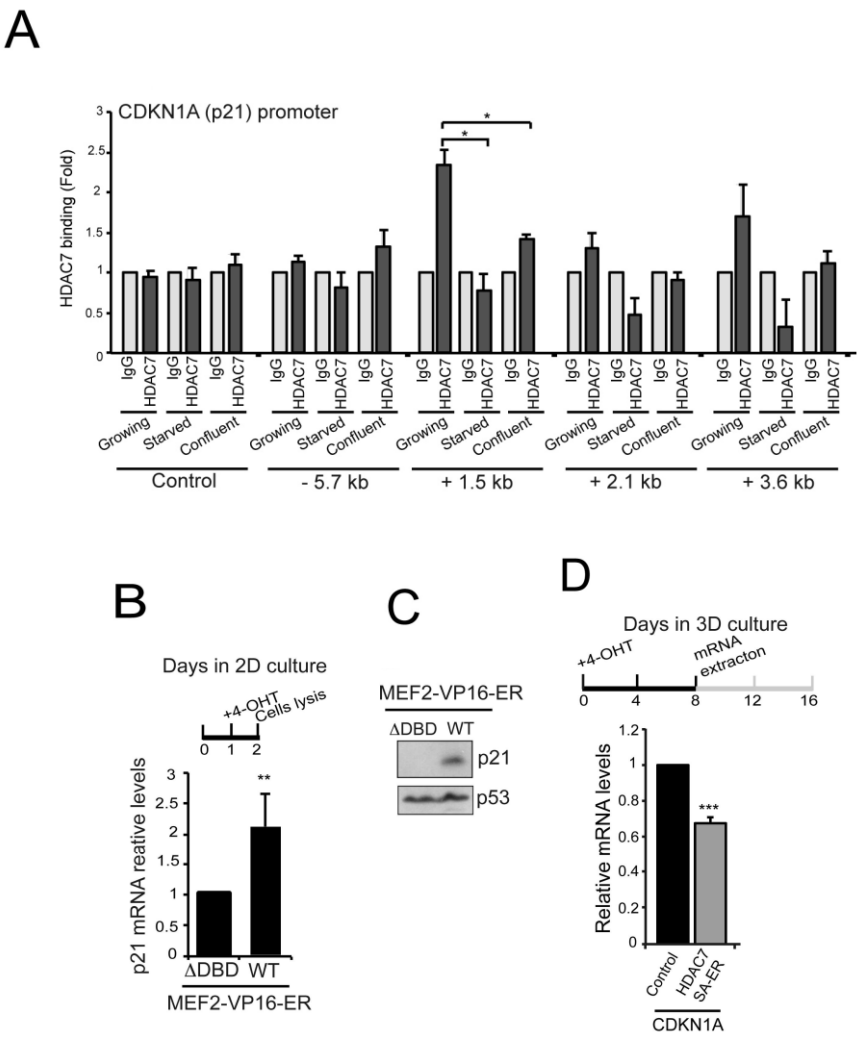

Figure 9: HDAC7 binds the p21 promoter.
A: qRT-PCR analysis on chromatin immunoprecipitated with the indicated antibodies in different conditions as showed. The different genomic regions of CDKN1A, containing putative MEF2 binding sites, are indicated starting from the transcription start site. An internal region (+4.7 Kb) of the CDKN1A gene was used as a negative control.
B: qRT-PCR was performed to quantify CDKN1A mRNA levels in cells in which MEF2-transcription was induced after treatment with 4-OHT. Fold induction was calculated as the ratio relative to cells in which the expression of MEF2 defective in DNA binding was induced by 4-OHT treatment as indicated.
C: Immunoblot analysis of MCF-10A cells expressing the indicated transgene and analysed for p21/CDKN1A levels. Induction of the transgenes was performed as in C.

D: mRNA expression levels of CDKN1A were measured by using qRT-PCR in MCF-10A cells expressing HDAC7/SA-ER or control grown in 3D culture for 8 days. 4-OHT was added to culture medium the day of seeding and the fourth day of culture.

The MEF2-HDAC axis is regulated during HER2-mediated transformation of mammary epithelial cells.

The contribution of the MEF2-HDAC axis to the regulation of mammary epithelial cells proliferation prompted us to determine whether oncogenic lesions, altering mammary epithelial morphogenesis, can provoke dysregulation of the MEF2-HDAC axis. The tyrosine kinase receptor HER2 (human epidermal growth factor receptor 2) is the key determinant of a subclass of breast tumors and its overexpression profoundly alters normal mammary epithelial morphogenetic process (Leung and Brugge, 2012). Hence, we generated MCF-10A cells overexpressing HER2 to assess dysregulations of the MEF2-HDAC axis. After 16 days in 3D culture, HER2 overexpressing cells showed an elevated proliferative index as proved by the development of larger acini (Fig. 10A), composed by higher numbers of cells per structure and marked by the presence of mitotic figures even at day 16 (Fig. 10B). Moreover the compromised epithelial organization is manifested by alterations in polarity and the presence of cells in the luminal cavity (Fig. 10B). Accordingly, HER2 significantly reduced the expression of the epithelial morphogenesis markers (BIM and BMF). Similarly, also the mRNA levels of certain MEF2-target genes (KLF2, RHOB, and CDKN1A) are reduced (Fig. 10C). Importantly, the decrease in MEF2-dependent transcription is coupled to the rescue of HDAC7 protein levels at day 16 (Fig. 10D). Curiously, MEF2D protein levels seem to be increased in HER2 expressing cells. Conversely, the inhibition of HER2 tyrosine kinase activity with lapatinib dramatically impacts on epithelial growth, thus limiting acinar size (Fig. 10E). The number of cells per structure and mitotic figures were also reduced in lapatinib treated cells (Fig. 10F). Lapatinib also restored the appearance of acini with hollow lumen (Fig. 10F). Interestingly, the effect of this inhibitor seems to be cell cycle preponderant, without interferences with the induction of apoptosis, as testified by the unchanged rate of picnotic and fragmented nuclei per acini (Fig. 10F).

In agreement with our studies, treatment of MCF-10A cells expressing HER2, grown for 16 days in 3D culture with lapatinib, up-regulated MEF2-dependent transcription, the expression of BIM and BMF morphogenetic markers (Fig. 10G), and elicited the down-regulation of HDAC7 (Fig. 10H). Interestingly also HDAC4 protein levels seem to be reduced after HER2 inhibition.

Importantly, induction of MEF2 transcription in MCF-10A cells expressing HER2 restores normal epithelial morphogenesis similarly to lapatinib. All the proliferative parameters (average nuclei/acinus, percentage of acini with mitotic figures and of acini with normal nuclei in the lumen) were reduced following MEF2 activation in HER2-overexpressing cells (Fig. 10I).

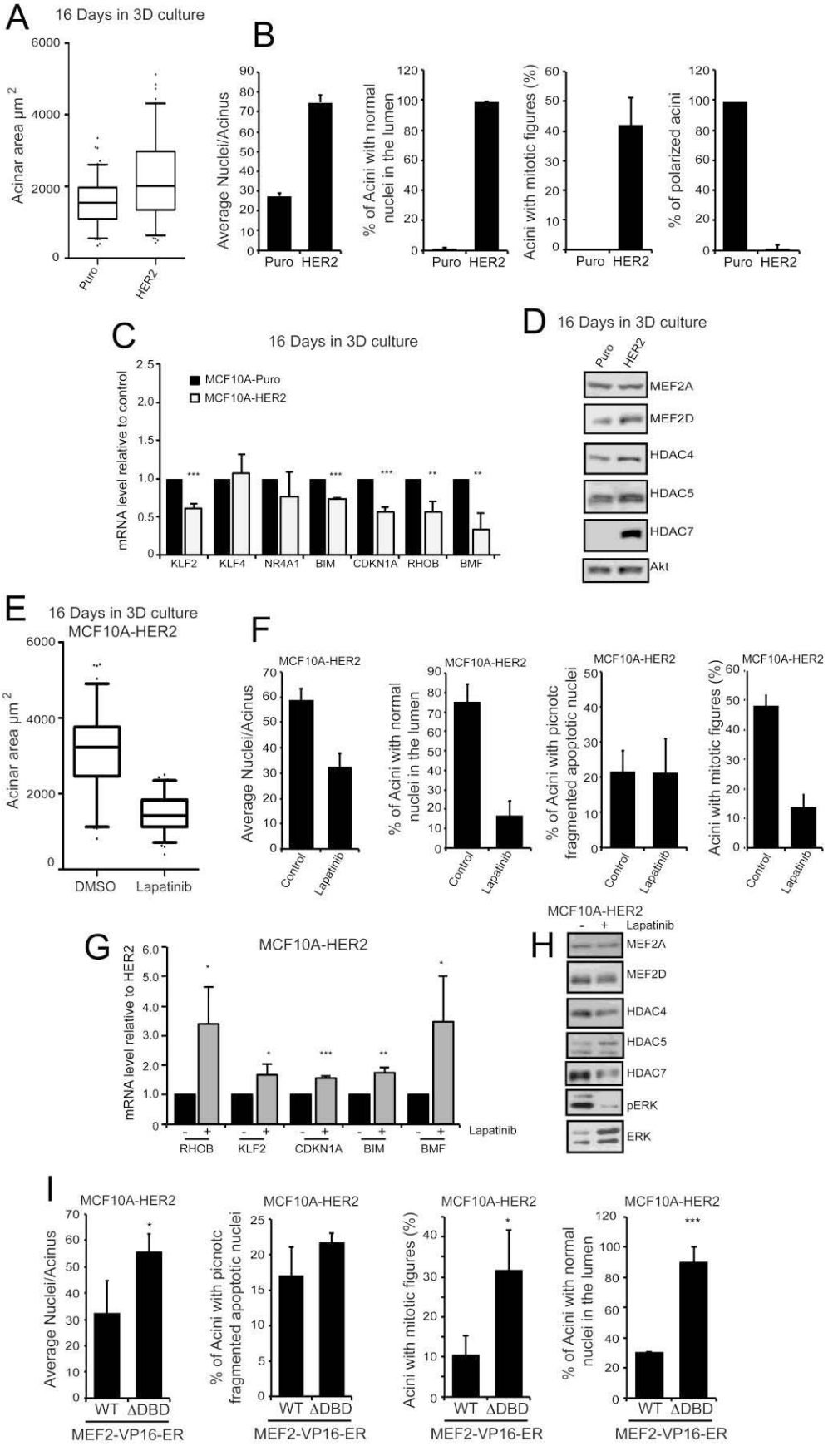
A
16 Days in 3D culture
Acinar area µm 2
Puro
HER2
B
Average Nuclei/Acinus
% of Acini with normal nuclei in the lumen
Acini with mitotic figures (%)
% of polarized acini
C
16 Days in 3D culture
MCF10A-Puro
MCF10A-HER2
mRNA level relative to control
KLF2
KLF4
NR4A1
BIM
CDKN1A
RHOB
BMF
D
16 Days in 3D culture
MEF2A
MEF2D
HDAC4
HDAC5
HDAC7
Akt
E
16 Days in 3D culture
MCF10A-HER2
DMSO
Lapatinib
F
MCF10A-HER2
% of Acini with picnotc fragmented apoptotic nuclei
Control
G
MCF10A-HER2
mRNA level relative to HER2
H
MCF10A-HER2
pERK
ERK
I
MCF10A-HER2
WT
ΔDBD
MEF2-VP16-ER

Figure 10: The MEF2-HDAC axis is regulated during HER2-mediated transformation of mammary epithelial cells.

A: Acinar size (μm^2) of MCF-10A cells expressing HER2 in 3D culture for 16 days.

B: Number of nuclei per acinus, number of acini with normal nuclei in the lumen, number of acini with mitotic figures and number of polarized acini, as generated by MCF-10A cells expressing HER2, after 16 days in 3D culture.

C: qRT-PCR was performed to evaluate mRNA levels of MEF2-target genes in MCF-10A cells expressing HER2 cultured in 3D for 16 days.

D: Immunoblot analysis of MEF2 family members and class IIa HDACs levels in MCF-10A cells expressing HER2 grown in 3D for 16 days. Akt was used as loading control.

E: Acinar size (μm^2) of MCF-10A cells expressing HER2 in 3D culture for 16 days and treated or not with lapatinib.

F: Number of nuclei per acinus, number of acini with normal nuclei in the lumen, number of acini with picnotic and fragmented apoptotic nuclei and number of acini with mitotic figures, as generated by MCF-10A cells expressing HER2 treated or not with lapatinib, after 16 days in 3D culture.

G: qRT-PCR was performed to evaluate mRNA levels of MEF2-target genes in MCF-10A cells expressing HER2 treated or not with lapatinib cultured in 3D for 16 days.

H: Immunoblot analysis of MEF2 family members and class IIa HDACs levels in MCF-10A cells expressing HER2, treated or not with lapatinib, grown in 3D for 16 days. Total ERK was used as loading control.

I: Number of nuclei per acinus, number of acini with picnotic and fragmented apoptotic nuclei, number of acini with mitotic figures and number of acini with normal nuclei in the lumen, as generated by MCF-10A cells expressing HER2-MEF2-VP16-ER chimera or its mutant defective in DNA binding MEF2-ΔDBD-VP16-ER, after 8 days in 3D culture. MEF2-VP16-ER-activation was induced by adding to growth medium 4-OHT after 4 days in 3D culture.

DISCUSSION

The mammary gland undergoes a complex remodeling during different phases like puberty, pregnancy, lactation, and involution (Gjorevski and Nelson, 2011). 3D cultures have become an important and attractive model for studying and understanding how some of these processes take place. Human mammary epithelial cells (MCF-10A) grown under 3D conditions develop structures that resemble the organization of epithelial cells within the terminal ductal lobular units (Schmeichel and Bissell, 2003). Although it is a simple model for epithelial morphogenesis, complex cellular decisions occur during the 16 days interval, necessary for acini formation. After the initial proliferation phase, cells begin to polarize and gradually exit from the cell cycle. The process terminates with the death of the cells in the lumen and cavity formation. This model, although does not induce terminal differentiation and milk protein production, imposes a 3D environment that influences cell behavior and mimics steps required for a proper developmental and homeostatic cue (Lo et al., 2012)(Shaw et al., 2004)(Leung and Brugge, 2012).

In this context we have studied the regulation of MEF2-HDAC axis and dissected its contribution to the epithelial morphogenetic program. Previous works have demonstrated that quantitative and qualitative changes in gene expression profiles characterize the morphogenetic process of MCF-10A cells grown under 3D condition (Yu et al., 2012). However, few studies have addressed the contribution of specific transcriptional factors and of the relative gene networks to this morphogenetic process. We have initially demonstrated that expression of MEF2-target genes is augmented during MCF-10A acini formation. This behavior resembles other differentiation contexts, such as skeletal muscle, where the contribution of the axis was previously studied (T A McKinsey et al., 2000)(Sebastian et al., 2013). Activation of MEF2-dependent transcription is coupled to a dramatic down-regulation of HDAC7 protein levels. In MCF-10A cells, differently from other cellular models, anti-proliferative signals unleash MEF2-dependent transcription, by impacting on HDAC7 levels, rather than by controlling nucleo-cytoplasmic shuttling of class IIa HDACs (T A McKinsey et al., 2000)(Paroni et al., 2008). We noticed that HDAC7 down-regulation is linked to cell growth arrest and it can be observed also in 2D culture condition, after growth factors starvation or density dependent inhibition. However at the moment the mechanism responsible for HDAC7 down-regulation is unknown. We can only exclude changes in mRNA levels, in proteasomal degradation or in autophagy.

Interestingly, HDAC5 and HDAC9 expression increases during acini formation. Being both MEF2-target genes, it is possible that such induction is part of the well-known negative feed-back loop activated by MEF2 itself (Haberland et al., 2007). Nevertheless, since HDAC7 is the highest expressed class IIa deacetylase in breast tissue and in MCF-10A cells, its withdrawal

justifies the up-regulation of MEF2-dependent transcription. Furthermore, some reports indicate a differential repressive capability of class IIa HDACs towards MEF2 factors with HDAC5 being the less prone enzyme (Lemercier et al., 2000).

We exploited different approaches to interfere with the MEF2 transcriptional activity. The down-regulation of MEF2D did not show any evident cellular changes/phenotypes. This failure can be explained with the presence of MEF2s compensatory mechanisms. This behavior was also observed and reported in other contexts (N. Liu et al., 2014). By contrast increasing MEF2-dependent transcription or boosting HDAC7-repressive activity has an effect on the proliferative phase of the morphogenic process, reducing cell division or favoring cell proliferation, respectively. However, in both cases, important steps that lead to acini formation, such as polarization and induction of cell death, were unaffected after modulation of the MEF2-HDAC axis.

In this work we proposed that the influence of the MEF2-HDAC axis on cell proliferation could be operated through the regulation of CDK inhibitor 1A (CDKN1A/p21). Previous works have shown that class IIa HDACs can control CDKN1A expression (Wilson et al., 2008)(Mottet et al., 2009)(R. Liu et al., 2009), however the mechanisms involved are debated. MEF2 binding sites are present in the genomic region embracing CDKN1A. In particular several of them lie within the first intron in correspondence of markers of open chromatin conformation (Ernst et al., 2011). Our results suggest that the MEF2-HDAC axis imposes a control on cell cycle by modulating CDKN1A expression through the recruitment of HDAC7 at position +1.5 Kb from the transcription start site, where a MEF2 binding site is located. HDAC7 binding is dramatically reduced under conditions stimulating cell cycle arrest. Although class IIa HDACs do not manifest catalytic activity, they can act as platforms beckoning class I enzymes (Lahm et al., 2007)(Di Giorgio et al., 2014). Interestingly the recruitment of HDAC7 on p21 promoter is confined in a region identified under the control of MEF2 factors also by ENCODE, in other different cell lineages.

Finally we decided to study the effect of the alteration of MEF2-HDAC axis on mammary epithelial cells proliferation, inducing HER2 overexpression, a frequent oncogenic event in breast tumor. HER2 is able to maintain HDAC7 levels and decrease MEF2-dependent transcription, compromising all the parameters/steps that are important for mammary epithelial organization. Interestingly forcing MEF2 activity in MCF-10A cells overexpressing HER2 reverts the transformed phenotype mainly by restraining proliferation, thus ensuring a correct epithelial organization. Furthermore treatment with the receptor tyrosine kinase inhibitor lapatinib rescued HDAC7 down-regulation and acini formation in 3D culture cells.

In conclusion our studies unveil a role of the MEF2-HDAC axis in the control of epithelial cells proliferation and suggest that class IIa HDACs specific inhibitors could be an interesting therapeutic strategy in addition to or in combination with RTK inhibitors for the treatment of breast cancer.

BIBLIOGRAPHY

Aranda, V., Haire, T., Nolan, M. E., Calarco, J. P., Rosenberg, A. Z., Fawcett, J. P., Pawson, T., Muthuswamy, S. K. (2006). Par6-aPKC uncouples ErbB2 induced disruption of polarized epithelial organization from proliferation control. *Nature Cell Biology*, *8*, 1235–1245.

Arnold, M. A., Kim, Y., Czubryt, M. P., Phan, D., McAnally, J., Qi, X., Shelton, J. M., Richardson, J. A., Bassel-Duby, R., Olson, E. N. (2007). MEF2C transcription factor controls chondrocyte hypertrophy and bone development. *Developmental Cell*, *12*(3), 377–89.

Barneda-Zahonero, B., Parra, M. (2012). Histone deacetylases and cancer. *Molecular Oncology*, *6(6),* 579-89.

Bartkova, J., Lukas, J., Muller, H., Lutzhoft, D., Strauss, M., Bartek, J. (1994). Cyclin D1 protein expression and function in human breast cancer. *Int J Cancer*, *57*, 0–353.

Besson, A., Dowdy, S. F., Roberts, J. M. (2008). CDK Inhibitors: Cell Cycle Regulators and Beyond. *Developmental Cell*, *14(2)*, 159-69.

Bissell, M. J. (2007). Modelling molecular mechanisms of breast cancer and invasion: lessons from the normal gland. *Biochemical Society Transactions*, *35*, 18–22.

Bissell, M. J., Radisky, D. C., Rizki, A., Weaver, V. M., Petersen, O. W. (2002). The organizing principle: Microenvironmental influences in the normal and malignant breast. *Differentiation*, *70(9-10),* 537-46.

Black, B. L., Olson, E. N. (1998). Transcriptional control of muscle development by myocyte enhancer factor-2 (MEF2) proteins. *Annual Review of Cell and Developmental Biology*, *14*, 167–196.

Bolger, T. A., Yao, T. P. (2005). Intracellular trafficking of histone deacetylase 4 regulates neuronal cell death. *The Journal of Neuroscience : The Official Journal of the Society for Neuroscience*, *25*, 9544–9553.

Butcher, D. T., Alliston, T., Weaver, V. M. (2009). A tense situation: forcing tumour progression. *Nature Reviews. Cancer*, *9*, 108–122.

Cernotta, N., Clocchiatti, A., Florean, C., Brancolini, C. (2011). Ubiquitin-dependent degradation of HDAC4, a new regulator of random cell motility. *Molecular Biology of the Cell*, *22(2)*, 278–89.

Chakrabarty, A., Rexer, B. N., Wang, S. E., Cook, R. S., Engelman, J. A., Arteaga, C. L. (2010). H1047R phosphatidylinositol 3-kinase mutant enhances HER2-mediated transformation by heregulin production and activation of HER3. *Oncogene*, *29*, 5193–5203.

Chandarlapaty, S., Sawai, A., Scaltriti, M., Rodrik-Outmezguine, V., Grbovic-Huezo, O., Serra, V., Majumder, P.K., Baselga, J., Rosen, N. (2011). AKT inhibition relieves feedback suppression of receptor tyrosine kinase expression and activity. *Cancer Cell*, *19*, 58–71.

Chang, S., Young, B. D., Li, S., Qi, X., Richardson, J. A., Olson, E. N. (2006). Histone Deacetylase 7 Maintains Vascular Integrity by Repressing Matrix Metalloproteinase 10. *Cell*, *126*, 321–334.

Choi, J., Jang, H., Kim, H., Lee, J. H., Kim, S. T., Cho, E. J., Youn, H. D. (2014). Modulation of lysine methylation in myocyte enhancer factor 2 during skeletal muscle cell differentiation. *Nucleic Acids Research*, *42*, 224–234.

Choi, S. J., Park, S. Y., Han, T. H. (2001). 14-3-3tau associates with and activates the MEF2D transcription factor during muscle cell differentiation. *Nucleic Acids Research*, *29*, 2836–2842.

Clocchiatti, A., Di Giorgio, E., Ingrao, S., Meyer-Almes, F. J., Tripodo, C., Brancolini, C. (2013). Class IIa HDACs repressive activities on MEF2-depedent transcription are associated with poor prognosis of ER^+ breast tumors. *FASEB Journal 27(3)*, 942–54.

Clocchiatti, A., Florean, C., Brancolini, C. (2011). Class IIa HDACs: from important roles in differentiation to possible implications in tumourigenesis. *Journal of Cellular and Molecular Medicine*, *15(9)*, 1833–46.

Collette, N. M., Genetos, D. C., Economides, A. N., Xie, L., Shahnazari, M., Yao, W. (2012). Targeted deletion of Sost distal enhancer increases bone formation and bone mass. *Proc Natl Acad Sci U S A*, *109(35)*, 14092-7.

Cox, D. M., Du, M., Marback, M., Yang, E. C. C., Chan, J., Siu, K. W. M., McDermott, J. C. (2003). Phosphorylation motifs regulating the stability and function of myocyte enhancer factor 2A. *Journal of Biological Chemistry*, *278*, 15297–15303.

Curtis, C., Shah, S. P., Chin, S. F., Turashvili, G., Rueda, O. M., Dunning, M. J., Speed, D., Lynch, A. G., Samarajiwa, S., Yuan, Y., Gräf, S., Ha, G., Haffari, G., Bashashati, A., Russell, R., McKinney, S.; METABRIC Group, Langerød, A., Green, A., Provenzano, E., Wishart, G., Pinder, S., Watson, P., Markowetz, F., Murphy, L., Ellis, I., Purushotham, A., Børresen-Dale, A. L., Brenton, J. D., Tavaré, S., Caldas, C., Aparicio, S. (2012). The genomic and transcriptomic architecture of 2,000 breast tumours reveals novel subgroups. *Nature*, *486(7403)*, 346-52.

Debnath, I., Roundy, K. M., Pioli, P. D., Weis, J. J., Weis, J. H. (2013). Bone marrow-induced Mef2c deficiency delays B-cell development and alters the expression of key B-cell regulatory proteins. *International Immunology*, *25(2)*, 99–115.

Debnath, J., Brugge, J. S. (2005). Modelling glandular epithelial cancers in three-dimensional cultures. *Nature Reviews. Cancer*, *5*, 675–688.

Debnath, J., Mills, K. R., Collins, N. L., Reginato, M. J., Muthuswamy, S. K., Brugge, J. S., Gudjonsson, V. (2002). The Role of Apoptosis in Creating and Maintaining Luminal Space within Normal and Oncogene-Expressing Mammary Acini Brigham and Women ' s Hospital, *111*, 29–40.

Debnath, J., Muthuswamy, S. K., Brugge, J. S. (2003). Morphogenesis and oncogenesis of MCF-10A mammary epithelial acini grown in three-dimensional basement membrane cultures. *Methods*, *30(3)*, 256-68.

Dequiedt, F., Van Lint, J., Lecomte, E., Van Duppen, V., Seufferlein, T., Vandenheede, J. R., Wattiez, R. Kettmann, R. (2005). Phosphorylation of histone deacetylase 7 by protein kinase D mediates T cell receptor-induced Nur77 expression and apoptosis. *The Journal of Experimental Medicine*, *201(5)*, 793–804.

Di Giorgio, E., Clocchiatti, A., Piccinin, S., Sgorbissa, A., Viviani, G., Peruzzo, P., Romeo, S., Rossi, S., Dei Tos, A. P., Maestro, R., Brancolini, C. (2013). MEF2 is a converging hub for HDAC4 and PI3K/Akt-induced transformation. *Molecular and Cellular Biology*, *33(22), 4473-91.*

Di Giorgio, E., Gagliostro, E., Brancolini, C. (2015). Selective class IIa HDAC inhibitors: myth or reality. *Cellular and Molecular Life Sciences, 72(1), 73-86.*

Edmondson, D. G., Lyons, G. E., Martin, J. F., Olson, E. N. (1994). Mef2 gene expression marks the cardiac and skeletal muscle lineages during mouse embryogenesis. *Development*, *120*, 1251–1263.

Ernst, J., Kheradpour, P., Mikkelsen, T. S., Shoresh, N., Ward, L. D., Epstein, C. B., Zhang, X., Wang, L., Issner, R., Coyne, M., Ku, M., Durham, T., Kellis, M., Bernstein, B. E. (2011). Mapping and analysis of chromatin state dynamics in nine human cell types. *Nature*, *473*, 43–49.

Fischle, W., Dequiedt, F., Hendzel, M. J., Guenther, M. G., Lazar, M. A., Voelter, W., Verdin, E. (2002). Enzymatic activity associated with class II HDACs is dependent on a multiprotein complex containing HDAC3 and SMRT/N-CoR. *Molecular Cell*, *9*, 45–57.

Flavell, S. W., Cowan, C. W., Kim, T. K., Greer, P. L., Lin, Y., Paradis, S., Griffith, E. C., Hu, L. S., Chen, C., Greenberg, M. E. (2006). Activity-dependent regulation of MEF2 transcription factors suppresses excitatory synapse number. *Science, 311*, 1008–1012.

Freed-Pastor, W. A., Mizuno, H., Zhao, X., Langerød, A., Moon, S. H., Rodriguez-Barrueco, R., Barsotti, A., Chicas, A., Li, W., Polotskaia, A., Bissell, M. J., Osborne, T. F., Tian, B., Lowe, S. W., Silva, J. M., Børresen-Dale, A. L., Levine, A. J., Bargonetti, J., Prives, C. (2012). Mutant p53 disrupts mammary tissue architecture via the mevalonate pathway. *Cell*, *148*, 244–258.

Fung, C., Lock, R., Gao, S., Salas, E., Debnath, J. (2008). Induction of autophagy during extracellular matrix detachment promotes cell survival. *Molecular Biology of the Cell*, *19*, 797–806.

Gillett, C., Fantl, V., Smith, R., Fisher, C., Bartek, J., Dickson, C., Barnes, D., Peters, G. (1994). Amplification and overexpression of cyclin D1 in breast cancer detected by immunohistochemical staining. *Cancer Research*, *54*, 1812–1817.

Gjorevski, N., Nelson, C. M. (2011). Integrated morphodynamic signalling of the mammary gland. *Nature Reviews. Molecular Cell Biology*, *12*, 581–593.

Godde, N. J., Sheridan, J. M., Smith, L. K., Pearson, H. B., Britt, K. L., Galea, R. C., Yates, L. L., Visvader, J. E., Humbert, P. O. (2014). Scribble Modulates the MAPK/Fra1 Pathway to Disrupt Luminal and Ductal Integrity and Suppress Tumour Formation in the Mammary Gland. *PLoS Genetics*, *10 (5)*.

Gogola, T. V., Rosen, J. M., Vargo-Gogola, T. (2007). Modelling breast cancer: one size does not fit all. *Nat Rev Cancer*, *7*, 659–672.

Gong, X., Tang, X., Wiedmann, M., Wang, X., Peng, J., Zheng, D., Blair, L. A., Marshall, J., Mao, Z. (2003). Cdk5-mediated inhibition of the protective effects of transcription factor MEF2 in neurotoxicity-induced apoptosis. *Neuron*, *38*, 33–46.

Grégoire, S., Tremblay, A. M., Xiao, L., Yang, Q., Ma, K., Nie, J., Mao, Z., Wu, Z., Giguère, V., Yang, X. J. (2006a). Control of MEF2 transcriptional activity by coordinated phosphorylation and sumoylation. *Journal of Biological Chemistry*, *281*, 4423–4433.

Haberland, M., Arnold, M. A., McAnally, J., Phan, D., Kim, Y., Olson, E. N. (2007). Regulation of HDAC9 gene expression by MEF2 establishes a negative-feedback loop in the transcriptional circuitry of muscle differentiation. *Molecular and Cellular Biology*, *27*, 518–525.

Haberland, M., Montgomery, R. L., Olson, E. N. (2009). The many roles of histone deacetylases in development and physiology: implications for disease and therapy. *Nature Reviews. Genetics*, *10*, 32–42.

Han, A., He, J., Wu, Y., Liu, J. O., Chen, L. (2005). Mechanism of recruitment of class II histone deacetylases by myocyte enhancer factor-2. *Journal of Molecular Biology*, *345*, 91–102.

Han, T. H., Prywes, R. (1995). Regulatory role of MEF2D in serum induction of the c-jun promoter. *Molecular and Cellular Biology*, *15*, 2907–2915.

Hansen, R. K., Bissell, M. J. (2000). Tissue architecture and breast cancer: the role of extracellular matrix and steroid hormones. *Endocr.Relat Cancer*, *7*, 95–113.

Hennighausen, L., Robinson, G. W. (2001). Signaling pathways in mammary gland development. *Developmental Cell*, *1*, 467–475.

Hennighausen, L., Robinson, G. W. (2005). Information networks in the mammary gland. *Nature Reviews. Molecular Cell Biology*, *6*, 715–725.

Homminga, I., Pieters, R., Langerak, A. W., de Rooi, J. J., Stubbs, A., Verstegen, M., Vuerhard, M., Buijs-Gladdines, J., Kooi, C., Klous, P., van Vlierberghe, P., Ferrando, A. A., Cayuela, J. M., Verhaaf, B., Beverloo, H. B., Horstmann, M., de Haas, V., Wiekmeijer, A. S., Pike-Overzet, K., Staal, F. J., de Laat, W., Soulier, J., Sigaux, F., Meijerink, J. P. P. (2011). Integrated Transcript and Genome Analyses Reveal NKX2-1 and MEF2C as Potential Oncogenes in T Cell Acute Lymphoblastic Leukemia. *Cancer Cell*, *19*, 484–497.

Hutchinson, J. N., Muller, W. J. (2000). Transgenic mouse models of human breast cancer. *Oncogene*, *19*, 6130–6137.

Ishikawa, F., Miyoshi, H., Nose, K., Shibanuma, M. (2010). Transcriptional induction of MMP-10 by TGF-beta, mediated by activation of MEF2A and downregulation of class IIa HDACs. *Oncogene*, *29*, 909–919.

Jackson, J. G., Lozano, G. (2013). The mutant p53 mouse as a pre-clinical model. *Oncogene*, *32*, 4325–30.

Kang, J., Gocke, C. B., Yu, H. (2006). Phosphorylation-facilitated sumoylation of MEF2C negatively regulates its transcriptional activity. *BMC Biochemistry*, *7*:5.

Kasler, H. G., Verdin, E. (2007). Histone deacetylase 7 functions as a key regulator of genes involved in both positive and negative selection of thymocytes. *Molecular and Cellular Biology*, *27*, 5184–5200.

Kasler, H. G., Victoria, J., Duramad, O., Winoto, A. (2000). ERK5 is a novel type of mitogen-activated protein kinase containing a transcriptional activation domain. *Mol Cell Biol*, *20*, 8382–8389.

Klefstrom, J., Partanen, J. I., Nieminen, A. I., Ma, T. P. (2007). Suppression of oncogenic properties of c-Myc by LKB1-controlled epithelial organization. *Proc Natl Acad Scid U S A, 104(37),* 14694-9.

Kleinman, H. K., McGarvey, M. L., Hassell, J. R., Star, V. L., Cannon, F. B., Laurie, G. W., Martin, G. R. (1986). Basement membrane complexes with biological activity. *Biochemistry*, *25*, 312–318.

Kramer, I., Baertschi, S., Halleux, C., Keller, H., Kneissel, M. (2012). Mef2c deletion in osteocytes results in increased bone mass. *Journal of Bone and Mineral Research, 27*(2), 360–73.

Lahm, A., Paolini, C., Pallaoro, M., Nardi, M. C., Jones, P., Neddermann, P., Sambucini, S., Bottomley, M. J., Lo Surdo, P., Carfí, A., Koch, U., De Francesco, R., Steinkühler, C., Gallinari, P. (2007). Unraveling the hidden catalytic activity of vertebrate class IIa histone deacetylases. *Proceedings of the National Academy of Sciences of the United States of America*, *104*, 17335–17340.

Lee, J. L., Streuli, C. H. (2014). Integrins and epithelial cell polarity. *Journal of Cell Science*, 1–9.

Lemercier, C., Verdel, A., Galloo, B., Curtet, S., Brocard, M. P., Khochbin, S. (2000). mHDA1/HDAC5 histone deacetylase interacts with and represses MEF2A transcriptional activity. *Journal of Biological Chemistry*, *275*, 15594–15599.

Leung, C. T., Brugge, J. S. (2012). Outgrowth of single oncogene-expressing cells from suppressive epithelial environments. *Nature*. *482(7385)*, 410-3.

Lin, Q. (1997). Control of Mouse Cardiac Morphogenesis and Myogenesis by Transcription Factor MEF2C. *Science*, *276(5317)*, 1404–1407.

Lin, Q., Lu, J., Yanagisawa, H., Webb, R., Lyons, G. E., Richardson, J. A., Olson, E. N. (1998). Requirement of the MADS-box transcription factor MEF2C for vascular development. *Development, 125(22)*, 4565–4574.

Liu, N., Nelson, B. R., Bezprozvannaya, S., Shelton, J. M., Richardson, J. a, Bassel-Duby, R., Olson, E. N. (2014). Requirement of MEF2A, C, and D for skeletal muscle regeneration. *Proceedings of the National Academy of Sciences of the United States of America*, *111*, 4109–14.

Liu, R., Wang, L., Chen, G., Katoh, H., Chen, C., Liu, Y., Zheng, P. (2009). F0XP3 Up-regulates p21 expression by site-specific inhibition of histone deacetylase 2/histone deacetylase 4 association to the locus. *Cancer Research*, *69*, 2252–2259.

Lo, A. T., Mori, H., Mott, J., Bissell, M. J. (2012). Constructing three-dimensional models to study mammary gland branching morphogenesis and functional differentiation. *Journal of Mammary Gland Biology and Neoplasia*, *17*, 103–110.

Lu, J., Mckinsey, T. A., Zhang, C., Olson, E. N. (2000). Regulation of Skeletal Myogenesis by Association of the MEF2 Transcription Factor with Class II Histone Deacetylases, *Mol Cell, 6(2)*, 233-44.

Lyons, G. E., Micales, B. K., Schwarz, J., Martin, J. F., Olson, E. N. (1995). Expression of mef2 genes in the mouse central nervous system suggests a role in neuronal maturation. *The Journal of Neuroscience, 15*, 5727–5738.

Ma, K., Chan, J. K. L., Zhu, G., Wu, Z. (2005). Myocyte enhancer factor 2 acetylation by p300 enhances its DNA binding activity, transcriptional activity, and myogenic differentiation. *Molecular and Cellular Biology*, *25*, 3575–3582.

Ma, L., Liu, J., Liu, L., Duan, G., Wang, Q., Xu, Y., Xia, F., Shan, J., Shen, J., Yang, Z., Bie, P., Cui, Y., Bian, X. W., Prieto, J., Avila, M. A., Qian, C. (2014). Overexpression of the transcription factor MEF2D in hepatocellular carcinoma sustains malignant character by suppressing G2-M transition genes. *Cancer Research*, *74*, 1452–1462.

Mailleux, A. A., Overholtzer, M., Brugge, J. S. (2008). Lumen formation during mammary epithelial morphogenesis: Insights from in vitro and in vivo models. *Cell Cycle*, *7(1)*, 57-62.

Martin, J. F., Miano, J. M., Hustad, C. M., Copeland, N. G., Jenkins, N. A., Olson, E. N. (1994). A Mef2 gene that generates a muscle-specific isoform via alternative mRNA splicing. *Molecular and Cellular Biology*, *14*, 1647–1656.

Martin, M., Kettmann, R., Dequiedt, F. (2007). Class IIa histone deacetylases: regulating the regulators. *Oncogene*, *26(37)*, 5450–67.

McKinsey, T. A., Zhang, C. L., Lu, J., Olson, E. N. (2000). Signal-dependent nuclear export of a histone deacetylase regulates muscle differentiation. *Nature*, *408*, 106–111.

McKinsey, T. A., Zhang, C. L., Olson, E. N. (2001). Identification of a signal-responsive nuclear export sequence in class II histone deacetylases. *Molecular and Cellular Biology*, *21*, 6312–6321.

McKinsey, T. A., Zhang, C. L., Olson, E. N. (2002). MEF2: A calcium-dependent regulator of cell division, differentiation and death. *Trends in Biochemical Sciences*, *27(1)*, 40-7.

Mills, K. R., Reginato, M., Debnath, J., Queenan, B., Brugge, J. S. (2004). Tumor necrosis factor-related apoptosis-inducing ligand (TRAIL) is required for induction of autophagy during lumen formation in vitro. *Proceedings of the National Academy of Sciences of the United States of America*, *101(10)*, 3438–43.

Miska, E. A., Langley, E., Wolf, D., Karlsson, C., Pines, J., Kouzarides, T. (2001). Differential localization of HDAC4 orchestrates muscle differentiation. *Nucleic Acids Research*, *29*, 3439–3447.

Molkentin, J. D., Li, L., Olson, E. N. (1996). Phosphorylation of the MADS-box transcription factor MEF2C enhances its DNA binding activity. *Journal of Biological Chemistry*, *271*, 17199–17204.

Mottet, D., Pirotte, S., Lamour, V., Hagedorn, M., Javerzat, S., Bikfalvi, A., Bellahcène, A., Verdin, E., Castronovo, V. (2009). HDAC4 represses p21(WAF1/Cip1) expression in human cancer cells through a Sp1-dependent, p53-independent mechanism. *Oncogene*, *28*, 243–256.

Muranen, T., Selfors, L. M., Worster, D. T., Iwanicki, M. P., Song, L., Morales, F. C., Gao, S., Mills, G. B., Brugge, J. S. (2012). Inhibition of PI3K/mTOR Leads to Adaptive Resistance in Matrix-Attached Cancer Cells. *Cancer Cell*, *21*, 227–239.

Muthuswamy, S. K., Li, D., Lelievre, S., Bissell, M. J., Brugge, J. S. (2001). ErbB2, but not ErbB1, reinitiates proliferation and induces luminal repopulation in epithelial acini. *Nature Cell Biology*, *3*, 785–792.

Naya, F. J., Black, B. L., Wu, H., Bassel-Duby, R., Richardson, J. A., Hill, J. A., Olson, E. N. (2002). Mitochondrial deficiency and cardiac sudden death in mice lacking the MEF2A transcription factor. *Nature Medicine*, *8*, 1303–1309.

Nebbioso, A., Manzo, F., Miceli, M., Conte, M., Manente, L., Baldi, A., De Luca, A., Rotili, D., Valente, S., Mai, A., Usiello, A., Gronemeyer, H., Altucci, L. (2009). Selective class II HDAC inhibitors impair myogenesis by modulating the stability and activity of HDAC-MEF2 complexes. *EMBO Reports*, *10*, 776–782.

Nedvetsky, P. I., Kwon, S. H., Debnath, J., Mostov, K. E. (2012). Cyclic AMP regulates formation of mammary epithelial acini in vitro. *Molecular Biology of the Cell. 23(15)*, 2973-81.

Neve, R. M., Chin, K., Fridlyand, J., Yeh, J., Baehner, F. L., Fevr, T., Clark, L., Bayani, N., Coppe, J. P., Tong, F., Speed, T., Spellman, P. T., DeVries, S., Lapuk, A., Wang, N. J., Kuo, W. L., Stilwell, J. L., Pinkel, D., Albertson, D. G., Waldman, F. M., McCormick, F., Dickson, R. B., Johnson, M. D., Lippman, M., Ethier, S., Gazdar, A., Gray, J. W. (2006). A collection of breast cancer cell lines for the study of functionally distinct cancer subtypes. *Cancer Cell*, *10*, 515–527.

Pallavi, S. K., Ho, D. M., Hicks, C., Miele, L., Artavanis-Tsakonas, S. (2012). Notch and Mef2 synergize to promote proliferation and metastasis through JNK signal activation in Drosophila. *The EMBO Journal*, *31(13)*, 2895–907.

Paroni, G., Cernotta, N., Dello Russo, C., Gallinari, P., Pallaoro, M., Foti, C., Talamo, F., Orsatti, L., Steinkühler, C., Brancolini, C. (2008). PP2A regulates HDAC4 nuclear import. *Molecular Biology of the Cell*, *19*, 655–667.

Paroni, G., Henderson, C., Schneider, C., Brancolini, C. (2001). Caspase-2-induced Apoptosis is Dependent on Caspase-9, but Its Processing during UV- or Tumor Necrosis Factor-dependent Cell Death Requires Caspase-3. *Journal of Biological Chemistry*, *276*, 21907–21915.

Paroni, G., Mizzau, M., Henderson, C., Del Sal, G., Schneider, C., Brancolini, C. (2004). Caspase-dependent regulation of histone deacetylase 4 nuclear-cytoplasmic shuttling promotes apoptosis. *Molecular Biology of the Cell*, *15*, 2804–2818.

Parra, M., Mahmoudi, T., Verdin, E. (2007). Myosin phosphatase dephosphorylates HDAC7, controls its nucleocytoplasmic shuttling, and inhibits apoptosis in thymocytes. *Genes and Development*, *21*, 638–643.

Peng, L., Seto, E. (2011). Deacetylation of nonhistone proteins by HDACs and the implications in cancer. *Handbook of Experimental Pharmacology*, *206*, 39–56.

Potthoff, M. J., Olson, E. N. (2007). MEF2: a central regulator of diverse developmental programs. *Development (Cambridge, England)*, *134(23)*, 4131–40.

Potthoff, M. J., Wu, H., Arnold, M. A., Shelton, J. M., Backs, J., McAnally, J., Richardson, J. A., Bassel-Duby, R., Olson, E. N. (2007). Histone deacetylase degradation and MEF2 activation promote the formation of slow-twitch myofibers. *Journal of Clinical Investigation*, *117*, 2459–2467.

Reginato, M. J., Mills, K. R., Becker, E. B. E., Lynch, D. K., Bonni, A., Muthuswamy, S. K., Brugge, J. S. (2005). Bim regulation of lumen formation in cultured mammary epithelial acini is targeted by oncogenes. *Molecular and Cellular Biology*, *25*, 4591–4601.

Reginato, M. J., Mills, K. R., Paulus, J. K., Lynch, D. K., Sgroi, D. C., Debnath, J., Muthuswamy, S. K., Brugge, J. S. (2003). Integrins and EGFR coordinately regulate the pro-apoptotic protein Bim to prevent anoikis. *Nature Cell Biology*, *5*, 733–740.

Reichenstein, M., Rauner, G., Barash, I. (2011). Conditional repression of STAT5 expression during lactation reveals its exclusive roles in mammary gland morphology, milk-protein gene expression, and neonate growth. *Molecular Reproduction and Development*, *78*, 585–596.

Riquelme, C., Barthel, K. K. B., Liu, X. (2006). SUMO-1 modification of MEF2A regulates its transcriptional activity. *Journal of Cellular and Molecular Medicine*, *10*, 132–144.

Robinson, G. W. (2007). Cooperation of signalling pathways in embryonic mammary gland development. *Nature Reviews. Genetics*, *8*, 963–972.

Rosenbloom, K. R., Sloan, C. A., Malladi, V. S., Dreszer, T. R., Learned, K., Kirkup, V. M., Wong, M. C., Maddren, M., Fang, R., Heitner, S. G., Lee, B. T., Barber, G. P., Harte, R. A., Diekhans, M., Long, J. C., Wilder, S. P., Zweig, A. S., Karolchik, D., Kuhn, R. M., Haussler, D., Kent, W. J. (2013). ENCODE Data in the UCSC Genome Browser: Year 5 update. *Nucleic Acids Research*, *41*.

Schafer, Z. T., Grassian, A. R., Song, L., Jiang, Z., Gerhart-Hines, Z., Irie, H. Y., Gao, S., Puigserver, P., Brugge, J. S. (2009). Antioxidant and oncogene rescue of metabolic defects caused by loss of matrix attachment. *Nature*, *461*, 109–113.

Schmeichel, K. L., Bissell, M. J. (2003). Modeling tissue-specific signaling and organ function in three dimensions. *Journal of Cell Science*, *116*, 2377–2388.

Schmelzle, T., Mailleux, A. A., Overholtzer, M., Carroll, J. S., Solimini, N. L., Lightcap, E. S., Veiby, O. P., Brugge, J. S. (2007). Functional role and oncogene-regulated expression of the BH3-only factor Bmf in mammary epithelial anoikis and morphogenesis. *Proceedings of the National Academy of Sciences of the United States of America*, *104*, 3787–3792.

Schuetz, C. S., Bonin, M., Clare, S. E., Nieselt, K., Sotlar, K., Walter, M., Fehm, T., Solomayer, E., Riess, O., Wallwiener, D., Kurek, R., Neubauer, H. J. (2006). Progression-specific genes identified by expression profiling of matched ductal carcinomas in situ and invasive breast tumors, combining laser capture microdissection and oligonucleotide microarray analysis. *Cancer Research*, *66*, 5278–5286.

Schwieger, M., Schüler, A., Forster, M., Engelmann, A., Arnold, M. A., Delwel, R., Valk, P. J., Löhler, J., Slany, R. K., Olson, E. N., Stocking, C. (2009). Homing and invasiveness of MLL/ENL leukemic cells is regulated by MEF2C. *Blood*, *114*, 2476–2488.

Sebastian, S., Faralli, H., Yao, Z., Rakopoulos, P., Palii, C., Cao, Y., Singh, K., Liu, Q. C., Chu, A., Aziz, A., Brand, M., Tapscott, S. J., Dilworth, F. J. (2013). Tissue-specific splicing of a ubiquitously expressed transcription factor is essential for muscle differentiation. *Genes and Development*, *27*, 1247–1259.

Shaw, K. R., Wrobel, C. N., Brugge, J. S. (2004). Use of three-dimensional basement membrane cultures to model oncogene-induced changes in mammary epithelial morphogenesis. *Journal of Mammary Gland Biology and Neoplasia*. *9(4)*, 297-310.

Simpson, D. R., Yu, M., Zheng, S., Zhao, Z., Muthuswamy, S. K., Tansey, W. P. (2011). Epithelial cell organization suppresses Myc function by attenuating Myc expression. *Cancer Research*, *71*, 3822–3830.

Smalley, M., Ashworth, A. (2003). Stem cells and breast cancer: A field in transit. *Nature Reviews. Cancer*, *3*, 832–844.

Song, K., Backs, J., McAnally, J., Qi, X., Gerard, R.D., Richardson, J. A., Hill, J. A., Bassel-Duby, R., Olson, E. N. (2006). The Transcriptional Coactivator CAMTA2 Stimulates Cardiac Growth by Opposing Class II Histone Deacetylases. *Cell*, *125*, 453–466.

Sørlie, T., Perou, C. M., Tibshirani, R., Aas, T., Geisler, S., Johnsen, H., Hastie, T., Eisen, M. B., van de Rijn, M., Jeffrey, S. S., Thorsen, T., Quist, H., Matese, J. C., Brown, P. O., Botstein, D., Lønning, P. E., Børresen-Dale, A. L. (2001). Gene expression patterns of breast carcinomas distinguish tumor subclasses with clinical implications. *Proceedings of the National Academy of Sciences of the United States of America*, *98*, 10869–10874.

Verdin, E., Dequiedt, F., Kasler, H. G. (2003). Class II histone deacetylases: Versatile regulators. *Trends in Genetics*, *19(5),* 286-93.

Verzi, M. P., Agarwal, P., Brown, C., McCulley, D. J., Schwarz, J. J., Black, B. L. (2007). The Transcription Factor MEF2C Is Required for Craniofacial Development. *Developmental Cell*, *12*, 645–652.

Visvader, J. E. (2009). Keeping abreast of the mammary epithelial hierarchy and breast tumorigenesis. *Genes and Development*, *23(22)*, 2563-77.

Wang, A. H., Kruhlak, M. J., Wu, J., Bertos, N. R., Vezmar, M., Posner, B. I., Bazett-Jones, D. P., Yang, X. J. (2000). Regulation of histone deacetylase 4 by binding of 14-3-3 proteins. *Molecular and Cellular Biology*, *20*, 6904–6912.

Weigelt, B., Bissell, M. J. (2008). Unraveling the microenvironmental influences on the normal mammary gland and breast cancer. *Seminars in Cancer Biology*, *18(5)*, 311-21.

Wilson, A. J., Byun, D. S., Nasser, S., Murray, L. B., Ayyanar, K., Arango, D., Figueroa, M., Melnick, A., Kao, G. D., Augenlicht, L. H., Mariadason, J. M. (2008). HDAC4 promotes growth of colon cancer cells via repression of p21. *Molecular Biology of the Cell*, *19*, 4062–4075.

Wu, H., Naya, F. J., McKinsey, T. A., Mercer, B., Shelton, J. M., Chin, E. R., Simard, A. R., Michel, R. N., Bassel-Duby, R., Olson, E. N., Williams, R. S. (2000). MEF2 responds to multiple calcium-regulated signals in the control of skeletal muscle fiber type. *The EMBO Journal*, *19*, 1963–1973.

Yang, X.-J., Seto, E. (2007). HATs and HDACs: from structure, function and regulation to novel strategies for therapy and prevention. *Oncogene*, *26*, 5310–5318.

Yang, X.-J., Seto, E. (2008). The Rpd3/Hda1 family of lysine deacetylases: from bacteria and yeast to mice and men. *Nature Reviews. Molecular Cell Biology*, *9*, 206–218.

Youn, H. D., Sun, L., Prywes, R., Liu, J. O. (1999). Apoptosis of T cells mediated by Ca2+-induced release of the transcription factor MEF2. *Science 286*, 790–793.

Yu, M., Lin, G., Arshadi, N., Kalatskaya, I., Xue, B., Haider, S., Nguyen, F., Boutros, P. C., Elson, A., Muthuswamy, L. B., Tonks, N. K., Muthuswamy, S. K. (2012). Expression Profiling during Mammary Epithelial Cell Three-Dimensional Morphogenesis Identifies PTPRO as a Novel Regulator of Morphogenesis and ErbB2-Mediated Transformation. *Molecular and Cellular Biology*, *32(19),* 3913-24.

Zhang, C. L., McKinsey, T. A., Chang, S., Antos, C. L., Hill, J. A., Olson, E. N. (2002). Class II histone deacetylases act as signal-responsive repressors of cardiac hypertrophy. *Cell*, *110*, 479–488.

Zhang, Y., Yan, W., Chen, X. (2011). Mutant p53 disrupts MCF-10A cell polarity in three-dimensional culture via epithelial-to-mesenchymal transitions. *Journal of Biological Chemistry*, *286*, 16218–16228.

Zhao, X., Sternsdorf, T., Bolger, T. A., Evans, R. M., Yao, T.-P. (2005). Regulation of MEF2 by histone deacetylase 4- and SIRT1 deacetylase-mediated lysine modifications. *Molecular and Cellular Biology*, *25*, 8456–8464.

Molecular and Cellular Biology

MEF2 Is a Converging Hub for Histone Deacetylase 4 and Phosphatidylinositol 3-Kinase/Akt-Induced Transformation

Eros Di Giorgio, Andrea Clocchiatti, Sara Piccinin, Andrea Sgorbissa, Giulia Viviani, Paolo Peruzzo, Salvatore Romeo, Sabrina Rossi, Angelo Paolo Dei Tos, Roberta Maestro and Claudio Brancolini

Mol. Cell. Biol. **2013, 33(22):4473. DOI: 10.1128/MCB.01050-13.**
Published Ahead of Print 16 September 2013.

MCB
Journals.ASM.org

MEF2 Is a Converging Hub for Histone Deacetylase 4 and Phosphatidylinositol 3-Kinase/Akt-Induced Transformation

Eros Di Giorgio,[a] Andrea Clocchiatti,[a] Sara Piccinin,[b] Andrea Sgorbissa,[a] Giulia Viviani,[a] Paolo Peruzzo,[a] Salvatore Romeo,[c] Sabrina Rossi,[c] Angelo Paolo Dei Tos,[c] Roberta Maestro,[b] Claudio Brancolini[a]

Dipartimento di Scienze Mediche e Biologiche, Università degli Studi di Udine, Udine, Italy[a]; Experimental Oncology 1, CRO National Cancer Institute, Aviano, Italy[b]; Department of Anatomical Pathology, Treviso General Hospital, Treviso, Italy[c]

The MEF2-class IIa histone deacetylase (HDAC) axis operates in several differentiation pathways and in numerous adaptive responses. We show here that nuclear active HDAC4 and HDAC7 display transforming capability. HDAC4 oncogenic potential depends on the repression of a limited set of genes, most of which are MEF2 targets. Genes verified as targets of the MEF2-HDAC axis are also under the influence of the phosphatidylinositol 3-kinase (PI3K)/Akt pathway that affects MEF2 protein stability. A signature of MEF2 target genes identified by this study is recurrently repressed in soft tissue sarcomas. Correlation studies depicted two distinct groups of soft tissue sarcomas: one in which MEF2 repression correlates with PTEN downregulation and a second group in which MEF2 repression correlates with HDAC4 levels. Finally, simultaneous pharmacological inhibition of the PI3K/Akt pathway and of MEF2-HDAC interaction shows additive effects on the transcription of MEF2 target genes and on sarcoma cells proliferation. Overall, our work pinpoints an important role of the MEF2-HDAC class IIa axis in tumorigenesis.

Gene transcription is under the influence of complex regulative networks integrating multiple signaling events that end up with the final decision of activating or repressing specific genetic programs. Histone deacetylases (HDACs) play important roles in the regulation of different genetic programs controlling differentiation, survival, tissue homeostasis and metabolism (1, 2). Among the different deacetylases, the class IIa HDACs, including HDAC4, HDAC5, HDAC7, and HDAC9, show a limited enzymatic activity but are equally powerful repressors of transcription by virtue of assembly into multiprotein complexes that recruit other transcriptional corepressor (3–5). Environmental signals control class IIa HDACs activities through different strategies, including regulation of transcription/translation, ubiquitin-dependent degradation, and selective proteolysis (6–11).

A widespread and rapid strategy to modulate class IIa repressive potential is operated through the control of their subcellular localization. These deacetylases shuttle in and out of the nucleus in a phosphorylation-dependent manner. A set of conserved serines, once phosphorylated become docking sites for 14-3-3 chaperone proteins, which escort the deacetylases from the nucleus into the cytoplasm, thus limiting their repressive influence (1, 5, 11–13). In contrast, phosphatases such as PP2A can promote HDAC nuclear import and consequently gene repression (14, 15).

Since class IIa HDACs omit DNA-binding domains, they must bind DNA-binding transcription factors in order to influence gene expression (1, 5, 16–18). Important partners of class IIa HDACs are the transcription factors of the MEF2 family. Genetic studies and the generation of animal models testified to the important role of the MEF2-HDAC axis during development, differentiation, and tissue homeostasis (19).

Molecular pathways that normally ensure proper embryogenesis and tissue maintenance in postembryonic life are subverted during the carcinogenetic process (20). Alterations of the class IIa HDACs and MEF2 transcription factors have been observed in certain cancers (11, 21–24). Overall, the data are scattered and debated, and, more importantly, the impact of the MEF2-HDAC axis on the tumorigenic process is still undefined. In the present study we addressed the prooncogenic role for class IIa HDACs. Since previous reports correlated HDAC4 with cell proliferation (25–27), we focused in particular on this deacetylase as a model.

MATERIALS AND METHODS

Cell cultures and reagents. NIH 3T3 mouse fibroblasts and human IMR90-E1A cells were grown in Dulbecco modified Eagle medium (DMEM; Lonza) supplemented with 10% fetal bovine serum (FBS), L-glutamine (2 mM), penicillin (100 U/ml), and streptomycin (100 μg/ml) (all from Lonza). Cells expressing the inducible form of MEF2 were grown in DMEM without phenol (Sigma-Aldrich). BALB/c 3T3 cells were generated from BALB/c primary MEF using the 3T3 protocol (28) and were grown in DMEM supplemented with 10% calf serum. The human leiomyosarcoma cell lines SKUT-1, DMR, and SK-LMS1 were cultivated as previously described (42). For analyses of cell growth, 10^4 cells were seeded, and the medium was changed every 2 days.

The following chemicals were used (the final concentrations are indicated): 20 μM LY (LY294002; LC laboratories); 2.5 μM MG132, 10 μM BML-210, 1 μM 4-hydroxytamoxifen (4-OHT), 10 μM resazurin, 0.5 mg of MTT [3-(4,5-dimethyl-2-thiazolyl)-2,5-diphenyl-2H-tetrazolium bromide]/ml, and dimethyl sulfoxide (DMSO) (all from Sigma-Aldrich); and leptomycin B (LC Laboratories). The primary antibodies were anti-green fluorescent protein (anti-GFP), anti-HDAC4 (29), antipaxillin, and anti-Ran (BD Transduction Laboratories), anti-VP16 (sc-7545; Santa Cruz), antihemagglutinin (anti-HA; Sigma-Aldrich), antiubiquitin (Covance), anti-nucleoporin p62, anti-RAN, anti-pp120, and anti-MEF2D

Received 13 August 2013 Accepted 9 September 2013
Published ahead of print 16 September 2013
Address correspondence to Claudio Brancolini, claudio.brancolini@uniud.it.
Supplemental material for this article may be found at http://dx.doi.org/10.1128/MCB.01050-13.

doi:10.1128/MCB.01050-13

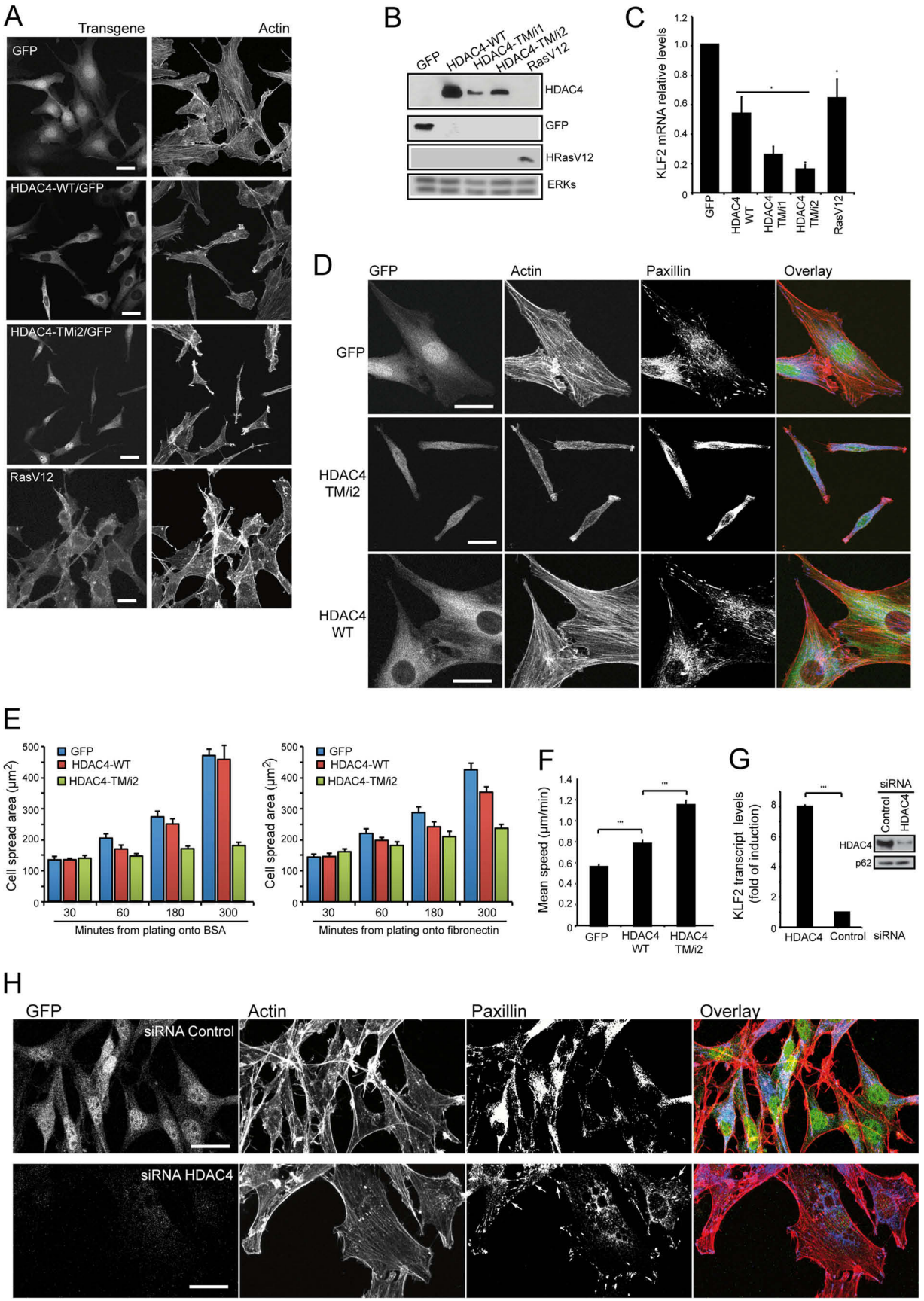
A
Transgene
Actin
GFP
HDAC4-WT/GFP
HDAC4-TMi2/GFP
RasV12
B
GFP
HDAC4-WT
HDAC4-TM/i1
HDAC4-TM/i2
RasV12
HDAC4
GFP
HRasV12
ERKs
C
KLF2 mRNA relative levels
GFP
HDAC4 WT
HDAC4 TM/i1
HDAC4 TM/i2
RasV12
D
GFP
Actin
Paxillin
Overlay
HDAC4 TM/i2
HDAC4 WT
E
Cell spread area (μm2)
GFP
HDAC4-WT
HDAC4-TM/i2
Minutes from plating onto BSA
Minutes from plating onto fibronectin
F
Mean speed (μm/min)
G
KLF2 transcript levels (fold of induction)
siRNA
Control
HDAC4
p62
H
GFP
Actin
Paxillin
Overlay
siRNA Control
siRNA HDAC4

(BD Transduction Laboratories), and anti-Erk, ant-pErk, anti-Akt, anti-Aktp473, anti-MEF2C D80C, and anti-MYC (Cell Signaling).

Plasmid construction, transfection, retroviral infection, and silencing. pEGFPN1 constructs expressing human HDAC4 and its mutants, pcDNA3.1 HA-MEF2C, 3×MEF2-Luc, and pRL-CMV, were previously described (9). All of the cDNAs used were from humans. Cells expressing the different transgenes were generated by retroviral infection as described previously (9). To generate pBABE-Puro-MEF2c-VP16-ER, p-BABE-MEF2cΔDBD-VP16-ER, pWZL-Hygro-MEF2c-VP16-ER, and pWZL-Hygro-MEF2c-ΔDBD-VP16-ER MEF2, the relative cDNAs were subcloned into pBABE-Puro and pWZL-Hygro plasmids using a PCR method and then checked by sequencing. The dominant-negative version of MEF2 encodes for amino acids (aa) 1 to 117. pWZL-HDAC4-TMΔMEF2 was generated in two steps. The N terminus (aa 1 to 166 and aa 184 to 221) was generated by PCR and cloned into pcDNA3+ (EcoRI/BamHI and BamHI/SalI). Finally, fragment 1-221 was subcloned into pWZL-HDAC4-TM-GFP restricted by using Eco-SalI. Silencing of NIH 3T3 and IMR90-E1A were performed with 70 μM small interfering RNA (siRNA; Invitrogen).

Immunofluorescence and immunoblotting. Cells were fixed with 3% paraformaldehyde and permeabilized with 0.1% Triton X-100. The secondary antibodies were Alexa Fluor 488-, 546-, or 633-conjugated anti-mouse and anti-rabbit secondary antibodies (Molecular Probes). Actin was labeled with phalloidin-AF546 (Molecular Probes) or phalloidin-ATTO 665 (Sigma-Aldrich). The cells were imaged with a Leica confocal scanner SP equipped with a 488 λ Ar laser and a 543 to 633 λ HeNe laser.

Cell lysates after SDS-PAGE and immunoblotting were incubated with primary antibodies. Secondary antibodies were obtained from Sigma-Aldrich, and blots were developed with Super Signal West Dura (Pierce). For antibody stripping, blots were incubated for 30 min at 60°C in stripping solution containing 100 mM β-mercaptoethanol.

RNA extraction and quantitative qRT-PCR. Cells were lysed using Tri-Reagent (Molecular Research Center). A total of 1 μg of total RNA was retrotranscribed by using 100 U of Moloney murine leukemia virus reverse transcriptase (Invitrogen). Quantitative reverse transcription-PCR (qRT-PCR) analyses were performed using Bio-Rad CFX96 and SYBR Green technology. The data were analyzed by use of a comparative threshold cycle using β_2-microglobulin, HPRT (hypoxanthine phosphoribosyltransferase), and β-actin as normalizer genes. All reactions were done in triplicate.

Adhesion and random motility measurements. Random motility was assayed by time-lapse video microscopy as previously described (9). To study adhesion and spreading, plates were coated with 10 μg of fibronectin/ml or bovine serum albumin (BSA; Sigma-Aldrich). Cells were seeded at 6×10^4/ml and, after 10 min, time-lapse analysis was performed. Time-lapse images were analyzed by using Metamorph software (Molecular Devices) and ImageJ. The results are pooled from eight independent experiments.

Soft agar and tumorigenicity assays. Equal volumes of 1.2% agar and DMEM were mixed to generate 0.6% base agar. A total of 10^5 NIH 3T3, BALB/c 3T3, or sarcoma cells expressing the different transgenes were seeded in 0.3% top agar, followed by incubation at 37°C in humidified conditions. The cells were grown for 15 days, and the culture medium was changed twice per week. Foci were visualized by using MTT staining. For tumorigenicity assays, 400,000 cells expressing the different transgenes were injected subcutaneously into immunocompromised nude mice. In parallel, 100,000 cells of the same cell suspension were plate counted 24 h after plating to check for equal number injection and cell viability. The tumor size was monitored twice per week.

RNA expression array and data analysis. Total RNA was isolated by using RNeasy (Qiagen). RNA samples were labeled according to the standard one-cycle amplification and labeling protocol (Affymetrix, Santa Clara, CA). Labeled cRNAs were hybridized on Affymetrix GeneChip Gene 1.0 ST mouse arrays. Scanning was performed using a GeneChip Scanner 3000 7G (Affymetrix), whereas Microarray Analysis Suite 5.0 software (Affymetrix) was used for preliminary data analysis. One-way analysis of variance was applied to replicates to discard missense gene expression values. We adopted a cutoff of 1.5 for the fold change. Gene set enrichment analysis (GSEA) (30) was used to investigate putative statistical association between genes modulated by HDAC4 and genes perturbed by other signal transduction pathways. The HDAC4 signature was used to interrogate 3,272 curated MSigDB gene sets and 91 data sets available on the GEO database (http://www.ncbi.nlm.nih.gov/geo/) and coming from DNA microarray experiment on murine fibroblasts. For the analysis, the maximum value of each probe was chosen; the ranking was done according to a signal-to-noise metric, and 1,000 permutations were used to generate the null distribution.

HDAC assay. HDAC assay was performed using a fluorogenic assay kit, the Fluor de Lys-Green HDAC assay (BIOMOL), according to manufacturer's instructions. Briefly, HDAC4 immunoprecipitates were resuspended in the HDAC assay buffer and incubated with Fluor de Lys-Green substrate for 30 min at 37°C. The fluorogenic reaction was triggered by adding developer according to the manufacturer's instructions, and the fluorescence was measured after 15 min and stopped with trichostatin A (TSA). HDAC inhibitor TSA (40 μM) was used as an internal control to measure the background signal. A total of 1.5 μg of anti-HDAC4 and anti-USP33, as a control IgG, were used for immunoprecipitations.

Chromatin immunoprecipitation. For each chromatin immunoprecipitation, 4.5×10^6 cells were used. DNA-protein complexes were cross-linked with 1% formaldehyde (Sigma-Aldrich) in phosphate-buffered saline (PBS) for 15 min at room temperature. After quenching and two washes in PBS, the cells were collected and then lysed for 10 min with lysis buffer (5 mM PIPES, 85 mM KCl, 0.5% NP-40) containing protease inhibitor cocktail (Sigma-Aldrich). The pellets were resuspended in RIPA-100 and sonicated using a Bioruptor UCD-200 (Diagenode) with pulses of 30 s for 15 min, resulting in an average size of ~500 bp for genomic DNA fragments. Samples were precleared and immunoprecipitated overnight with 2 μg of anti-GFP or anti-USP33 antibodies, followed by incubation with protein A blocked with BSA and salmon sperm DNA (1 μg/μl) at 4°C for 2 h. Beads and inputs were treated with proteinase K overnight at 68°C to degrade proteins and reverse cross-linking. Genomic DNA was finally purified with Qiagen QIAquick PCR purification kit and eluted in 65 μl of water.

FIG 1 Morphological changes in cells expressing HDAC4/TM. (A) Confocal pictures of NIH 3T3 cells expressing GFP and the different chimeras. Immunofluorescence analysis was performed to visualize HRasV12. AF546-phalloidin was used to decorate F-actin. Scale bar, 50 μm. (B) Immunoblot assays were performed to visualize the different transgenes. The antibodies used were anti-GFP to detect GFP and HDAC4-GFP, anti-HRas, and anti-Erks as a loading control. (C) qRT-PCR analysis was performed to quantify mRNAs levels of the HDAC4-target gene, *Klf2*. *Gapdh* was used as a control gene. The *Klf2* mRNA levels were relative to GFP-expressing cells. (D) Confocal pictures of cells expressing GFP, GFP-HDAC4/WT, and GFP-HDAC4/TMi2. Immunofluorescence analysis was performed to visualize paxillin subcellular localization. AF546-phalloidin was used to decorate F-actin. Scale bar, 50 μm. (E) NIH 3T3 cells expressing HDAC4/WT, HDAC4/TMi2, or GFP were plated onto BSA- or fibronectin-covered dishes and subjected to time-lapse analysis for the indicated times. The data are presented as the average areas. (F) At 24 h after seeding, NIH 3T3 cells expressing HDAC4/WT, HDAC4/TMi2, or GFP were subjected to time-lapse analysis for 6 h. The data are presented as the average migration rates. (G) qRT-PCR analysis was performed to quantify *Klf2* mRNAs after the transfection of cells expressing HDAC4/TMi2 with siRNA against HDAC4 or control siRNA. *Klf2* mRNA levels were relative to GFP-expressing cells. Immunoblotting was performed with anti-GFP antibodies to prove the siRNA efficiency. (H) Confocal pictures of cells expressing HDAC4/TMi2 transfected with siRNAs against HDAC4 or control siRNA. Immunofluorescence analysis was performed as described in panel D. Scale bar, 50 μm. *, $P < 0.05$; ***, $P < 0.001$.

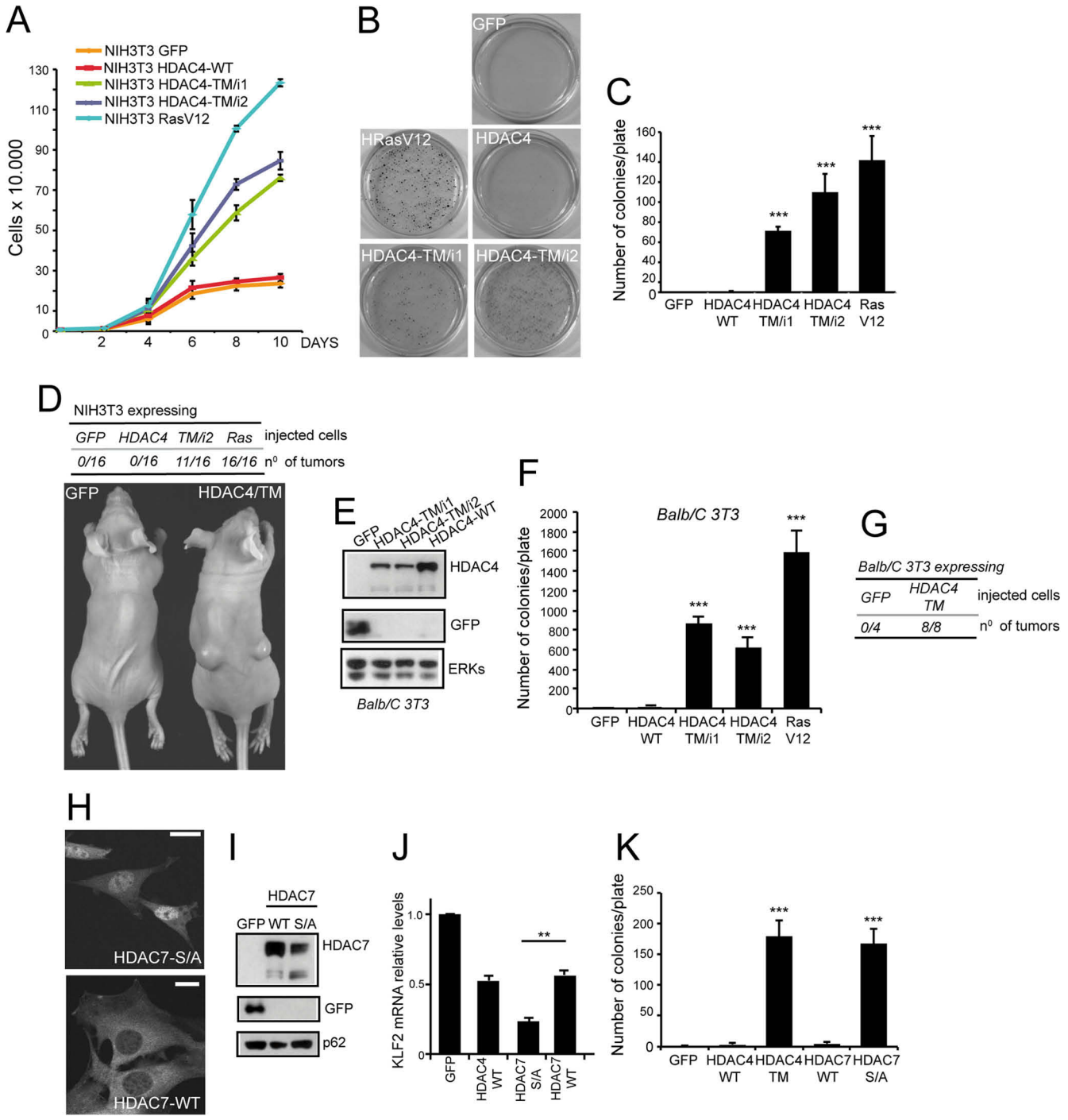

FIG 2 Transforming ability of HDAC4/TM. (A) NIH 3T3 cells expressing the indicated transgenes were grown in DMEM supplemented with 10% FBS. (B) Growth in soft agar of NIH 3T3 expressing the indicated transgenes, foci were stained with MTT. (C) Quantitative results of colony formation. (D) Analysis of the tumorigenic properties of NIH 3T3 cells expressing the indicated genes when injected into immunocompromised nude mice. HDAC4/TM-expressing cells generate tumors, with nodules becoming palpable ~20 days later compared to HRasV12-transformed cells. Pictures were obtained at week 6. (E) Immunoblot assays were performed to visualize the different transgenes expressed in the BALB/c 3T3 cell lines. The antibodies used were anti-GFP to detect GFP and HDAC4-GFP. Anti-Erks antibody was used as a loading control. (F) Quantitative results of colony formation in soft agar of BALB/c cells expressing the indicated transgenes. (G) Analysis of the tumorigenic properties of BALB/c 3T3 cells expressing the indicated genes when injected into immunocompromised nude mice. (H) Confocal pictures of NIH 3T3 cells expressing GFP chimeras of HDAC7-WT and a mutant defective in the four serine binding sites for 14-3-3 proteins (HDAC7-S/A). Scale bar, 50 μm. (I) Immunoblot assays were performed to visualize the different transgenes expressed in the NIH 3T3 cell lines. The antibodies used were anti-GFP to detect GFP, HDAC7-WT, and HDAC7-S/A. Anti-p62 antibody was used as a loading control. (J) qRT-PCR analysis was performed to quantify mRNAs levels of *Klf2*. *Gapdh* was used as control gene. *Klf2* mRNA levels were relative to GFP-expressing cells. (K) Quantitative results of colony formation in soft agar of NIH 3T3 cells expressing the indicated transgenes. **, $P < 0.01$; ***, $P < 0.001$.

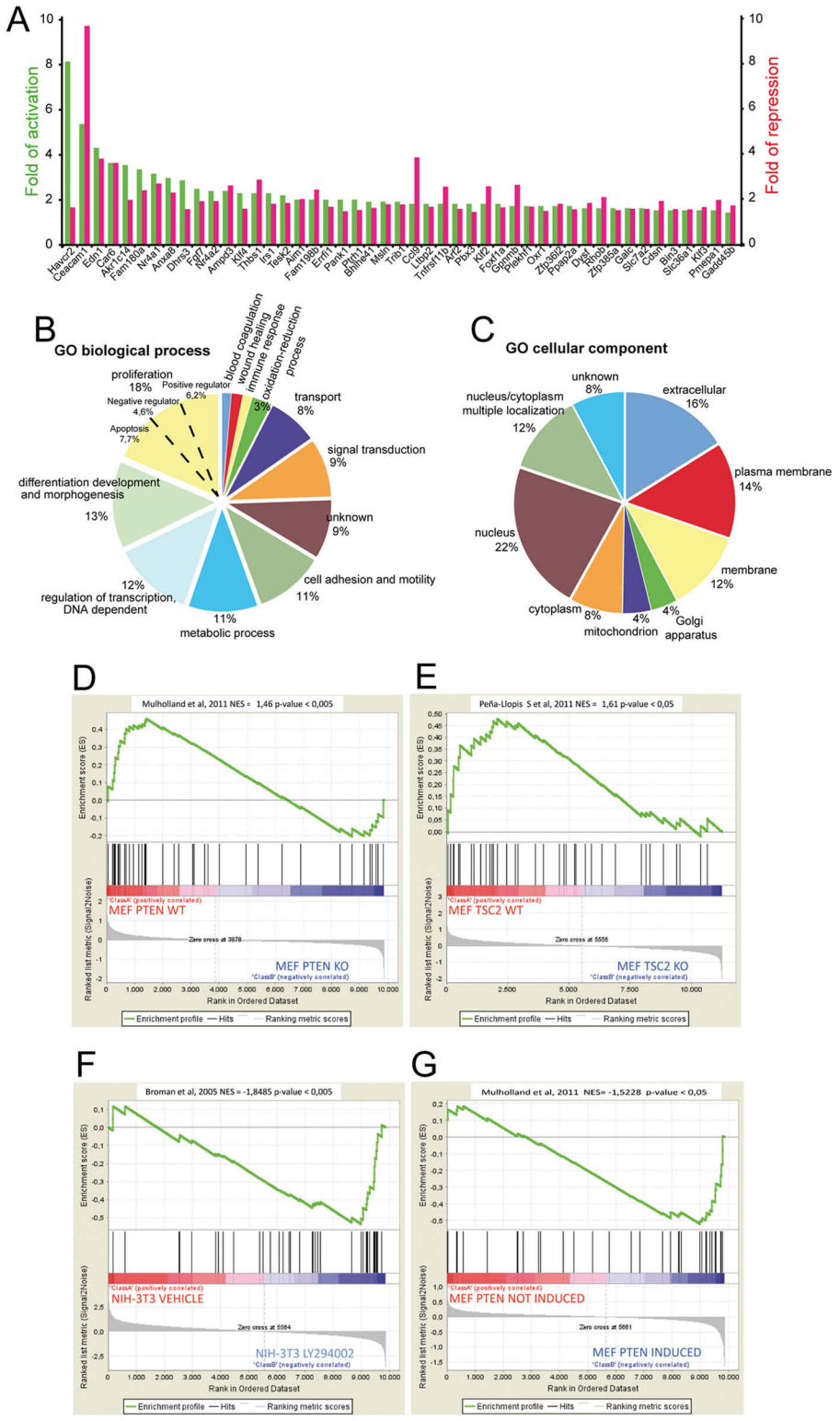

FIG 3 Identification of genes repressed by HDAC4/TM. (A) Diagram representation of the HDAC4/TM target genes. Microarray analyses were performed on GFP- and HDAC4/TM-expressing cells (repressed genes are indicated in red) and in HDAC4/TM cells transfected with control siRNA and the same cells transfected with a siRNA against human HDAC4 (induced genes are indicated in green). (B) Gene ontology (GO) analysis using the PANTHER database was performed to interpret the biological processes under the regulation of the 47 genes repressed by HDAC4. (C) GO analysis using the PANTHER database was performed to classify the 47 genes repressed by HDAC4 in terms of subcellular localization. (D to G) GSEA plots show the enrichment of HDAC4-repressed genes among protein coding genes ranked according to PTEN and TSC2 status and the fold change in LY-treated cells versus control cells. See Materials and Methods for details.

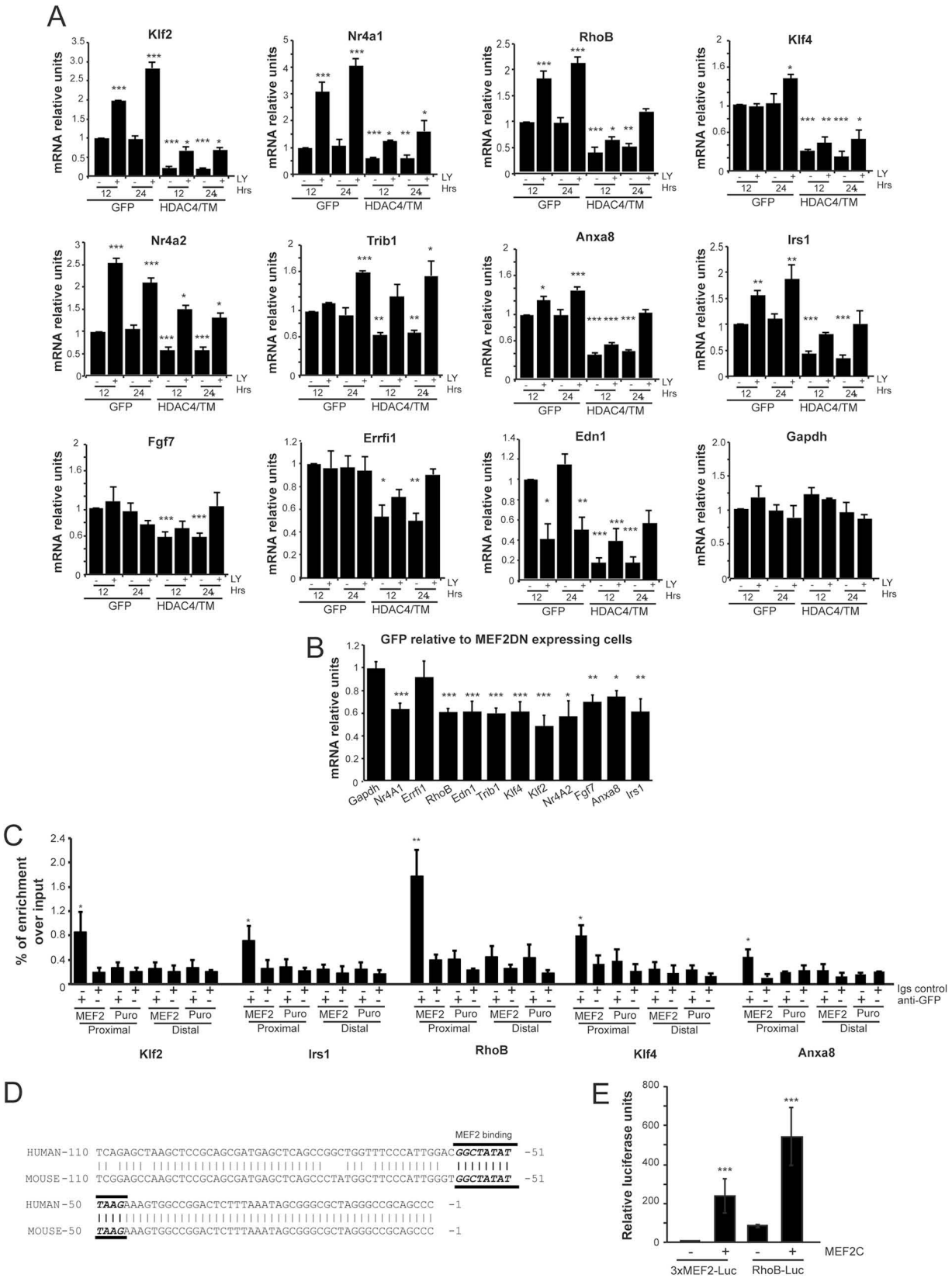
A
Klf2
Nr4a1
RhoB
Klf4
Nr4a2
Trib1
Anxa8
Irs1
Fgf7
Errfi1
Edn1
Gapdh
mRNA relative units
LY
Hrs
GFP
HDAC4/TM
B
GFP relative to MEF2DN expressing cells
mRNA relative units
Gapdh
Nr4A1
Errfi1
RhoB
Edn1
Trib1
Klf4
Klf2
Nr4A2
Fgf7
Anxa8
Irs1
C
% of enrichment over input
MEF2
Puro
Proximal
Distal
Igs control
anti-GFP
Klf2
Irs1
RhoB
Klf4
Anxa8
D
MEF2 binding
HUMAN-110 TCAGAGCTAAGCTCCGCAGCGATGAGCTCAGCCGGCTGGTTTCCCATTGGAC GGCTATAT -51
MOUSE-110 TCGGAGCCAAGCTCCGCAGCGATGAGCTCAGCCCTATGGCTTCCCATTGGGT GGCTATAT -51
HUMAN-50 TAAGAAAGTGGCCGGACTCTTTAAATAGCGGGCGCTAGGGCCGCAGCCC -1
MOUSE-50 TAAGAAAGTGGCCGGACTCTTTAAATAGCGGGCGCTAGGGCCGCAGCCC -1
E
Relative luciferase units
MEF2C
3xMEF2-Luc
RhoB-Luc

Reporter gene assay. The promoter of *RhoB* (300 bp) was cloned from NIH 3T3 genomic DNA by PCR into the pGL3 plasmid. The following oligonucleotides were used: *RhoB*_FW_XhoI, 5′-ATC CTC GAG CAA TCG GAG CCA AGC TCC GC-3′; and *RhoB*_RV_HindIII, 5′-ATC AAG CTT GAG CTG GCC GGG CGC GGG CA-3′. IMR90-E1A cells were transfected at 30 to 40% confluence with the indicated mammalian expression plasmids. In the LY experiments, cells were collected 12 h after transfection, split into two plates, and treated after 6 h with LY-294002 or DMSO. The luciferase activity was measured and normalized for *Renilla* luciferase activity using the dual-luciferase reporter assay system according to the vendor's instructions (Promega). The empty vectors pEGFP or pUSE were used to normalize the total amounts of transfected DNA.

Immunoprecipitation. Coimmunoprecipitations were performed as previously described (9). Briefly, cells were collected directly from culture dishes into radioimmunoprecipitation assay buffer (50 mM Tris-HCl [pH 8], 150 mM NaCl, 0.2% SDS, 1% NP-40, 0.5% sodium deoxycholate) and supplemented with protease inhibitors. Lysates were incubated for 5 h with the antibody against green fluorescent protein (GFP). After 1 h of incubation with protein A-beads (GE), several washes were performed. Samples were resolved by SDS-PAGE and analyzed by immunoblotting.

Bioinformatics analysis. To analyze MEF2 target gene expression in human cancers, the presence of a putative MEF2 binding site in the proximal promoters was scored using Cister (zlab.bu.edu/~mfrith/cister.shtml). Among our list of 29 human MEF2 target genes, we selected 25 that have good-quality probes and a proximal MEF2 binding site. For this analysis, 40 human cancer data sets available on GEO were selected according to sample abundance and the platform used (Affymetrix Human Genome U95 version 2 array; Affymetrix Human Genome U133B/Plus2). The data from each DNA microarray experiment were considered separately and were $\log_2$ transformed, normalized at the probe set level, and median centered. In the case of multiple probe sets, we discarded any that could hybridize with other transcripts, in addition to the expected level for >33% of the probes (scored using PLANdbAffy [http://affymetrix2.bioinf.fbb.msu.ru] [31] and Genecruiser [http://genecruiser.broadinstitute.org]). In the case of missing information about a probe set, we used the class A probe set according to the NetAffy (www.affymetrix.com/analysis/index.affx) classification. We then collapsed the multiple values of each gene by averaging them.

The median values representing this signature in each sample were plotted, resulting in a series of box plots. The significance was calculated considering as positive events the samples in which the median of the 25 MEF2 genes is less than zero and applying a Poisson test of significance. The resulting *P* value was corrected for multiple testing by applying Holm-Bonferroni correction ($P < 0.05$). For correlation analysis, the Spearman rank correlation coefficient and the corresponding statistical significance were calculated using the R package.

Tissue array construction and immunohistochemistry. Paraffin-embedded samples from leiomyosarcoma were available from 26 patients. All cases were histologically and immunohistochemically validated. Multiple tissue cores (three per sample) with a diameter of 1 mm were taken by using a Tissue Arrayer (TMA Master 3dHistech) and arrayed on a recipient block according to standard procedures. Immunohistochemistry for HDAC4 (1:100) was performed by using an automated immunostainer (Autostainer; Dako Cytomation). Antigen retrieval was performed with citrate buffer at pH 6 for HDAC4 and at pH 9 with EnVision FLEX target retrieval solution (Dako Cytomation), respectively. As a negative control, sections were stained without adding the primary antibody. Slides were independently evaluated by two observers. All tumors were scored for the intensity of signal (scoring range: 0 = no expression; 1 = weak expression; 2 = moderate expression; 3 = strong expression). The presence of subcellular localization (i.e., nuclear or cytoplasmic) was recorded as well. Mean intensities and percentages of duplicate cores were used for the final analysis.

Statistics. For experimental data, a Student *t* test was used. A *P* value of <0.05 was chosen as the statistical limit of significance. Unless otherwise indicated, all of the data in the figures are arithmetic means ± the standard deviations from at least three independent experiments.

RESULTS

Nucleus-localized HDAC4 triggers morphological changes and increased proliferation in NIH 3T3 cells. To investigate the role of HDAC4 in the control of cell growth and proliferation, we engineered NIH 3T3 cells to express GFP-tagged HDAC4/WT or its nucleus-localized version (TM), which is defective in 14-3-3 binding. This mutant, by mimicking the dephosphorylated form (Ser/Ala mutations) of the deacetylase, displays nuclear localization and exhibits increased repressive transcriptional activity (12, 13). NIH 3T3 cells expressing oncogenic HRasV12 or GFP were used as positive and negative controls, respectively. Two independent infections with the TM allele were exploited (TM/i1 and TM/i2).

Immunofluorescence analysis proved that HDAC4/WT is mainly cytosolic (Fig. 1A) and subjected to nuclear/cytoplasmic shuttling (data not shown). In contrast, the TM mutant is predominantly nuclear, with some cells showing pan/cytoplasmic localization. Figure 1B illustrates the expression levels of the different transgenes. In general HDAC4/TM was expressed to less extent compared to the WT.

The repressive influence of HDAC4 was then measured by using an MEF2 target, the transcription factor *Klf2* (24) (Fig. 1C). qRT-PCR experiments demonstrated that in HDAC4 expressing cells *Klf2* mRNA is reduced and, as expected, the TM mutant is a more potent repressor. *Klf2* mRNA levels were also decreased in cells expressing HRasV12.

Morphological inspection of engineered cells revealed that whereas no relevant changes in cell shape were detectable after ectopic expression of the WT allele, the expression of the nuclear allele (both TM/i1 and TM/i2) resulted in the gain of a spindle-like morphology, characterized by reduced size and reduced spreading/adhesion (Fig. 1A and D). Moreover, the nuclear allele promoted an overt reorganization of actin cytoskeleton characterized by the loss of stress fibers and by an increase in membrane ruffles.

To gain more insight into the morphological changes induced by HDAC4/TM we compared the organization of focal adhesions (FA) in the different cell lines. Since TMi1 and TMi2 evidenced the same morphological changes but TMi2 expressed a higher level of

FIG 4 Several HDAC4-repressed genes are MEF2 targets. (A) The mRNA expression levels for 11 HDAC4 target genes and *Gapdh*, as a control, were measured using qRT-PCR in GFP- and HDAC4/TM-expressing cells. Cells were also treated with LY for 12 or 24 h. The mRNA levels were relative to untreated GFP-expressing cells. (B) The mRNA expression levels of 11 HDAC4 target genes were measured using qRT-PCR in GFP- and MEF2DN-expressing cells. (C) Chromatin immunoprecipitation of NIH 3T3 cells overexpressing MEF2-GFP or control Puro. Chromatin was immunoprecipitated with anti-GFP antibody or anti-USP33 (2 μg) as a control. For each of the genes examined, we compared the fold enrichment over input (1/100) between the proximal (1 to 1,000 bp) and the distal (>3,000 bp) promoters, as indicated. (D) Nucleotide sequence analysis of the human and mouse *RhoB* proximal promoters. The putative MEF2 binding site is underlined. (E) Relative luciferase activity after cotransfection in IMR90-E1A cells of the reporter plasmids p*RhoB-Luc* (−300/−1) and p3×MEF2-luc, together with *MEF2C*, as indicated. The *Renilla* luciferase plasmid was used as an internal control. *, $P < 0.05$; **, $P < 0.01$; ***, $P < 0.001$.

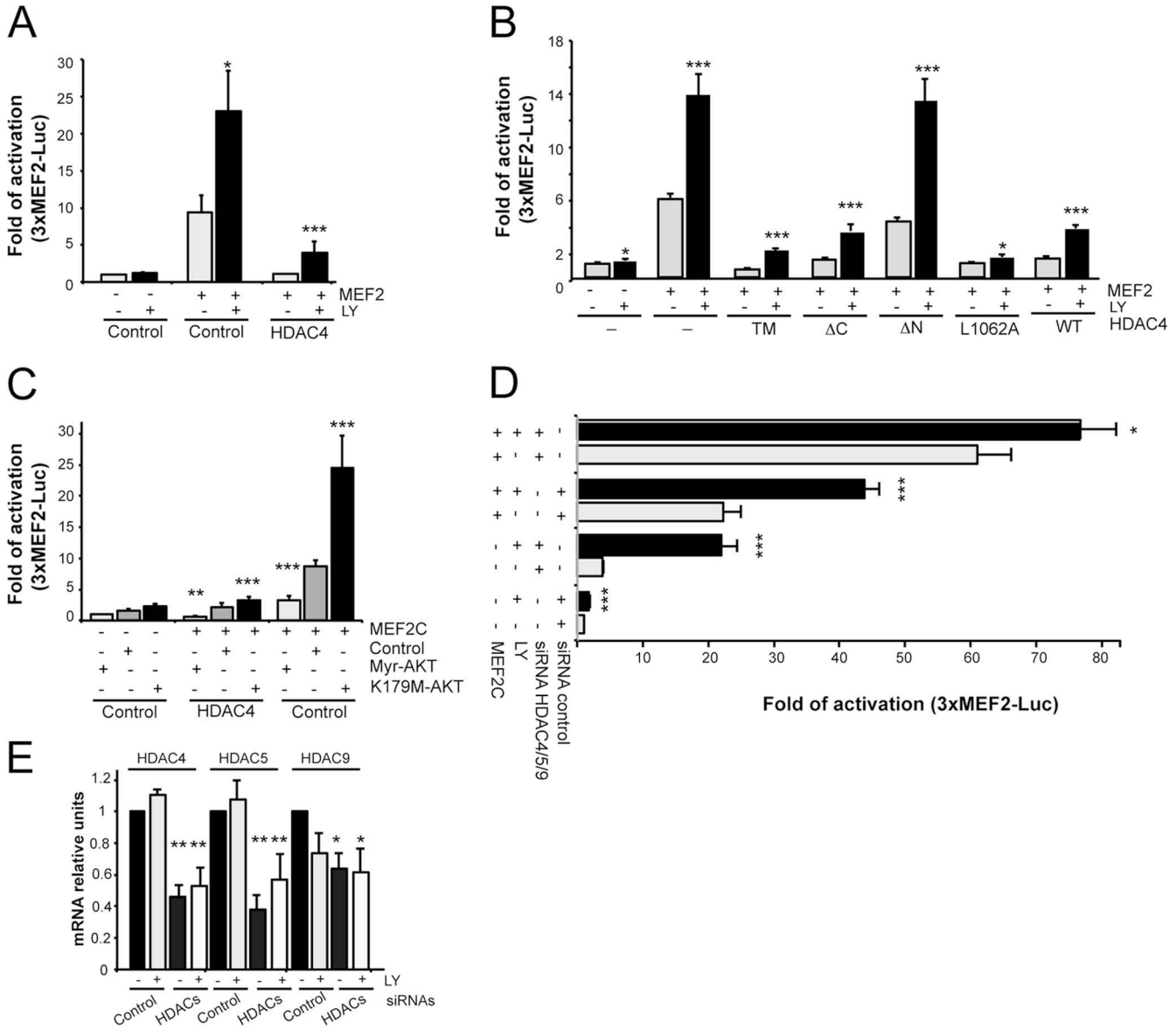

FIG 5 Regulation of the MEF2-dependent transcription by the PI3K/Akt pathway. (A) IMR90-E1A cells were transfected with the 3×MEF2-Luc (1 μg), the internal control pRL-CMV (20 ng), pcDNA3.1-HA-MEF2C (1 μg), and 300 ng of pEGFP expressing HDAC4. Cells were treated or not for 24 h with LY. (B) IMR90-E1A cells were transfected as in panel A, together with the indicated HDAC4 mutants. Cells were treated or not for 24 h with LY. (C) IMR90-E1A cells were transfected with the 3×MEF2-Luc (1 μg), the internal control pRL-CMV (20 ng), pcDNA3.1-HA-MEF2C (1 μg), and 1 μg of pUSE vectors expressing Myr-Akt or its catalytically inactive point mutant K179M. (D) IMR90-E1A cells transfected with siRNAs against HDAC4, HDAC5, and HDAC9 or with the same amount of a control siRNA were cotransfected after 12 h with 3×MEF2-Luc (1 μg), the internal control pRL-CMV (20 ng), and eventually pcDNA3.1-HA-MEF2C (1 μg), as indicated. After 12 h, the cells were split into two plates and treated or not for 24 h with LY. (E) qRT-PCR analysis was performed to quantify the mRNA levels of *HDAC4*, *HDAC5*, and *HDAC9* in IMR90-E1A cells, cotransfected with the indicated siRNAs. *GAPDH* was used as a control gene. *, $P < 0.05$; **, $P < 0.01$; ***, $P < 0.001$.

the transgene and more efficiently repressed *Klf2* expression, we used TMi2 for the subsequent analysis. In GFP- and HDAC4-expressing cells, paxillin marking FA is localized at the cell periphery, with distinct punctate staining (Fig. 1D). In contrast, in HDAC4/TM cells, a prominent diffuse staining of paxillin is evident, thus confirming the profound changes of actin cytoskeleton and of FA.

To quantify the differences in adhesion/spreading elicited by HDAC4/TM, we analyzed the behavior of the three cell lines when plated onto BSA or fibronectin. Figure 1E demonstrates that HDAC4/TM cells evidence a restricted spreading under both conditions. Defects in cells spreading could be responsible for the reduced size observed in Fig. 1A/D.

HDAC4 can influence cell motility (9). Since we have observed an insightful rearrangement of actin cytoskeleton in HDAC4/TM cells, we compared the random cell motility of the different cell lines by performing a time-lapse microscopy analysis. Figure 1F shows that HDAC4/WT-expressing cells increase motility to 0.78 μm/min (standard error of the mean [SEM] = 0.026; $n = 141$) compared to GFP-expressing cells

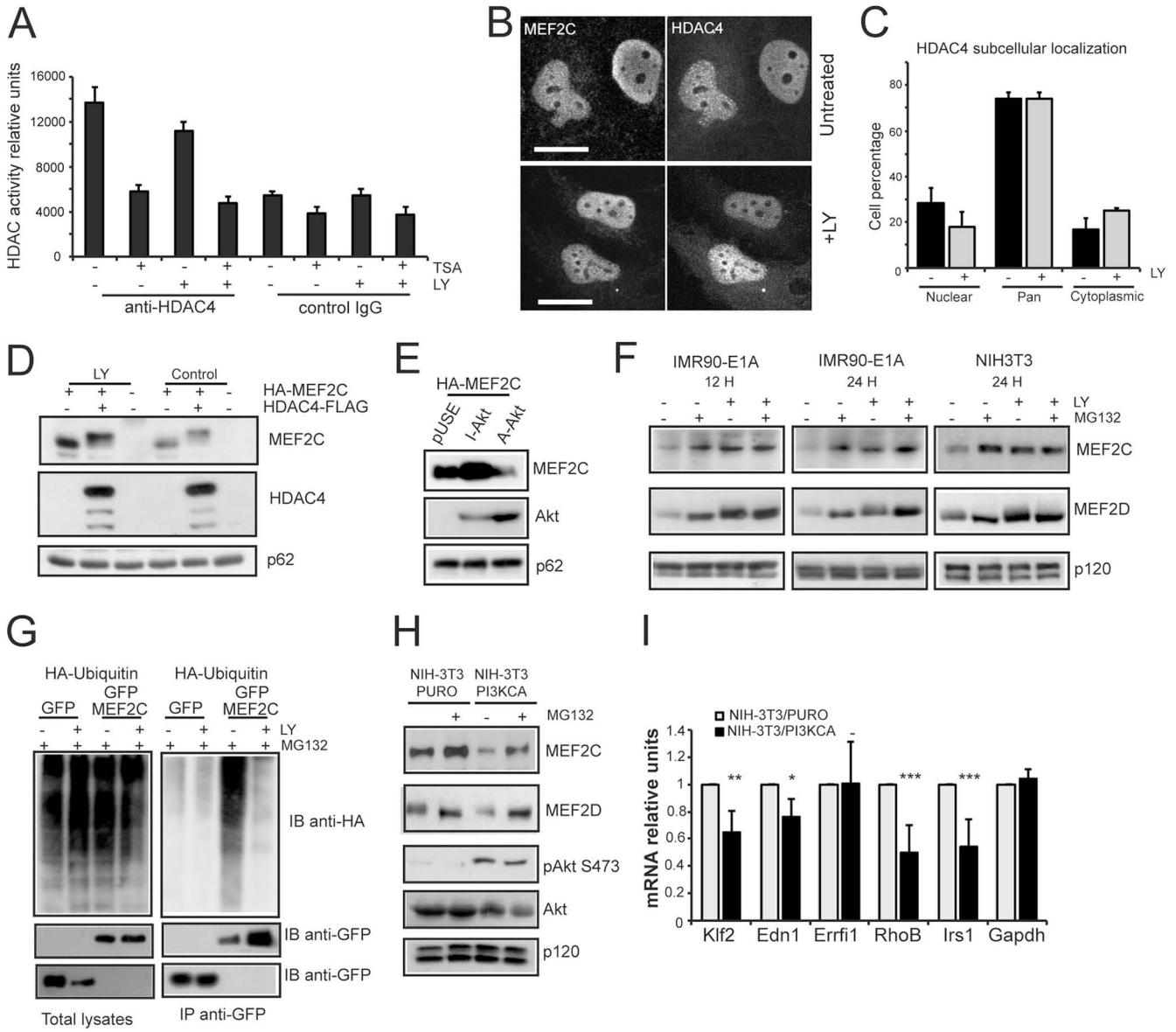

FIG 6 The PI3K/Akt pathway influences MEF2 protein stability. (A) HDAC4 was immunoprecipitated from NIH 3T3 cells treated or not for 18 h with LY. The HDAC activity was measured 15 min after the addition of the developer. (B) Confocal pictures of IMR90-E1A cells transfected with pcDNA3.1-HA-MEF2C (1 μg) and pEGFPN1-HDAC4 (300 ng) and treated or not with LY for 24 h. Immunofluorescence analysis was performed to visualize HDAC4 and MEF2C subcellular localization. Scale bar, 50 μm. (C) Quantification of endogenous HDAC4 subcellular localization in IMR90-E1A cells after the treatment with LY or DMSO for 24 h. For each experiment, at least 200 cells were counted ($n = 3$). (D) IMR90-E1A cells were transfected with pcDNA3.1-HA-MEF2C (1 μg), and 300 ng of pEGFP expressing HDAC4, as indicated. After 12 h, cells were harvested, split into two plates and treated with the PI3K inhibitor LY. After 24 h, cellular lysates were generated and subjected to immunoblot analysis using the anti-GFP and the anti-HA antibodies. Nucleoporin (p62) was used as loading control. (E) IMR90-E1A cells were transfected with pcDNA3.1-HA-MEF2C (1 μg), and 1 μg of pUSE vectors expressing Myr-Akt or its catalytically inactive point mutant K179M. After 24 h, cellular lysates were generated and subjected to immunoblot analysis with the anti-Akt and the anti-HA antibodies. Nucleoporin (p62) was used as loading control. (F) Immunoblot analysis of MEF2 family members in IMR90-E1A and NIH 3T3 cells treated with LY and the proteasome inhibitor MG132 as indicated. p120 was used as loading control. (G) IMR90-E1A cells were cotransfected with HA-ubiquitin and MEF2C-GFP or GFP. After 24 h, the cells were treated or not for 12 h with LY, followed by 12 h with MG132. GFP fusions were immunoprecipitated with an antibody to GFP and subjected to immunoblotting with an antiubiquitin antibody. After being stripped, the filter was probed with an anti-GFP antibody. Inputs have been included. (H) Immunoblot analysis of MEF2C and MEF2D levels in NIH 3T3 cells expressing the catalytically active PI3K (PI3KCA) treated with MG132 as indicated. Cellular lysates were generated and subjected to immunoblot analysis with the specific antibodies. The Akt phosphorylation levels were also probed. p120 was used as a loading control. (I) mRNA expression levels of selected MEF2-HDAC4 target genes and *Gapdh*, as a control, were measured using qRT-PCR in NIH 3T3 cells expressing PI3KCA or Puro. Samples were normalized to HPRT, GAPDH, and β-actin. *, $P < 0.05$; **, $P < 0.01$; ***, $P < 0.001$.

(0.56 μm/min; SEM = 0.02; $n = 136$). This increase is significantly more pronounced in cells expressing HDAC4/TM (1.15 μm/min; SEM = 0.04; $n = 171$).

To confirm that the observed changes were elicited by HDAC4/TM, we silenced its expression using a human specific siRNA. The efficiency of silencing was proved by immunoblotting and by augmented *Klf2* expression (Fig. 1G). The downregulation of HDAC4/TM led to a reversion to the morphological changes de-

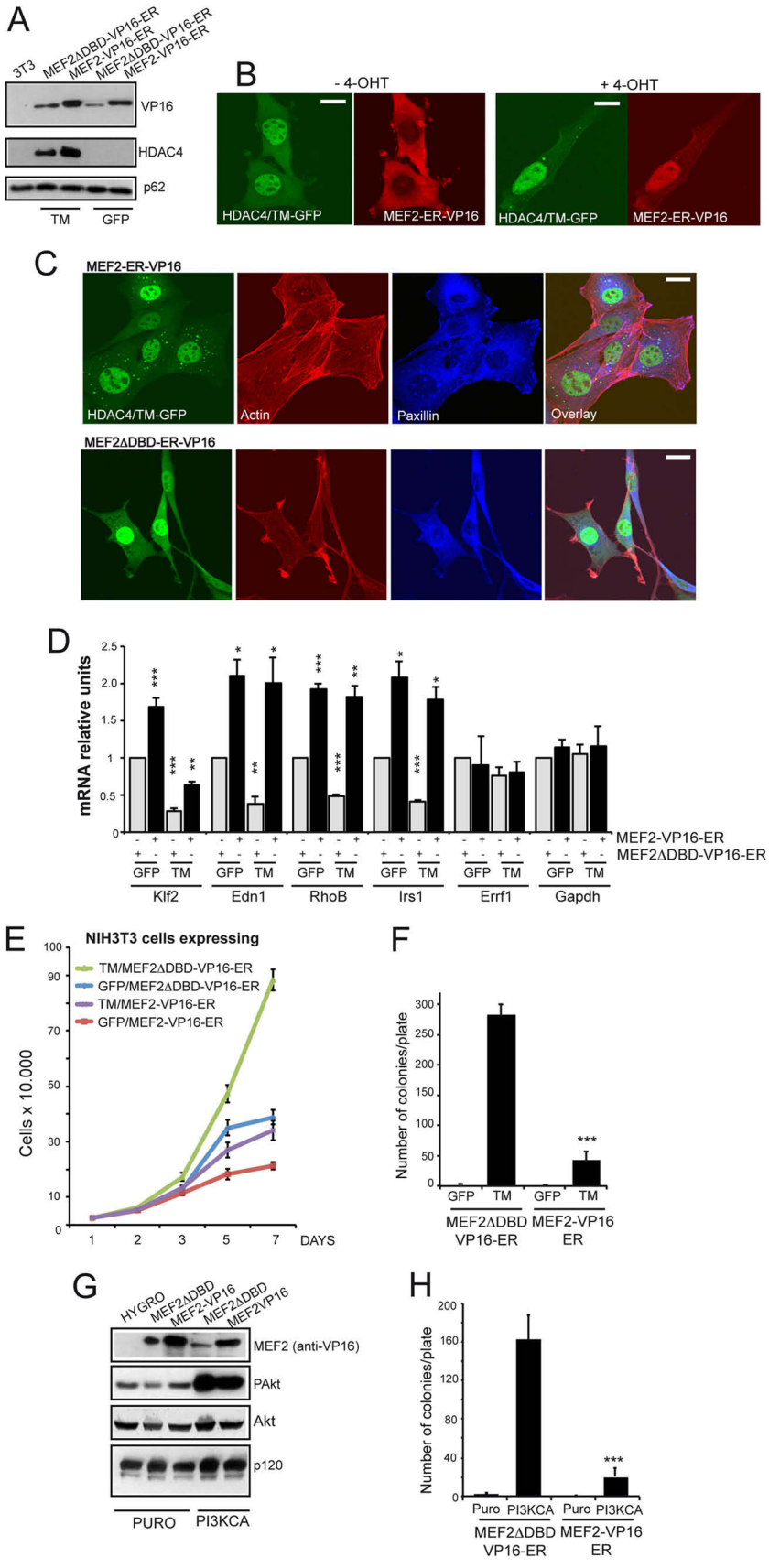
A
3T3
MEF2ΔDBD-VP16-ER
MEF2-VP16-ER
MEF2ΔDBD-VP16-ER
MEF2-VP16-ER
VP16
HDAC4
p62
TM
GFP
B
- 4-OHT
+ 4-OHT
HDAC4/TM-GFP
MEF2-ER-VP16
HDAC4/TM-GFP
MEF2-ER-VP16
C
MEF2-ER-VP16
HDAC4/TM-GFP
Actin
Paxillin
Overlay
MEF2ΔDBD-ER-VP16
D
mRNA relative units
2.5
2.0
1.5
1
0.5
0
MEF2-VP16-ER
MEF2ΔDBD-VP16-ER
GFP
TM
Klf2
Edn1
RhoB
Irs1
Errf1
Gapdh
E
NIH3T3 cells expressing
TM/MEF2ΔDBD-VP16-ER
GFP/MEF2ΔDBD-VP16-ER
TM/MEF2-VP16-ER
GFP/MEF2-VP16-ER
Cells x 10.000
100
90
70
50
30
10
0
1
2
3
5
7
DAYS
F
Number of colonies/plate
300
250
200
150
100
50
0
GFP
TM
GFP
TM
MEF2ΔDBD VP16-ER
MEF2-VP16 ER
G
HYGRO
MEF2ΔDBD
MEF2-VP16
MEF2ΔDBD
MEF2VP16
MEF2 (anti-VP16)
PAkt
Akt
p120
PURO
PI3KCA
H
Number of colonies/plate
200
160
120
80
40
0
Puro
PI3KCA
Puro
PI3KCA
MEF2ΔDBD VP16-ER
MEF2-VP16 ER

scribed above. The cells increase spreading, rebuild stress fibers, and reorganize FA (Fig. 1H).

HDAC4/TM induces cell transformation and tumorigenesis. The altered morphology and the increased motility of cells expressing HDAC4/TM are reminiscent of a transformed phenotype. Moreover, the two cell lines expressing the TM allele have a proliferative potential greater than cells expressing GFP or HDAC4/WT, overcoming the contact inhibition, similarly to HRasV12 transformed cells (Fig. 2A). To assess whether TM-expressing cells acquire parameters of transformation, we investigated their ability to form colonies in soft agar (Fig. 2B and C). Cells expressing HDAC4/TM but not GFP or HDAC4/WT developed large colonies in soft agar, similarly to HRasV12-expressing cells. In summary, HDAC4/TM dismisses contact-dependent inhibition and confers anchorage-independent growth. Finally, HDAC4/TM-engineered NIH 3T3 cells but not GFP or HDAC4/WT cells generated tumors when subcutaneously injected into athymic nude mice (Fig. 2D).

The oncogenic properties of the HDAC4/TM allele were confirmed also in BALB/c 3T3 cells, ruling out the possibility that the observed phenotypes were context dependent (Fig. 2E to G). As expected, HDAC4/WT was largely cytoplasmic, whereas the TM mutant accumulated in the nucleus (data not shown). HDAC4/TM-expressing but not HDAC/WT- or GFP-expressing BALB/c 3T3 cells were able to grow in soft agar (Fig. 2F). When BALB/c 3T3 cells expressing HDAC4/TM were subcutaneously injected into nude mice, they efficiently generated tumors (Fig. 2G).

To understand whether HDAC4 shares with other class IIa members this prooncogenic activity, we generated NIH 3T3 cells expressing HDAC7/WT or its nucleus-localized version (S/A), which is defective in all four serine binding sites for 14-3-3 proteins (32). Similar to HDAC4/TM, HDAC7-S/A was mostly nuclear (Fig. 2H) and, although expressed to a lower extent compared to the cytosolic HDAC7/WT (Fig. 2I), it exerted a stronger repression on *Klf2* expression (Fig. 2J). HDAC7-S/A cells mimicked the morphological changes observed in HDAC4/TM-expressing cells (data not shown). Moreover, similar to HDAC4/TM, HDAC7-S/A conferred the NIH 3T3 transformed phenotype and anchorage-independent growth capability (Fig. 2K). Overall, our findings suggest that nucleus-resident class IIa HDACs can elicit tumorigenic conversion of immortalized mouse fibroblasts.

Identification of genes under the influence of HDAC4. To identify key mediators of class II HDAC oncogenic properties, the transcriptional expression profiles of HDAC4/TM and HDAC4/GFP were compared. To further corroborate our results, microarray analysis was also performed when HDAC4 expression was silenced in TM cells. In this manner, we identified 47 genes whose expression is both repressed in HDAC4/TM cells, compared to GFP cells, and induced in HDAC4/TM cells after HDAC4 silencing (Fig. 3A).

We next examined the publicly available databases Gene Ontology (www.geneontology.com) and Panther (www.pantherdb.org) to assess the representation of different biological functions among genes repressed by HDAC4/TM (Fig. 3B). The top-ranking GO biological functions were proliferation (18%) and differentiation/development/morphogenesis (13%). Interestingly, the third category was the regulation of transcription/DNA binding, and the top GO subcellular component is the nucleus (22%) (Fig. 3C). These evidences indicate that HDAC4 profoundly reprograms the expression profile and thus the cell fate. Not surprisingly, several transcription factor genes (*Nr4a1*, *Nr4a2*, *Klf2*, *Klf3*, *Klf4*, *Bhlhe41*, *Pbx3*, and *Foxf1a*) can be found among the 47 genes repressed by HDAC4.

To gain insight into the signaling pathways deregulated by HDAC4/TM, we used GSEA (30). We compared our DNA microarray data with gene sets from the 3,272 curated MSigDB data sets. From this analysis we found that the phosphatidylinositol 3-kinase (PI3K)/Akt/mTOR signature is among the most enriched (data not shown). To confirm this result, we used as data sets 91 DNA microarray experiments available on GEO, including different models of transformation in murine fibroblasts and our gene list as a gene set. The signature of HDAC4 significantly overlaps genes repressed by the PI3K/Akt/mTOR pathway (Fig. 3D to G) through PTEN ablation (33) (normalized enrichment score [NES] = 1.46, $P < 0.005$) or TSC2 inhibition (34) (NES = 1.61, $P < 0.05$). Furthermore, the HDAC4 signature is negatively enriched for gene expression profiles elicited by the inhibition of the PI3K/Akt/mTOR pathway, using the PI3K inhibitor LY (35) (NES = −1.8485, $P < 0.005$), or induced PTEN expression in *Pten*$^{-/-}$ MEFs (33) (NES = −1.5228, $P < 0.05$).

Several genes repressed by HDAC4 are MEF2 targets and are negatively regulated by the PI3K/Akt pathway. To validate the microarray studies, we performed qRT-PCR analysis on a panel of 11 genes of the 47 described above, among which we included some MEF2 targets (*Klf2*, *Klf4*, *Edn1*, and *Nr4a1*) and others not previously associated with MEF2 (*RhoB*, *Nr4a2*, *Trib1*, *Anxa8*, *Irs1*, *Fgf7*, and *Errfi1*). *Gapdh* was used as control. Furthermore, GFP and HDAC4/TM cells were also treated with the PI3K inhibitor LY for 12 and 24 h to validate the GSEA. Except for *Fgf7*, *Errfi1*, and *Edn1*, the expression of all HDAC4 targets was upregu-

FIG 7 MEF2 transcriptional activation can revert the oncogenic phenotype. (A) Immunoblot analysis of MEF2-VP16-ER levels in NIH 3T3 cells expressing GFP or HDAC4-TM/GFP or control vector (Hygro-Puro). MEF2-VP16-ER-dependent transcription was induced by treating cells with 4-OHT for 24 h. Cellular lysates were generated and subjected to immunoblot analysis with anti-VP16 or anti-GFP antibodies. p62 (nucleoporin) was used as loading control. (B) Confocal pictures showing MEF2-ER-VP16 nuclear accumulation after the induction with 4-OHT in NIH 3T3 HDAC4/TM cells (Hygro) stably expressing MEF2-VP16-ER (Puro). Immunofluorescence analyses to visualize MEF2-VP16-ER subcellular localization were performed with an anti-VP16 antibody. Scale bar, 50 μm. (C) Confocal pictures of HDAC4/TM cells expressing MEF2-ER-VP16 chimera or its mutant defective in DNA binding MEF2ΔDBD-ER-VP16 grown in the presence of 4-OHT. Immunofluorescence analysis was performed to visualize HDAC4 and paxillin subcellular localizations. AF546-phalloidin was used to decorate F-actin. Scale bar, 50 μm. (D) mRNA expression levels of selected MEF2-HDAC4 target genes and *Gapdh*, as a control, were measured by using qRT-PCR in HDAC4/TM cells expressing MEF2-ER-VP16 or the mutant MEF2ΔDBD-ER-VP16. (E) HDAC4/TM cells were grown in DMEM supplemented with 10% FBS. The day after seeding, 4-OHT was added. (F) Quantitative results of colony formation in soft agar of NIH 3T3 cells expressing GFP or HDAC4/TM and the two MEF2 forms. The day after seeding, 4-OHT was added to culture medium. (G) Immunoblot analysis of MEF2-VP16-ER and MEF2ΔDBD-VP16-ER levels in NIH 3T3 cells expressing PI3KCA or the control vector (Puro). MEF2-dependent transcription was induced by treating cells with 4-OHT for 24 h. Cellular lysates were generated and subjected to immunoblot analysis with anti-VP16 or the indicated antibodies to monitor PI3K activation. p120 was used as a loading control. (H) Quantitative results of colony formation in soft agar of NIH 3T3 cells expressing Puro or PI3KCA and the two MEF2 forms. The day after seeding, 4-OHT was added to the culture medium. *, $P < 0.05$; **, $P < 0.01$; ***, $P < 0.001$.

lated after inhibition of the PI3K signaling. Interestingly, addition of the PI3K inhibitor reduces but did not abrogate the repressive activity of HDAC4 on these genes (Fig. 4A).

In order to clarify which genes of the panel are MEF2 targets, we generated NIH 3T3 cells expressing MEF2DN, a dominant-negative version of MEF2C (36) fused to GFP. MEF2DN-GFP was expressed at a lower level compared to HDAC4-GFP and less efficiently repressed MEF2-dependent transcription (data not shown). Except for *Errfi1*, all of the selected HDAC4 target genes were also downregulated after the expression of MEF2DN (Fig. 4B). To further attest the identified genes as MEF2 targets, we performed chromatin immunoprecipitation experiments in MEF2C-GFP-overexpressing cells. We selected a set of genes whose expression was influenced by MEF2DN, namely, *Irs1*, *RhoB*, *Klf4*, *Anxa8*, and *Klf2*. All of the selected genes are significantly enriched for MEF2 binding in the proximal promoter (Fig. 4C). Interestingly, several MEF2 targets identified by our study (*Irs1*, *RhoB*, *Klf2*, *Nr4a1*, *Nr4a2*, *Fgf7*, and *Trib1*) have recently been proposed as MEF2 targets in a lymphoblastic cell line by the ENCODE project (37).

Since *RhoB* showed the highest enrichment in the ChIP experiments, we decided to further prove its relationships with MEF2 by cloning its proximal promoter. The MEF2 consensus sequence embedded in the *RhoB* proximal promoter is highlighted in Fig. 4D. Its coexpression, together with MEF2C, dramatically augmented the luciferase activity, used as a reporter gene (Fig. 4F).

The PI3K/Akt pathway represses MEF2 transcriptional activity. The GSEA and the effect of the PI3K inhibitor LY suggest that the PI3K/Akt pathway could be involved in the regulation of genes, which are also under the influence of MEF2/HDAC4 axis. To further prove this relationship, we evaluated the ability of LY to directly influence MEF2-dependent transcription. Human fibroblasts expressing the E1A oncogene were used for these studies because of their high transfection efficiency. Treatment with LY increased MEF2C-dependent transcription but modestly affected the HDAC4 repressive influence (Fig. 5A). Similar results were obtained in NIH 3T3 cells (data not shown). Afterward, we explored the susceptibility of a set of HDAC4 variants to LY treatment. All of the different mutants show a behavior similar to that of the WT, being able to suppress MEF2C-dependent transcription also in the presence of the inhibitor (Fig. 5B). The only exception was the HDAC4 mutant lacking the amino terminus, which is defective for MEF2 binding and thus for repressive activity (8).

The repressive effect of PI3K/Akt signaling pathway on MEF2-dependent transcription was corroborated in IMR90-E1A cells expressing a constitutive active (A) version (Myr-Akt) of Akt (Fig. 5C). IN contrast, a dominant-negative (I) form of Akt (K179M) increased the MEF2C-dependent transcriptional activity (Fig. 5C). Similarly to the effect of LY, the repressive influence of HDAC4 was only weakly affected by the coexpression of the Akt variants.

HDAC4 and PI3K/Akt could exert their repressive influence on MEF2-depedent transcription as components of the same pathway or as independent arms of different signaling pathways. To answer this question, we evaluated whether the depletion of HDAC4 and LY showed additive effects on MEF2-dependent transcription. Because of compensatory mechanisms and redundant functions among class IIa HDACs (24), HDAC4, HDAC5, and HDAC9 were simultaneously silenced. Together with the three siRNAs, the MEF2-Luc reporter was cotransfected. Subsequently, the cells were incubated or not with LY. As a further control, in an additional set of experiments, we ectopically expressed MEF2C.

Transcription from the MEF2 promoter was upregulated 2-fold after PI3K inhibition (Fig. 5D). Silencing of class IIa HDAC4/5/9 increased transcription by ~4-fold. Downregulation of class IIa HDACs in the presence of LY dramatically augmented MEF2-dependent transcription (20-fold). When the experiment was repeated in the presence of ectopic MEF2C, the trend was similar. Silencing of class IIa HDACs and inhibition of the PI3K pathway demonstrated additive effects on MEF2-dependent transcription. Figure 5E shows the siRNA efficiency, as measured by qRT-PCR.

The PI3K/Akt pathway influences MEF2 protein stability. Although we have provided data that the PI3K/Akt pathway can influence MEF2 transcriptional activity, the mechanism involved remains obscure. In order to gain insight into the mechanisms exerted by PI3K/Akt signaling on MEF2s, we analyzed whether LY could influence the deacetylase activity associated with HDAC4 (Fig. 6A) or HDAC4 and MEF2C colocalization (Fig. 6B and C). All of the analyzed parameters were unaffected by LY.

We next compared the levels of MEF2C when expressed in the presence or absence of LY. We also coexpressed HDAC4 to evaluate its effect on MEF2C under these conditions. Immunoblot analysis confirmed that HDAC4 influences the electrophoretic mobility of MEF2C (Fig. 6D) (38). Importantly, LY augmented MEF2C protein levels independently from HDAC4. Similarly, the coexpression of the inactive mutant of Akt sustained MEF2 expression, whereas the active form reduced its level (Fig. 6E).

To confirm that the PI3K/Akt can impact MEF2 stability, we treated IMR90-E1A and NIH 3T3 cells with LY, in the presence or not of the proteasome inhibitor MG132. Extracts were generated, and the protein levels of MEF2C and MEF2D compared. LY and MG132 can augment the levels of the two MEF2 isoforms, and the effect is not addictive (Fig. 6F). These data suggest that the PI3K/Akt pathway impinges on MEF2 by controlling its turnover via the ubiquitin-proteasome system. To prove this hypothesis, we evaluated MEF2C polyubiquitination in the presence of LY. Coimmunoprecipitation studies in E1A cells, coexpressing MEF2C-GFP and HA-ubiquitin, demonstrated that the PI3K/Akt pathway is required for the polyubiquitination of MEF2C (Fig. 6G).

To further strengthen the relationships between MEF2 transcription, protein degradation, and the PI3K/Akt pathway, we generated NIH 3T3 cells expressing catalytic active PI3K. The levels of both MEF2C and MEF2D are reduced in cells expressing the PI3KCA compared to control cells, and treatment with the proteasome inhibitor rescued the levels of both MEF2 isoforms (Fig. 6H). In agreement with this observation, the expression levels of several MEF2 targets (*Klf2*, *End1*, *Irs1*, and *RhoB*) were reduced in cells expressing constitutive active PI3K (Fig. 6I).

Activation of MEF2 reverses the oncogenic properties of cells expressing HDAC4/TM and PI3K/CA. In addition to MEF2, HDAC4 can influence other transcription factors and, of the identified 47 genes, some are not MEF2 targets. To understand whether the oncogenic phenotype of cells expressing HDAC4 depends on the repression of the MEF2 genetic program, we decided to reactivate MEF2-dependent transcription in HDAC4-transformed cells. We took advantage from a MEF2-VP16-ER chimera in which the ligand-binding domain of the estrogen receptor (ER)

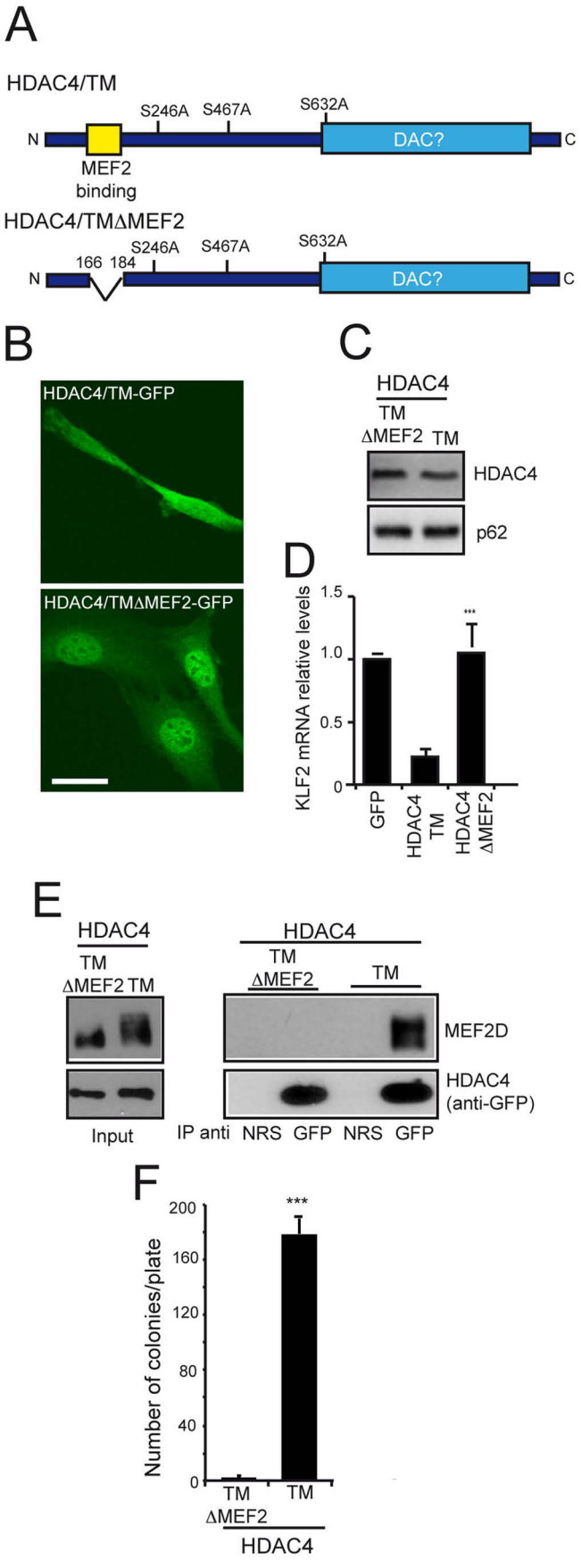

is fused to the C terminus of the constitutively active MEF2-VP16 fusion protein (39). We also used as a control the MEF2-VP16-ER lacking the DNA-binding domain (ΔDBD aa58-86). Immunoblot analysis of the different transgenes expressed in HDAC4/TM or GFP cells is shown in Fig. 7A. We also monitored the subcellular localization of MEF2-VP16-ER in HDAC4/TM cells to verify its nuclear accumulation after 4-OHT treatment (Fig. 7B). Induction of MEF2-VP16 in HDAC4/TM transformed cells reversed the morphological alterations and promoted stress fiber formation and focal adhesion assembling. In contrast, induction of MEF2ΔDBD-VP16 was ineffective (Fig. 7C).

Induction of MEF2-VP16 but not of its deletion version (ΔDBD) elicited the upregulation of MEF2 target genes also in cells expressing HDAC4/TM (Fig. 7D). The reactivation of the MEF2 program was sufficient to dramatically limit the proliferative potential of cells expressing HDAC4/TM to a level similar to GFP-expressing cells (Fig. 7E). Finally, growth in soft agar of HDAC4/TM-expressing cells was suppressed as well upon induction of MEF2-VP16 expression (Fig. 7F).

To corroborate the key role of MEF2 in counteracting transformation, we introduced the MEF2-VP16-ER chimera or its DNA-binding deletion version in PI3KCA-trasformed cells (Fig. 7G). Also in this case, the induction of MEF2-VP16 but not of its deleted version (ΔDBD) suppressed the ability of the transformed cells to grow in soft agar (Fig. 7H). These results indicate that MEF2 is an important target of the HDAC4 and PI3K transforming activity and suggest that the repression of the MEF2 genetic program is sufficient to confer oncogenic properties to NIH 3T3 cells.

HDAC4/TM defective in MEF2 binding loses its transforming activity. To show that the repression of MEF2 transcription is a key step for HDAC4 transforming activity, we constructed a nuclear mutant of HDAC4 unable to complex MEF2. The MEF2 binding region, which comprises aa 166 to 184, was deleted from HDAC4/TM to produce HDAC4/TMΔMEF2 (Fig. 8A). NIH 3T3 cells expressing HDAC4/TM and HDAC4/TMΔMEF2 were next generated. The 166-184 mutant shows a clear nuclear localization (Fig. 8B) and is expressed at levels similar to the HDAC4/TM (Fig. 8C). The repressive activity of HDAC4/TM on *Klf2* expression was abrogated after the removal of aa 166 to 184 (Fig. 8D). A coimmunoprecipitation study confirmed that the binding to MEF2D was impaired in the HDAC4/TMΔMEF2 mutant (Fig. 8E). Having characterized the properties of this new mutant, we next investigated its transforming ability. Figure 8F testifies that cells expressing HDAC4/TMΔMEF2 are unable to grow in soft agar in contrast

FIG 8 HDAC4/TM defective in MEF2 binding loses its transforming activity. (A) Scheme of HDAC4/TM highlighting the deacetylase domain and the region involved in MEF2 binding. The deletion mutant generated for the present study is also illustrated. (B) Confocal pictures of NIH 3T3 cells expressing HDAC4/TM-GFP or its deleted version for MEF2 binding. Scale bar, 50 μm. (C) Immunoblot analysis of HDAC4/TM and HDAC4/TM/ΔMEF2 levels in NIH 3T3 cells. Immunoblot analysis was performed with anti-GFP antibodies. p62 (nucleoporin) was used as a loading control. (D) qRT-PCR analysis was performed to quantify mRNAs levels of the HDAC4 target gene, *Klf2*. *Gapdh* was used as a control gene. *KLF2* mRNA levels were relative to GFP-expressing cells. (E) Cellular lysates from NIH 3T3 cells expressing HDAC4/TM and HDAC4/TM/ΔMEF2 were immunoprecipitated with an anti-GFP antibody. Immunoblots were performed with anti-MEF2D and anti-GFP antibodies. NRS, normal rabbit serum. (F) Quantitative results of colony formation in soft agar of NIH 3T3 cells expressing the indicated transgenes. ***, $P < 0.001$.

A

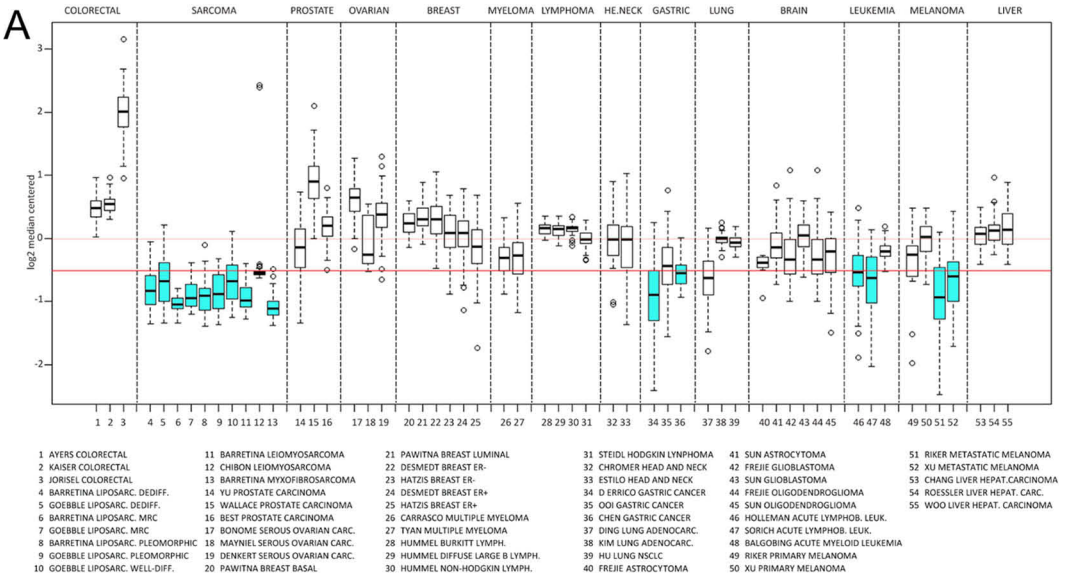

B **GSEA on STSs using the MEF2 signature**

DESCRIPTION	ACCESSION	NES	*P*
Normal tissue vs Liposarcoma (dedifferentiated)	GSE2719	1.66	0.016
Normal tissue vs Liposarcoma (myxoid and round cell)	GSE2719	2.52	0.001
Normal tissue vs Liposarcoma (pleomorphic)	GSE2719	1.74	0.026
Normal fat vs Liposarcoma (dedifferentiated)	GSE21122	1.79	0.0079
Normal fat vs Liposarcoma (myxoid and round cell)	GSE21122	2.05	0.001
Normal fat vs Liposarcoma (pleomorphic)	GSE21122	1.92	0.002
Lipoma vs Liposarcoma (myxoid and round cell)	GSE6481	1.96	0.001
STS Grade 1 vs STS Grade 3	GSE12972	1.78	0.003

C **STS: Correlations of the expression levels (ρ) between the MEF2 signature and the indicated genes**

TUMOR	REF.	ACCESSION	N. SAMPLES	PTEN ρ	*P*	HDAC4 ρ	*P*
Liposarcoma	[40]	GSE21122	89	0.48	0.0001	-0.10	0.33
Liposarcoma	[41]	GSE23980	84	0.44	0.001	-0.32	0.046
Leiomyosarcoma	[40]	GSE21122	25	0.38	0.05	-0.30	0.13
Leiomyosarcoma	[41]	GSE23980	57	0.48	0.0002	-0.21	0.12

D **PTEN clustered STS: Correlations of the expression levels (ρ) between the MEF2 signature and HDAC4**

TUMOR	REF.	ACCESSION	N. SAMPLES	PTEN levels	HDAC4 ρ	*P*
Liposarcoma	[40]	GSE21122	61	<-0.5	-0.05	0.7
Liposarcoma	[40]	GSE23980	52	<-0.5	-0.28	0.086
Leiomyosarcoma	[40]	GSE21122	17	<-0.5	-0.19	0.44
Leiomyosarcoma	[41]	GSE23980	45	<-0.5	-0.11	0.46
Liposarcoma	[40]	GSE21122	28	>-0.5	-0.56	0.002
Liposarcoma	[41]	GSE23980	32	>-0.5	-0.49	0.006
Leiomyosarcoma	[40]	GSE21122	8	>-0.5	-0.54	0.06
Leiomyosarcoma	[41]	GSE23980	13	>-0.5	-0.68	0.02

E

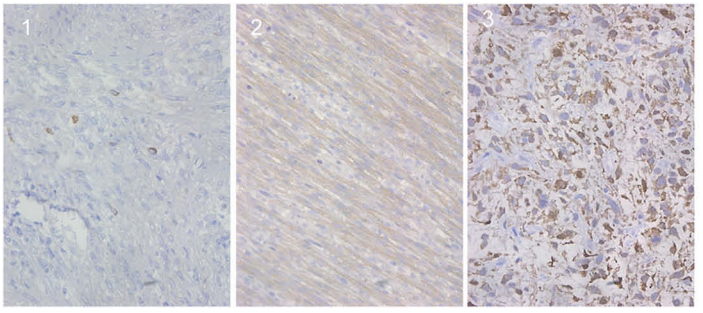

to HDAC4/TM cells. In conclusion, these results further support the idea that the repression of MEF2 transcription is essential for HDAC4 transforming activity.

A signature of 25 MEF2 target genes repressed by HDAC4 in NIH 3T3 cells is significantly repressed in human in STS. Data collected thus far suggest that dysfunctions of the MEF2-HDAC4 axis could play a role in tumorigenesis. As a first step for understanding our discovery in the context of human tumors, we decided to explore whether the expression of 25 genes (see Fig. S1A and B in the supplemental material), containing MEF2-binding sites in the proximal promoters and whose expression was repressed by HDAC4, is also repressed in human cancers. The transcriptomes of 14 tumor types coming from 40 DNA microarray GEO data sets were interrogated with this signature. This analysis allowed us to discover that the MEF2 signature was significantly repressed in soft tissue sarcoma (STS), gastric cancer, lymphoblastic leukemia, and metastatic melanoma (Fig. 9A). In particular, STSs turned out to be the tumors scoring the strongest repression of these 25 genes. The downregulation of this MEF2 signature in STSs was also confirmed by means of GSEA. The MEF2 signature resulted significantly enriched in normal tissues compared to tumors, and its repression parallels the progression of tumor malignancy (Fig. 9B).

To further portray the association between STSs and the MEF2 signature, we applied a statistical analysis to determine the correlation values, in terms of expression levels, between the 25 MEF2 targets and genes influencing their expression, including MEF2s, class IIa HDACs, and PTEN, using two data sets (40, 41). Among the MEF2 family members, MEF2C shows the highest expression in STSs. As expected, the MEF2C levels correlate with the levels of the 25 MEF2 target genes ($\rho = 0.35$; $P < 0.05$). This result implies that although MEF2 downregulation can contribute to the repression of MEF2 target gene in STSs, additional mechanisms also exists. In both studies, PTEN was generally repressed, and its repression correlated well with the levels of the 25 MEF2 target genes (Fig. 9C).

In STSs HDAC4 evidenced a heterogeneous pattern of expression (see Fig. S1C in the supplemental material and also Fig. 9D). With the exclusion of the liposarcomas from the Gibault study (Fig. 9C), we failed to observe a significant inverse correlation between MEF2 target genes and HDAC4 expression. Interestingly, when STSs were clustered into two groups based on the level of PTEN expression: negative (<-0.5) or residual (≥ -0.5), HDAC4 levels negatively correlated with the MEF2 signature only in tumors displaying residual PTEN expression (Fig. 9D). The expression of other class IIa members did not correlate with the repression of the 25 MEF2 target genes (data not shown).

Immunohistochemical analysis of a series of 26 human primary leiomyosarcomas revealed a diffuse/pan, although weak reactivity for anti-HDAC4 antibody in 12 cases (Fig. 9E2) and an intense diffuse signal in 5 cases, with prominent nuclear accumulation in 2 cases (Fig. 9E3). Immunohistochemical data are summarized in Fig. S2 in the supplemental material. This result is in line with our *in silico* predictions, evoking a contribution of HDAC4 to the repression of MEF2 transcription only in a subgroup of STSs.

MEF2 negatively impacts on the proliferation of human sarcoma cells. Having discovered a correlation between MEF2 transcriptional activity and STSs, we examined the contribution of MEF2 to the tumorigenic phenotype of a panel of human leiomyosarcoma cell lines (LMS) (42). We initially verified whether, similarly to NIH 3T3 cells, MEF2D and MEF2C levels are under the control of the PI3K/Akt pathway. Experiments with LY and MG123, alone or in combination, indicated that in LMS cells the PI3K/Akt pathway also controls MEF2C and MEF2D protein stability via the proteasome (Fig. 10A). Next, we engineered LMS cells with the MEF2-VP16-ER chimera for inducible MEF2-dependent transcription. The induction of MEF2 was sufficient to reduce the proliferation (Fig. 10B), as well as the anchorage-independent growth, of LMS cell lines (Fig. 10C). Overall, these results support the hypothesis of MEF2 as a tumor suppressor in STSs.

Pharmacological cotargeting of the PI3K/Akt pathway and of the MEF2-HDAC axis in sarcoma cells. To additionally prove the independent and synergistic action of HDAC4 and of the PI3K/Akt pathway on MEF2s and to evaluate the therapeutic perspective of our discovery, we used LY in conjunction with BML-210, a recently defined inhibitor of the interaction between class IIa HDACs and MEF2s (17).

BML-210 discharges the binding between HDAC4 and MEF2D (Fig. 11A) and MEF2 transcriptional activity is augmented in the presence of BML-210 (Fig. 11B). Moreover, both BML-210 and LY inhibit the proliferation of LMS cell lines and, most importantly, the combination of the two drugs shows additive effects in terms of the suppression of proliferation (Fig. 11C), which stems from a delayed cell cycle progression, as shown in Fig. 11D. Moreover, the transcription of the MEF2 target genes *KLF2*, *NR4A1*, and *RHOB* was in general augmented in LMS cells when grown in the presence of both drugs compared to single treatments (Fig. 11E).

DISCUSSION

This study provides unprecedented and compelling evidence of the tumorigenic potential of the MEF2-HDAC axis. Murine fibroblasts engineered to express nuclear active HDAC4 gain a transformed phenotype, including elongated morphology, loss of contact inhibition, anchorage-independent growth, and tumorigenicity in a xenograft assay. Cell transformation as elicited by HDAC4 is accompanied by the repression of a limited number of genes, including several transcription factors. The selective influence of HDAC4 on the transcription of important regulatory nodes can explain the dramatic shift in the proliferative attitude of the cells.

FIG 9 Expression of the MEF2 target genes in human tumors. (A) Box plots depicted in light-blue mark tumors where the MEF2 signature is significantly below zero and with at least the 50% of the values below an arbitrary threshold of −0.5. Significance was calculated by using the Poisson test (Holm-Bonferroni correction, $P < 0.05$). (B) GSEA on STSs, using the MEF2 signature as a gene set. (C) Expression level correlations between the MEF2 signature and HDAC4 or PTEN in three different types of STSs. Statistically significant correlations are indicated in green, whereas statistically significant inverse correlations are indicated in red. (D) Expression level correlations between MEF2 signature and HDAC4 in different types of STS subdivided into two subclasses according to the expression of PTEN. Log_2(PTEN) of −0.5 was selected as the cutoff to identify the two populations. Statistically significant inverse correlations are shown in red. (E) Immunohistochemical analysis of HDAC4 expression in leiomyosarcoma. HDAC4 showed absent E1 (few positive inflammatory cells are present), low pan/cytoplasmic expression E2, or increased expression and nuclear localization E3.

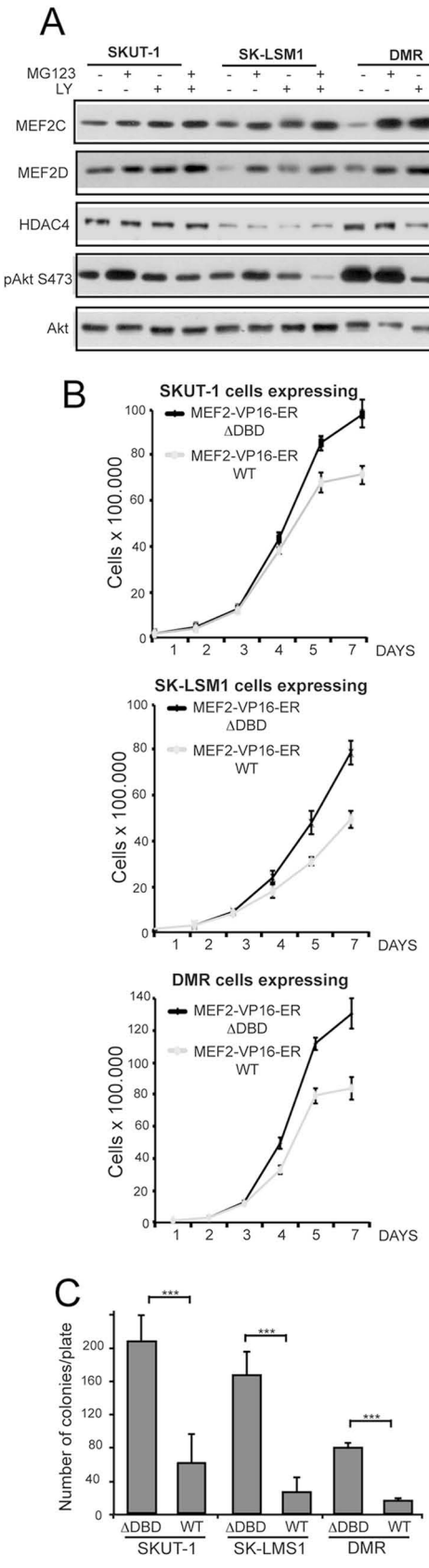

Although MEF2s are important partners of HDAC4, the literature provide a long list of other proteins able to complex with HDAC4 (18). Hence, whether the dysregulation of the MEF2-HDAC4 axis is accountable for the oncogenic behavior cannot be automatically evoked. Our results indicate that repression of the MEF2 genetic program is crucial for the HDAC4 transforming action. First, most (70%) of the genes repressed by HDAC4 are putative MEF2 targets. Second, the restoration of the MEF2-dependent transcription in cells expressing nuclear HDAC4 reverts the transformed phenotype. Third, loss of MEF2 binding abrogates the transforming capability of nuclear active HDAC4.

The oncogenic potential appears to be shared among class IIa members. An HDAC7 mutant defective for 14-3-3 binding was also able to transform NIH 3T3 cells. Of note, a mutation in serine 155 of HDAC7, a binding site for 14-3-3 proteins, has been recently described in non-Hodgkin lymphoma (43). Although overexpression of the WT forms of HDAC4 and HDAC7 was insufficient for a robust transformation, we cannot exclude that *in vivo* an increase of class IIa HDACs levels might have an impact on MEF2 and on tumor development (11, 24, 44).

Genes identified as targets of the MEF2-HDAC4 axis can also be repressed by PI3K/Akt signaling. HDAC4 and the PI3K/Akt pathway repress MEF2 transcription through independent routes. Although HDAC4 binds MEF2s and possibly generates a repressed state on chromatin (1), the PI3K/Akt signaling promotes polyubiquitination and proteasome-mediated degradation of MEF2s. Previous studies have reported that, in the context of muscle differentiation, the PI3K/Akt pathway could enhance MEF2 transcriptional activity (45, 46). However, the mechanism engaged by Akt is debated, and there are evidences contrasting with the idea of Akt as an activator of MEF2 (47). Most importantly, the positive influence of the PI3K/Akt pathway on MEF2s was not confirmed in cancer cells (45). Analogous to our findings, the phosphorylation-dependent degradation of MEF2C has been previously reported (48).

The subset of MEF2 targets repressed by HDAC4 turned out to be significantly repressed in certain tumors, particularly in STSs, which share with NIH 3T3 the mesenchymal origin, highlighting the relevance of the cell context in HDAC4/MEF2-mediated phenotypes (19). Importantly, reactivation of MEF2 transcription in PI3K-transformed cells and also in human sarcoma cell lines was sufficient to reduce proliferation and to impact on anchorage-independent growth.

In STSs, repression of the MEF2 targets mainly correlates with the downregulation of PTEN, the negative regulator of the PI3K/Akt pathway. Intriguingly, in tumors that retain partial PTEN expression, MEF2 targets are still repressed. In these cases, repression inversely correlates with HDAC4 levels. This suggests that PTEN loss and HDAC4 overexpression could represent two alternative mechanisms for suppressing the MEF2 genetic program in STS.

FIG 10 Regulation and functions of MEF2s in human sarcoma cells. (A) Immunoblot analysis of MEF2C and MEF2D levels in human sarcoma cell lines treated or not with LY. Cellular lysates were generated and subjected to immunoblot analysis with the indicated antibodies. (B) Human sarcoma cells expressing MEF2-VP16-ER or MEF2ΔDBD-VP16-ER were grown in DMEM supplemented with 10% FBS. The day after seeding, 4-OHT was added to culture medium. (C) Quantitative results of colony formation in soft agar of human sarcoma cells expressing MEF2-VP16-ER or MEF2ΔDBD-VP16-ER. The day after seeding, 4-OHT was added to culture medium. ***, $P < 0.001$.

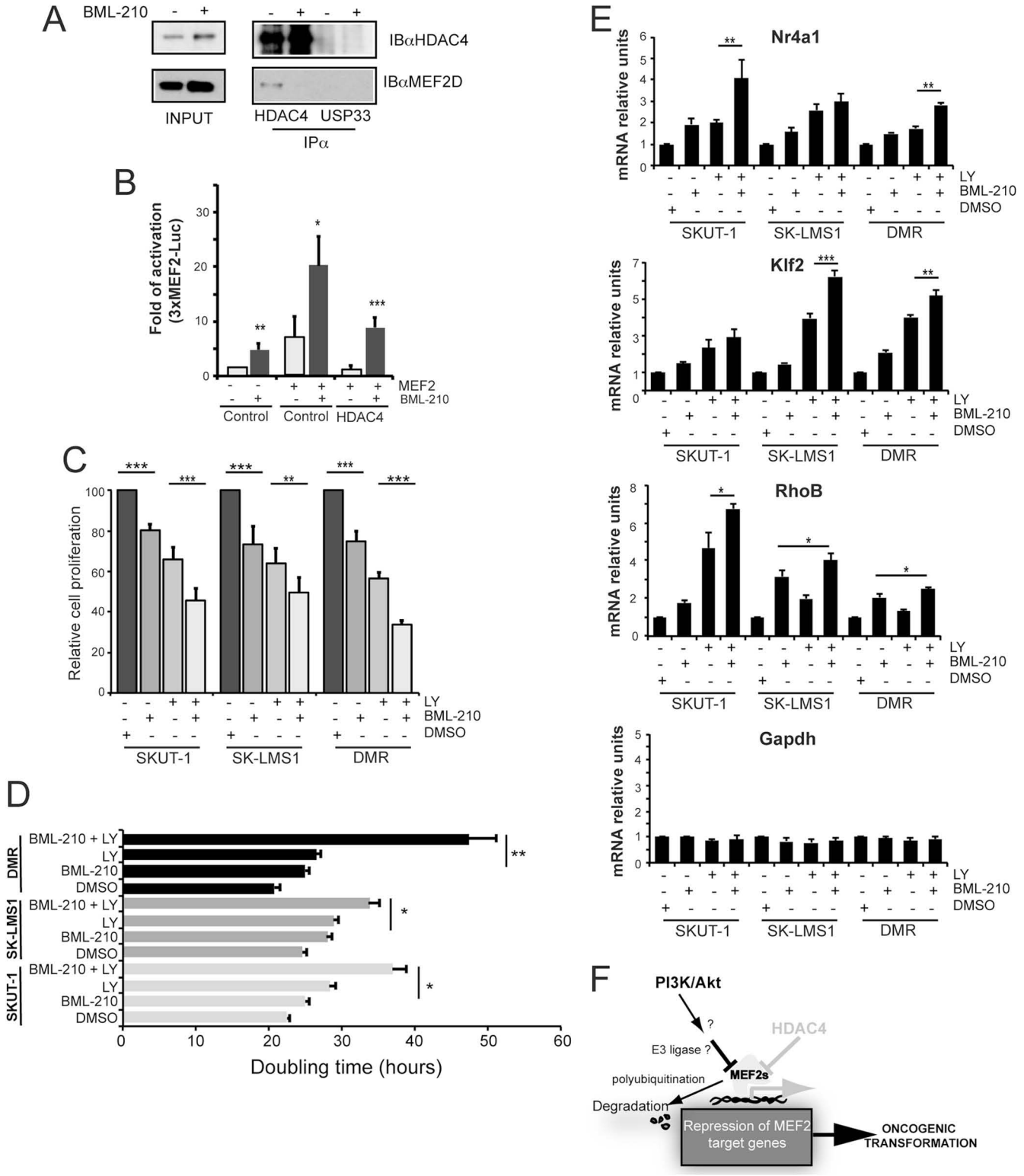

FIG 11 Pharmacological targeting of MEF2-HDAC axis and PI3K/Akt pathway. (A) Cellular lysates from IMR90-E1A cells treated or not for 36 h with BML-210 were immunoprecipitated with an anti-HDAC4 antibody. Immunoblots were performed with the anti-MEF2D and anti-HDAC4 antibodies. (B) IMR90-E1A cells were transfected as described in Fig. 5A. After 12 h, the cells were treated or not with BML-210 for 36 h. (C) Human sarcoma cells were seeded in 96-well and treated for 48 h with LY and/or BML-210. The proliferative rate was scored by using a resazurin assay. (D) Doubling time (DB) of human sarcoma cells (5×10^4) treated as in panel C. The DB was calculated according to the following formula: $DB = (t_2 - t_1) \cdot [\log_2/\log(q_2/q_1)]$, where t_2 is time 2, t_1 is time 1, q_1 is the number cells at t_1, and q_2 is the number of cells at t_2. (E) mRNA expression levels of selected MEF2-HDAC4 target genes and *Gapdh*, as a control, were measured using qRT-PCR in human sarcoma cells treated for 36 h as in panel C. (F) Model representing the two different actions of PI3K/Akt signaling and of HDAC4 on MEF2-dependent transcription. *, $P < 0.05$; **, $P < 0.01$; ***, $P < 0.001$.

The independent action of HDAC4 and of PI3K/Akt on MEF2 was confirmed also by the use of selective inhibitors. Blocking the PI3K/Akt pathway and impeding the interaction between MEF2 and class IIa HDACs produced additive effects on the transcription of MEF2 target genes and much strongly suppressed proliferation in sarcoma cell lines. This observation highlights the importance of targeting both pathways for the development of more efficient therapies for the treatment of STS.

In conclusion, our work suggests a model (Fig. 11F) wherein MEF2 is a converging hub for the transformation promoted by different oncogenic pathways. In this context, MEF2s behave as tumor suppressors, which suggests that the restoration of MEF2 activity could be exploited as a novel therapeutic avenue.

ACKNOWLEDGMENTS

This study was supported by Associazione Italiana per la Ricerca contro il Cancro (AIRC) grant IG-10437 and FIRB Progetto RBAP11S8C3_002 (C.B.) and by the AIRC and Ministero della Salute (R.M.). A.C. received a Gemma del Cornò fellowship from the AIRC.

We thank F. Dequiedt for the HDAC7 plasmids (University of Liège, Liège, Belgium) and M. E. Greenberg (Harvard University, Boston, MA) for the estrogen-inducible MEF2C plasmids.

REFERENCES

1. **Martin M, Kettmann R, Dequiedt F.** 2007. Class IIa histone deacetylases: regulating the regulators. Oncogene **26:**5450–5467.
2. **Haberland M, Montgomery RL, Olson EN.** 2009. The many roles of histone deacetylases in development and physiology: implications for disease and therapy. Nat. Rev. Genet. **10:**32–42.
3. **Fischle W, Dequiedt F, Hendzel MJ, Guenther MG, Lazar MA, Voelter W, Verdin E.** 2002. Enzymatic activity associated with class II HDACs is dependent on a multiprotein complex containing HDAC3 and SMRT/N-CoR. Mol. Cell **9:**45–57.
4. **Lahm A, Paolini C, Pallaoro M, Nardi MC, Jones P, Neddermann P, Sambucini S, Bottomley MJ, Lo Surdo P, Carfí A, Koch U, De Francesco R, Steinkühler C, Gallinari P.** 2007. Unraveling the hidden catalytic activity of vertebrate class IIa histone deacetylases. Proc. Natl. Acad. Sci. U. S. A. **104:**17335–17340.
5. **Yang XJ, Seto E.** 2008. The Rpd3/Hda1 family of lysine deacetylases: from bacteria and yeast to mice and men. Nat. Rev. Mol. Cell. Biol. **9:**206–218.
6. **Chen JF, Mandel EM, Thomson JM, Wu Q, Callis TE, Hammond SM, Conlon FL, Wang DZ.** 2006. The role of microRNA-1 and microRNA-133 in skeletal muscle proliferation and differentiation. Nat. Genet. **38:**228–233.
7. **Liu F, Pore N, Kim M, Voong KR, Dowling M, Maity A, Kao GD.** 2006. Regulation of histone deacetylase 4 expression by the SP family of transcription factors. Mol. Biol. Cell **17:**585–597.
8. **Paroni G, Fontanini A, Cernotta N, Foti C, Gupta MP, Yang XJ, Fasino D, Brancolini C.** 2007. Dephosphorylation and caspase processing generate distinct nuclear pools of histone deacetylase 4. Mol. Cell. Biol. **27:**6718–6732.
9. **Cernotta N, Clocchiatti A, Florean C, Brancolini C.** 2011. Ubiquitin-dependent degradation of HDAC4, a new regulator of random cell motility. Mol. Biol. Cell **22:**278–289.
10. **Backs J, Worst BC, Lehmann LH, Patrick DM, Jebessa Z, Kreusser MM, Sun Q, Chen L, Heft C, Katus HA, Olson EN.** 2011. Selective repression of MEF2 activity by PKA-dependent proteolysis of HDAC4. J. Cell Biol. **195:**403–4015.
11. **Clocchiatti A, Florean C, Brancolini C.** 2011. Class IIa HDACs: from important roles in differentiation to possible implications in tumorigenesis. J. Cell. Mol. Med. **15:**1833–1846.
12. **Grozinger CM, Schreiber SL.** 2000. Regulation of histone deacetylase 4 and 5 and transcriptional activity by 14-3-3-dependent cellular localization. Proc. Natl. Acad. Sci. U. S. A. **97:**7835–7840.
13. **Wang AH, Kruhlak MJ, Wu J, Bertos NR, Vezmar M, Posner BI, Bazett-Jones DP, Yang XJ.** Regulation of histone deacetylase 4 by binding of 14-3-3 proteins. Mol. Cell. Biol. **20:**6904–6912.
14. **Martin M, Potente M, Janssens V, Vertommen D, Twizere JC, Rider MH, Goris J, Dimmeler S, Kettmann R, Dequiedt F.** 2008. Protein phosphatase 2A controls the activity of histone deacetylase 7 during T cell apoptosis and angiogenesis. Proc. Natl. Acad. Sci. U. S. A. **105:**4727–4732.
15. **Paroni G, Cernotta N, Dello Russo C, Gallinari P, Pallaoro M, Foti C, Talamo F, Orsatti L, Steinkühler C, Brancolini C.** 2008. PP2A regulates HDAC4 nuclear import. Mol. Biol. Cell **19:**655–667.
16. **Miska EA, Karlsson C, Langley E, Nielsen SJ, Pines J, Kouzarides T.** 1999. HDAC4 deacetylase associates with and represses the MEF2 transcription factor. EMBO J. **18:**5099–50107.
17. **Jayathilaka N, Han A, Gaffney KJ, Dey R, Jarusiewicz JA, Noridomi K, Philips MA, Lei X, He J, Ye J, Gao T, Petasis NA, Chen L.** 2012. Inhibition of the function of class IIa HDACs by blocking their interaction with MEF2. Nucleic Acids Res. **40:**5378–5388.
18. **Clocchiatti A, Di Giorgio E, Demarchi F, Brancolini C.** 2013. Beside the MEF2 axis: unconventional functions of HDAC4. Cell Signal **25:**269–276.
19. **Potthoff MJ, Olson EN.** 2007. MEF2: a central regulator of diverse developmental programs. Development **134:**4131–4140.
20. **Hanahan D, Weinberg RA.** 2011. Hallmarks of cancer: the next generation. Cell **144:**646–674.
21. **Schwieger M, Schüler A, Forster M, Engelmann A, Arnold MA, Delwel R, Valk PJ, Löhler J, Slany RK, Olson EN, Stocking C.** 2009. Homing and invasiveness of MLL/ENL leukemic cells is regulated by MEF2C. Blood **114:**2476–2488.
22. **Milde T, Oehme I, Korshunov A, Kopp-Schneider A, Remke M, Northcott P, Deubzer HE, Lodrini M, Taylor MD, von Deimling A, Pfister S, Witt O.** 2010. HDAC5 and HDAC9 in medulloblastoma: novel markers for risk stratification and role in tumor cell growth. Clin. Cancer Res. **16:**3240–3252.
23. **Homminga I, Pieters R, Langerak AW, de Rooi JJ, Stubbs A, Verstegen M, Vuerhard M, Buijs-Gladdines J, Kooi C, Klous P, van Vlierberghe P, Ferrando AA, Cayuela JM, Verhaaf B, Beverloo HB, Horstmann M, de Haas V, Wiekmeijer AS, Pike-Overzet K, Staal FJ, de Laat W, Soulier J, Sigaux F, Meijerink JP.** 2011. Integrated transcript and genome analyses reveal NKX2-1 and MEF2C as potential oncogenes in T cell acute lymphoblastic leukemia. Cancer Cell **19:**484–497.
24. **Clocchiatti A, Di Giorgio E, Ingrao S, Meyer-Almes FJ, Tripodo C, Brancolini C.** 2013. Class IIa HDACs repressive activities on MEF2-depedent transcription are associated with poor prognosis of ER^{+} breast tumors. FASEB J. **27:**942–954.
25. **Mottet D, Pirotte S, Lamour V, Hagedorn M, Javerzat S, Bikfalvi A, Bellahcène A, Verdin E, Castronovo V.** 2009. HDAC4 represses $p21^{WAF1/Cip1}$ expression in human cancer cells through a Sp1-dependent, p53-independent mechanism. Oncogene **28:**243–256.
26. **Wilson AJ, Byun DS, Nasser S, Murray LB, Ayyanar K, Arango D, Figueroa M, Melnick A, Kao GD, Augenlicht LH, Mariadason JM.** 2008. HDAC4 promotes growth of colon cancer cells via repression of p21. Mol. Biol. Cell **19:**4062–4075.
27. **Cadot B, Brunetti M, Coppari S, Fedeli S, de Rinaldis E, Dello Russo C, Gallinari P, De Francesco R, Steinkühler C, Filocamo G.** 2009. Loss of histone deacetylase 4 causes segregation defects during mitosis of p53-deficient human tumor cells. Cancer Res. **69:**6074–6082.
28. **Todaro GJ, Green H.** 1963. Quantitative studies of the growth of mouse embryo cells in culture and their development into established lines. J. Cell Biol. **17:**299–313.
29. **Paroni G, Mizzau M, Henderson C, Del Sal G, Schneider C, Brancolini C.** 2004. Caspase-dependent regulation of histone deacetylase 4 nuclear-cytoplasmic shuttling promotes apoptosis. Mol. Biol. Cell **15:**2804–2818.
30. **Subramanian A, Tamayo P, Mootha VK, Mukherjee S, Ebert BL, Gillette MA, Paulovich A, Pomeroy SL, Golub TR, Lander ES, Mesirov JP.** 2005. Gene set enrichment analysis: a knowledge-based approach for interpreting genome-wide expression profiles. Proc. Natl. Acad. Sci. U. S. A. **102:**15545–15550.
31. **Nurtdinov RN, Vasiliev MO, Ershova AS, Lossev IS, Karyagina AS.** 2010. PLANdbAffy: probe-level annotation database for Affymetrix expression microarrays. Nucleic Acids Res. **38:**D726–D730.
32. **Dequiedt F, Kasler H, Fischle W, Kiermer V, Weinstein M, Herndier BG, Verdin E.** 2003. HDAC7, a thymus-specific class II histone deacetylase, regulates Nur77 transcription and TCR-mediated apoptosis. Immunity. **18:**687–698.
33. **Mulholland DJ, Tran LM, Li Y, Cai H, Morim A, Wang S, Plaisier S, Garraway IP, Huang J, Graeber TG, Wu H.** 2011. Cell autonomous role of PTEN in regulating castration-resistant prostate cancer growth. Cancer Cell **19:**792–804.

34. **Peña-Llopis S, Vega-Rubin-de-Celis S, Schwartz JC, Wolff NC, Tran TA, Zou L, Xie XJ, Corey DR, Brugarolas J.** 2011. Regulation of TFEB and V-ATPases by mTORC1. EMBO J. **30:**3242–3258.
35. **Bromann PA, Korkaya H, Webb CP, Miller J, Calvin TL, Courtneidge SA.** 2005. Platelet-derived growth factor stimulates Src-dependent mRNA stabilization of specific early genes in fibroblasts. J. Biol. Chem. **280:** 10253–10263.
36. **Molkentin JD, Black BL, Martin JF, Olson EN.** 1996. Mutational analysis of the DNA binding, dimerization, and transcriptional activation domains of MEF2C. Mol. Cell. Biol. **16:**2627–2636.
37. **Rosenbloom KR, Dreszer TR, Pheasant M, Barber GP, Meyer LR, Pohl A, Raney BJ, Wang T, Hinrichs AS, Zweig AS, Fujita PA, Learned K, Rhead B, Smith KE, Kuhn RM, Karolchik D, Haussler D, Kent WJ.** 2010. ENCODE whole-genome data in the UCSC Genome Browser. Nucleic Acids Res. **38:**D620–D625.
38. **Grégoire S, Tremblay AM, Xiao L, Yang Q, Ma K, Nie J, Mao Z, Wu Z, Giguère V, Yang XJ.** 2006. Control of MEF2 transcriptional activity by coordinated phosphorylation and sumoylation. J. Biol. Chem. **281:**4423–4433.
39. **Flavell SW, Cowan CW, Kim TK, Greer PL, Lin Y, Paradis S, Griffith EC, Hu LS, Chen C, Greenberg ME.** 2006. Activity-dependent regulation of MEF2 transcription factors suppresses excitatory synapse number. Science **311:**1008–10012.
40. **Barretina J, Taylor BS, Banerji S, Ramos AH, Lagos-Quintana M, Decarolis PL, Shah K, Socci ND, Weir BA, Ho A, Chiang DY, Reva B, Mermel CH, Getz G, Antipin Y, Beroukhim R, Major JE, Hatton C, Nicoletti R, Hanna M, Sharpe T, Fennell TJ, Cibulskis K, Onofrio RC, Saito T, Shukla N, Lau C, Nelander S, Silver SJ, Sougnez C, Viale A, Winckler W, Maki RG, Garraway LA, Lash A, Greulich H, Root DE, Sellers WR, Schwartz GK, Antonescu CR, Lander ES, Varmus HE, Ladanyi M, Sander C, Meyerson M, Singer S.** 2010. Subtype-specific genomic alterations define new targets for soft-tissue sarcoma therapy. Nat. Genet. **42:**715–721.
41. **Gibault L, Ferreira C, Pérot G, Audebourg A, Chibon F, Bonnin S, Lagarde P, Vacher-Lavenu MC, Terrier P, Coindre JM, Aurias A.** 2012. From PTEN loss of expression to RICTOR role in smooth muscle differentiation: complex involvement of the mTOR pathway in leiomyosarcomas and pleomorphic sarcomas. Mod. Pathol. **25:**197–211.
42. **Piccinin S, Tonin E, Sessa S, Demontis S, Rossi S, Pecciarini L, Zanatta L, Pivetta F, Grizzo A, Sonego M, Rosano C, Dei Tos AP, Doglioni C, Maestro R.** 2012. A "twist box" code of p53 inactivation: twist box: p53 interaction promotes p53 degradation. Cancer Cell **22:**404–415.
43. **Morin RD, Mendez-Lago M, Mungall AJ, Goya R, Mungall KL, Corbett RD, Johnson NA, Severson TM, Chiu R, Field M, Jackman S, Krzywinski M, Scott DW, Trinh DL, Tamura-Wells J, Li S, Firme MR, Rogic S, Griffith M, Chan S, Yakovenko O, Meyer IM, Zhao EY, Smailus D, Moksa M, Chittaranjan S, Rimsza L, Brooks-Wilson A, Spinelli JJ, Ben-Neriah S, Meissner B, Woolcock B, Boyle M, McDonald H, Tam A, Zhao Y, Delaney A, Zeng T, Tse K, Butterfield Y, Birol I, Holt R, Schein J, Horsman DE, Moore R, Jones SJ, Connors JM, Hirst M, Gascoyne RD, Marra MA.** 2011. Frequent mutation of histone-modifying genes in non-Hodgkin lymphoma. Nature **476:**298–303.
44. **Rad R, Rad L, Wang W, Cadinanos J, Vassiliou G, Rice S, Campos LS, Yusa K, Banerjee R, Li MA, de la Rosa J, Strong A, Lu D, Ellis P, Conte N, Yang FT, Liu P, Bradley A.** 2010. PiggyBac transposon mutagenesis: a tool for cancer gene discovery in mice. Science **330:**1104–1107.
45. **Xu Q, Wu Z.** 2000. The insulin-like growth factor-phosphatidylinositol 3-kinase-Akt signaling pathway regulates myogenin expression in normal myogenic cells but not in rhabdomyosarcoma-derived RD cells. J. Biol. Chem. **275:**36750–36757.
46. **Kaneko S, Feldman RI, Yu L, Wu Z, Gritsko T, Shelley SA, Nicosia SV, Nobori T, Cheng JQ.** 2002. Positive feedback regulation between Akt2 and MyoD during muscle differentiation: cloning of Akt2 promoter. J. Biol. Chem. **277:**23230–23235.
47. **Wilson EM, Tureckova J, Rotwein P.** 2004. Permissive roles of phosphatidyl inositol 3-kinase and Akt in skeletal myocyte maturation. Mol. Biol. Cell **15:**497–505.
48. **Magli A, Angelelli C, Ganassi M, Baruffaldi F, Matafora V, Battini R, Bachi A, Messina G, Rustighi A, Del Sal G, Ferrari S, Molinari S.** 2010. Proline isomerase Pin1 represses terminal differentiation and myocyte enhancer factor 2C function in skeletal muscle cells. J. Biol. Chem. **285:** 34518–34527.